REPUBLIC OF TURKEY
YILDIZ TECHNICAL UNIVERSITY
GRADUATE SCHOOL OF NATURAL AND APPLIED SCIENCES

SYNTHESIS OF NANOMATERIALS FOR PHOTOVOLTAIC SYSTEMS

SELEN EZGİ ÇELİK

MSc. THESIS
DEPARTMENT OF CHEMICAL ENGINEERING
PROGRAM OF CHEMICAL ENGINEERING

ADVISER
PROF. DR. HANİFİ SARAÇ

İSTANBUL, 2015

REPUBLIC OF TURKEY

YILDIZ TECHNICAL UNIVERSITY

GRADUATE SCHOOL OF NATURAL AND APPLIED SCIENCES

SYNTHESIS OF NANOMATERIALS FOR PHOTOVOLTAIC SYSTEMS

A thesis submitted by Selen Ezgi ÇELİK in partial fulfillment of the requirements for the degree of **MASTER OF SCIENCE** is approved by the committee on 11.06.2016 in Department of Chemical Engineering, Chemical Engineering Program.

Thesis Adviser

Prof. Dr. Hanifi SARAÇ

Yıldız Technical University

Approved By the Examining Committee

Prof. Dr. Hanifi SARAÇ

Yıldız Technical University _____

Prof. Dr. Belma KIN ÖZBEK, Member

Yıldız Technical University _____

Prof. Dr. İsmail AYDIN, Member

İstanbul University _____

ACKNOWLEDGEMENTS

I would like to express the deepest appreciation to my advisor, Prof Hanifi SARAÇ, who has the attitude and substance of a leader. Without his guidance and persistent help this dissertation would not have been possible. He gave me perfect research opportunity and always supported me in scientific way.

I also would like to thank Prof Ismail AYDIN, for his guidance, support, advices, valuable comments and provision since my bachelor days until today. His knowledge and vision helped me to step into academic career.

This thesis would not have been completed without the assistance of members of Sarac Labs research group and Zeynep ERPOLAT and Birsen Cansın BUDAN.

I am also grateful to Yıldız Technical University, Central Lab employees, for carrying out my analysis's.

I would like to express my sincere gratitude to two important companies. To GAMA-PLAS employers, who helped me during my reactor design and production process and to ARÇELİK – R&D Department employers who completed some of my analysis.

Last but not least, I would like to thank sincerely to my mother, Nurhan AÇIKYILDIZ, my father, Mehmet AÇIKYILDIZ and my brother Ahmet Eren AÇIKYILDIZ for supporting me at every stage of my life.

And finally, I would like to thank and apologize my husband, Hüseyin ÇELİK, for the times I take from our lives to write this thesis.

June, 2015

Selen Ezgi ÇELİK

TABLE OF CONTENTS

LIST OF SYMBOLS

K	Kelvin
Å	Angstrom
SA:V	Surface Area-to-Volume Ratio
S/N	Signal to Nosie
V	Voltage
P	Porosity
TW	Terawatt
CSP	Concentrating Solar Power

LIST OF ABBREVIATIONS

AAM	Anodized Alumina Membrane
AAO	Anodic Aluminium Oxide
AES	Auger-Electron Spectroscopy
ALD	Atomic Layer Deposition
BET	Brunauer, Emmett And Teller
CAS	Chemical Abstracts Service
CB	Conduction Band
CNT	Carbon Nanotubes
DI	Deionized Water
DOE	Design Of Experiment
DSSC	Dye Sensitized Solar Cell
EELS	Electron-Energy-Loss Spectroscopy
FE-SEM	Field Emission Scanning Electron Microscopy
HOMO	Highest Occupied Molecular Orbitals
INS	International Numbering System
LALD	Liquid-Phase Atomic Layer Deposition
LUMO	Lowest Unoccupied Molecular Orbitals
PC	Polycarbonate
PCE	Photoelectric Conversion Efficiency
RBA	Rapid Breakdown Anodization
SCE	Saturated Calomel Electrode
SEM	Scanning Electron Microscope
SFIL	Step and Flash Imprint Lithography
STC	Standard Test Conditions
TEM	Transmission Electron Microscopy
TNT	TiO_2 Nanotubes
TTIP	Titaniumtetraisopropoxide
USP	Ultraviolet Photoemission Spectroscopy
UV	Ultraviolet
VOC	Volatile Organic Compounds
XPS	X-Ray Photoemission Spectroscopy
XRD	X-Ray Powder Diffraction

LIST OF FIGURES

LIST OF TABLES

ABSTRACT

SYNTHESIS OF NANOMATERIALS FOR PHOTOVOLTAIC SYSTEMS

Selen Ezgi ÇELİK

Department of Chemical Engineering

MSc. Thesis

Adviser: Prof. Dr. Hanifi SARAÇ

Increasing energy demand and running out of fossil fuels led researchers to find alternative energy solutions. Solar cells are one of the most promising options in that field, because of the unlimited potential of solar power.

Dye-sensitized solar cells (DSSCs) are under the class of the third generation solar cells. They have been studied widely since their invitation by Grätzel, because of their low cost and versatile technology. Here, a condense TiO_2 film, usually made from nanosized TiO_2, carries an organic dye. In this system, dye absorbs the light and carries excited electron into conduction band.

For the sake of reduce irregular movement of the electrons, one-dimensional morhologies such as nanowires, nanorods and nanotbues have been synthesized as an option to nanoparticle based films. Due to having easy production methods and ordered geometric arrays, TiO_2 nanotube (TNT) films became popular in this application area in recent years. In order to achieve reasonable convertion rates in solar cells, most of these researches

deal with improving properties of TNT's such as surface area-to-volume ratio, length-to-diameter ratio, homogenous porosity, desired crystal structure, conductivity or reactivity values etc. For being relatively new discovered field, scientists need numbers of experiments to achieve desired optimized conditions of TNT's.

In this research it is aimed to find out the relationship between temperature, type of TiO_2 raw material, time, concentration of NaOH solution and physical and chemical properties of TNT's in hydrothermal synthesis. Rutile and anatase bulk TiO_2, Degussa P25 and ultrasounded anatase TiO_2 (which have been synthesized on previous studies) used as different TiO_2 sources. Without using any Design of Experiment (DOE) software, there should be 4^4=256 experiments for investigation of four different parameters in four levels. Nevertheless the required number of experiment sharply decreases to 16 by applying Taguchi method. Properties of TNT's characterized by SEM, XRD and BET surface area analysis. Finally optimized conditions determined by Minitab Statistical Software.

Key words: TiO_2, solar cell, photovoltaics, TiO_2 nanotube, Taguchi method

ÖZET

FOTOVOLTAİK SİSTEMLER İÇİN NANOMALZEME ÜRETİMİ

Selen Ezgi ÇELİK

Kimya Mühendisliği Anabilim Dalı

Yüksek Lisans Tezi

Tez Danışmanı: Prof. Dr. Hanifi SARAÇ

Enerji talebindeki artış ve fosil yakıtların tükenmesi araştırmacıları alternatif enerji çözümleri bulmaya yönlendirmiştir. Sınırsız enerji potansiyeli nedeniyle, güneş bu konuda en çok umut vadeden seçeneklerden biridir.

Üçüncü nesil güneş panelleri sınıfının bir parçası olan, boyayla duyarlaştırılmış güneş panelleri, düşük maliyetleri ve istenilen şekilde üretilmeye elverişli olmaları sebebiyle, Grätzel tarafından icat edildiğinden beri geniş çapta süren araştırmalara konu olmaktadır. Hücrenin yapısına bakıldığında, genellikle nano boyutlarda üretilen, yoğunlaşmış bir TiO_2 film üzerine organik boya uygulandığı görülür. Bu sistemde, boya ışığı emer ve uyarılmış elektronu iletkenlik bandına taşır.

Elektronların rastgele hareketlerinin azaltılması için, nano parçacık temelli filmlere alternatif olarak, nano çubuk ve nano tüpler gibi tek boyutlu yapılar sentezlenmiştir. Kolay üretim yöntemlerine sahip olmaları ve düzgün geometrik dizilimleri sebebiyle TiO_2 nanotüp (TNT) filmlerinin bu konuda kullanımları son yıllarda oldukça hız kazanmıştır. Güneş hücrelerinden makul dönüştürme değerleri alabilmek için, çoğu araştırma TNT'lerin alan-hacim oranı, uzunluk-çap oranı, homojen gözeneklilik, kristal yapı, iletkenlik veya reaktiflik değerleri gibi özelliklerinin geliştirilmesi üzerine yoğunlaşmıştır. Yeni keşfedilmiş bir alan olması nedeniyle, TNT'ler için en uygun koşulların bulunması için bilim insanlarının çok sayıda deneye ihtiyacı var.

Bu çalışmada, hidrotermal sentez yöntemi ile TiO_2 hammedde tipi, zaman, sıcaklık ve NaOH konsantrasyonu ile TNT'lerin fiziksel ve kimyasal özellikleri arasındaki ilişki

araştırılmıştır. Farklı hammadde tipleri olarak, Degussa P25, rutil, anataz ve daha önceki çalışmalarda sentezlenmiş olan ultrasona maruz bırakılmış anataz TiO_2 örnekleri kullanılmıştır.

Hiç bir deneysel tasarım yöntemi kullanılmadığı takdirde, dört değişkenin dört seviyede incelenmesi için 4^4=256 adet örnek sentezlenmesi gerekmektedir. Ancak Taguchi yöntemi kullanılması halinde, bu sayı keskin bir şekilde 16'ya düşmektedir.

Sentezlenen örnekler, SEM, XRD ve BET yüzey analizleri ile incelenmiş, optimazasyon çalışmaları Minitab İstatistik Yazılımı ile gerçekleştirilmiştir.

Anahtar Kelimeler: TiO_2, güneş hücresi, fotovoltaik, TiO_2 nanotüp, Taguchi yöntemi

CHAPTER 1

INTRODUCTION

1.1 Literature Review

Effects of industrial revolution and increasing population resulted a great global energy demand for the last 150 years. According to statics, by 2015 world total energy consumption has been increased to 300 times comparing to 1900 and it is expected to be 1500 times greater by the year 2300. [1] On the other hand, traditional energy sources have been running out sharply and existing alternatives cause great environmental problems. Therefore renewable energy sources such as wind, oxygen, fresh water, solar, timber, and biomass have great attention from scientist because they are reusable, green, replaced naturally and much more economic in long term comparing to traditional resources.

According to US - Department of Energy reports, the maximum possible power we could capture from the sun is 120.000 TW, while our global energy usage is around 15 TW annualy. This means solar power could provide almost 10.000 times as much energy as the world needs. The closest alternative to sun is biomass with 100 TW, while other renewable sources such as geothermal (12 TW), wind (4 TW), hydroelectric (3 TW) are not even close to it. [2]

Solar energy technologies are divided into two main groups so far: Thermal energy conversion systems and electricity production. Thermal energy systems can be categorized into different subtitles such as water heating, cooling, process heat, water treatment, etc. These practices are very useful for different purposes such as domestic hot water supply, space heating, space cooling and process heat generation.

Electricity production has also two main subtitles: Concentrated solar power (CSP) systems and photovoltaics. CSP systems, focuses sunlight into a small beam by using lenses or mirrors. This concentrated heat then used in a conventional power plant. CSP uses the sunlight indirectly, while photovoltaics use directly.

Photovoltaic systems have three different generations that differentiate by their raw material. First generation solar cells are made of silicon and have the highest conversion value so far. They are the most common installed solar power types in the world but they have disadvantages such as being expensive and having complicated production processes. Second generation photovoltaics are thin-film solar cells. They have lower production costs comparing to silicon based solar cells, and they have less material requirement. The third generation solar cells are dye synthesized solar cells (DSSC). They have the least expensive production process and they are very suitable for optimization due to their many alternatively raw material options.

DSSC's are made from a TiO_2 based film covered by a dye layer. They have electrolyte solution up and down and sandwiched between two conductive glass layers. The TiO_2 films used in this systems mostly consist of nanomaterials because of their high surface area and advantages in electron transportation.

TiO_2 nanotubes are one of the most researched nano TiO_2 materials so far. But still many investigations should be made to develop their unique properties to achieve reasonable conversation ratios in DSSC's.

1.2. Objective of Thesis

TNT's are very suitable options for DSSC's because of their advantages such as strong light-scattering effects, high surface-to-volume ratio, being vertically oriented and high dye-loading capacity. But, use of TNT's in DSSC's is a relatively new idea and there are only few researches that consider many parameters at the same time. Furthermore it is known that production of any kind of nanomaterial is a delicate process and it is hard to control each parameter at the same time.

In this study, it is aimed to observe the difference in products synthesised by hydrothermal method, by experimenting four different critical parameters with four levels. After

determining the optimum conditions for each analyse result, the best production arrangement for the highest DSSC yield will be recommended. In further studies, it is aimed to produce real DSSC cells with the samples of this study and find out the overall conversion ratio for each sample.

1.3. Hypothesis

In this study, first the most important hydrothermal method parameters have been determined. These are, TiO_2 raw material type, time, temperature and NaOH concentration. In order to investigate the effect of these parameters on TNT properties, a Teflon reactor has been designed and produced and it has been used for each experiment during the thesis.

The important properties such as morphologic pattern, BET surface area, crystal structure, pore size and pore volume have been analysed with SEM, XRD and BET analysis's. As a difference with other TNT studies, for each result, cumulative results that covers each parameter have been suggested.

CHAPTER 2

GENERAL INFORMATION

2.1. Titanium Dioxide Nanotubes (TNT)

2.1.1 Structure, Physical and Chemical Properties of TiO_2

Titanium dioxide (TiO_2) (INS no. 171; CAS no. 13463-67-7) is one of the most consumed products around the world with higher than 10 billion $ market capacity. Currently only pigment industry consumes 5 million tonnes of bulk TiO_2 and it is expected to reach 6.8 million tonnes by 2016. [3] Plastic, fiber and ink sectors are following pigment industry by means of global sales. Only about 5% of the world's annual production of titanium minerals goes to make titanium metal. The other 95% of such production is used primarily to make white TiO_2 pigment.

Because of being very compatible, white, clean, non-toxic, chemically stabile, low cost, corrosion-resistant, photo catalytically active, having high refractive index and light-scattering ability TiO_2 is the predominant material for different products such as paint, sun-blockers, solar cell, cosmetics, vitamins, toothpaste, food colorants, nutritional supplements etc. [4] [5]

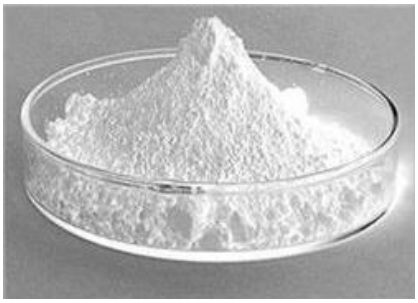

Figure 2.1 Physical appearance of TiO_2

TiO_2 molecule has a conventional transition metal oxide structure. It has three most popular crystal forms: Rutile (tetragonal), anatase (tetragonal), and brookite (orthorhombic). There also some other less known formations such as TiO_2 (B), TiO_2 (II) with a PbO_2 structure and TiO_2 (H) with a hollandite structure, baddeleyite-type high-pressure phase of TiO_2, [6] Last two structures are high-pressure forms of rutile phase. Figure 2.2 shows 3D models of unit cells and Figure 2.3 shows XRD analysis of these formations for anatase, rutil and brookite phases.

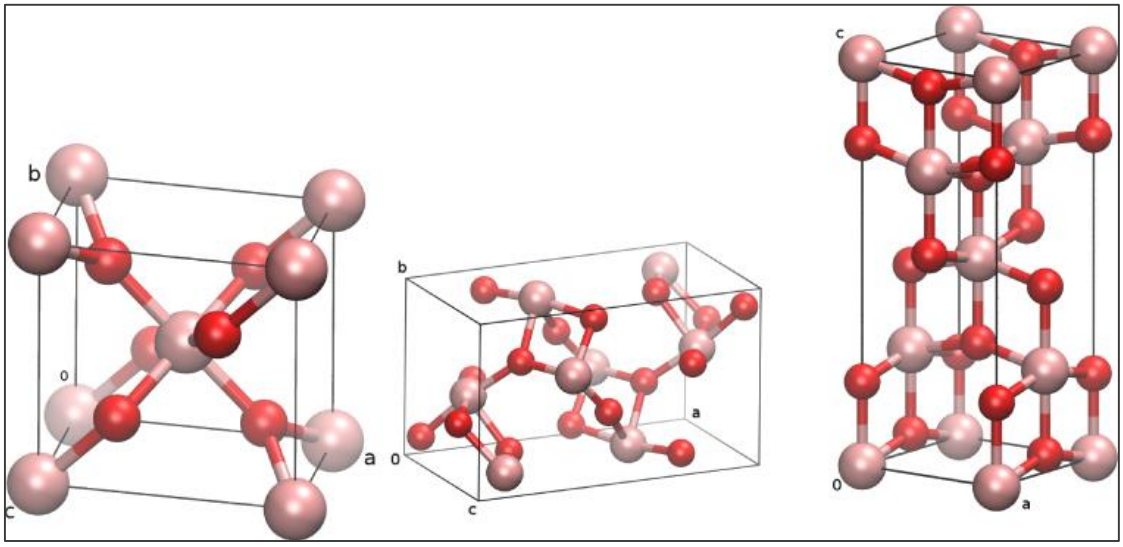

Figure 2.2 Unit cell structures of rutile, brookite and anatase (from left to right). (Red and pink balls represents oxygen and titanium atoms, respectively.)

As can be seen from the Figure 2.2, in rutil and anatase structures, each O atom is coordinated to three Ti atoms while each Ti atom is coordinated to six O atoms. They both have tetragonal structure but have six and twelve atoms per unit cell, respectively.

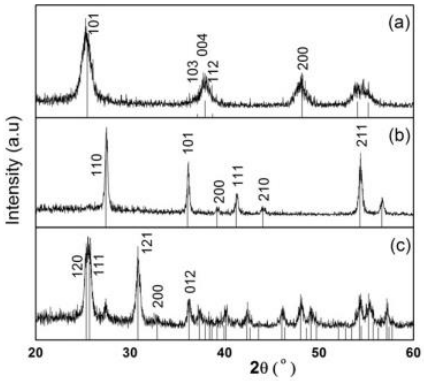

Figure 2.3 XRD analysis of different TiO_2 crystal structures. (a) anatase (b) rutile and (c) brookite

Rutile is the most common natural form of TiO_2. Its lowest molecular volume among other phases makes it the primary titanium carrying phase in most metamorphic rocks which are under high-pressure.[7] It is also the most stable form of titanium dioxide but up to 14 nm particle size. After this limit, with decreasing particle size, the total free energy of rutile (contributed by bulk and surface) becomes higher than that of anatase, the relative phase stability of anatase and rutile reverses, and anatase becomes the stable phase.[8] [9] Yet it is also found that stability of rutile nanoparticles increases relative to anatase and brookite at low pH due to surface charges. [10]

By means of crystal structure, rutile phase has a slightly distorted TiO_6 formation. Two Ti-O bonds are greater than the other four and with some of the O-Ti-O bond angles deviating from 90^o. [11] Both anatase and rutile crystals has been explained as chains of TiO_6 octahedra that has common edges. Each Ti atom is coordinated to the six neighbouring oxygens via two (long) apical and four (short) equatorial bonds, of lengths 1.976 and 1.946 Å, respectively, at 15 K. [12] In rutile phase, there are two edges in common, while anatase has four.

Anatase phase of TiO_2 is most commonly known with its high photocatalytic activity. Mainly, the surface properties of anatase eventuate in that difference between rutile and anatase phases. With increasing crystal defect, catalytic activity also increases. Furthermore, (101) anatase crystal surface is even more active than (001) anatase phase due to same parameter. [13] [14] Figure 2.4 shows FE-SEM images of different surfaces of anatase form. [15]

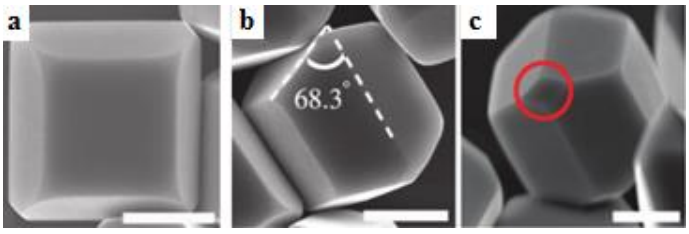

Figure 2.4 (a) FE-SEM image of the anatase single crystals (b) Interfacial angle between {001} and {101} faces (68.3 ± 0.3° on average). The white dashed line indicate the (001) and (101) crystal planes of anatase TiO_2, respectively (c) Small rhombus {110} facets (indicated by red circle) of the anatase single crystals [11]

Morphologically, anatase also has tetragonal structure like rutile but distortion of the TiO_6 octahedron is slightly larger with apical and equatorial bonds of 1.979 and 1.932 Å, respectively.[12]. It is 9% less dense than rutile in metastable form and contains four TiO_2 units.[17] The coordination of Ti and O atoms is the same as in rutile. Ti-Ti inter-ionic

distances are larger in anatase (3.79 and 3.04 A) than in the rutile (3.57 and 2.96 A), whereas Ti-O distances are shorter in the former (1.91 and 1.95 A) than in the latter (1.94 and 1.99 A). [18]

Ti-O interatomic distances, O-Ti-O bond angles and overall crystal parameters are shown in Table 2.1. [11]

Table 2.2 Crystal Structure Data of TiO_2

Crystal Structure	**Rutile**	**Anatase**	**Brookite**
Lattice Constants (Å)	Tetragonal	Tetragonal	Orthotrhombic
	a =4.5936	*a*=3.784	*a*=9.184
	c=2.9587	*c*=9.515	*b*=5.447
			c=5.145
Space Group	$P4_2/mnm$	$I4_I/amd$	*Pbca*
Molecule/Cell	2	4	8
Volume/Molecule ($Å^3$)	31.2160	34.061	32.172
Density (g/cm^3)	4.13	3.79	3.99
Ti—O Bond Length (Å)	1.949(4)	1.937(4)	1.87~2.04
O—Ti—O Bond Angle	1.980(2)	1.965(2)	
	81.2^o	77.7^o	77.0^o~105^o
	90.0^o	92.6^o	

2.1.2 TiO_2 Nanoparticles

Nanotechnology is a brand new developing science area of bringing new properties to present materials by modification them at very small scales such as atomic, molecular and macromolecular or fine-tuning of new kind of nanomaterials. Nanomaterials as defined in a 2011 European Commission Recommendation are materials which natural, incidental or manufactured material containing particles, in an unbound state or as an aggregate or as an agglomerate and where, for 50 % or more of the particles in the number size distribution, one or more external dimensions is in the size range 1 nm-100 nm. [19]

Although carbon nanotubes (CNT) are the most researched structures due to their wide application especially in electronics, other inorganic nanotubes (especially metal sulphides and oxides) are also preferred because of their specific properties in areas such as biomedical, photochemical, electrical and environmental.

Among all the other transition metal oxides, TiO_2 has become the most common interested compound, with more than 40.000 publications in last ten years. As a specific point of interest, nano-sized TiO_2 particles started to take much attention from researchers in meanwhile. Figure 2.5 shows the number of published articles between 2003 and 2013[20]. It can be seen that there is a certain increase in number of researches in that area.

The size dependency of most of the properties of TiO_2 is the most important reasons of that fact. All of the optical, electrical, chemical, catalytic and physical properties of TiO_2 change with respect to molecular size.

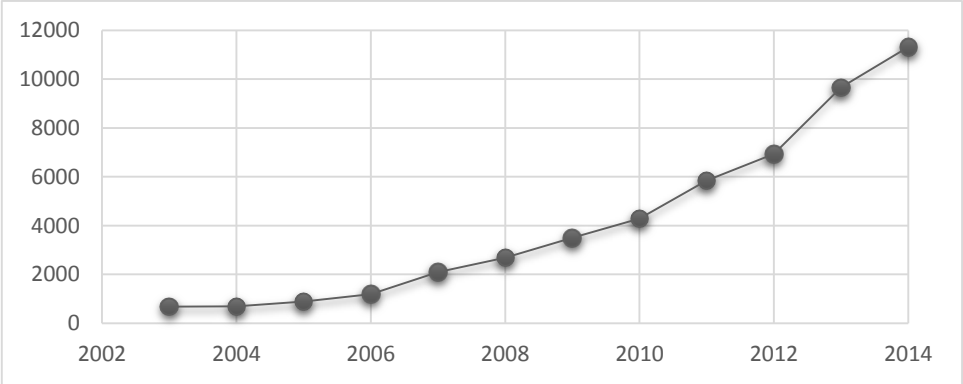

Figure 2.5 Number of articles in scientific database with using keywords "Nano" and "Titanium Dioxide / TiO_2"

One of the important research areas of TiO_2 is photocatalysts. It is now clear that photocatalytic effect of TiO_2 is greater in nanoparticle form than in bulk powder. [21] It is also known that anatase form of TiO_2 is much more effective as photocatalyzer than rutile as in bulk phase. Another fact is that smaller molecular size leads higher yields. This result is due to getting higher surface areas by using smaller diameters. [22–25]

Optical properties of nano titania is also a popular research topic. The reflectance of visible light decreases and material also becomes more transparent with reducing crystallite size (to <100 nm). That feature provides nano TiO_2 a wide market in paint,

plastics, paper and pharmaceuticals. It is also distinct that nanocrystalline TiO_2 has a markable absorption of ultraviolet (UV) radiation. These two important optical properties; UV absorption and the concurrent high transparency for visible light, make TiO_2 particles with a size of <100 nm find widespread use in such diverse areas as sun cosmetics, packaging materials, or wood protection coatings. [26]

The electron structure of TiO_2 has been studied by various of techniques such as ultraviolet photoemission spectroscopy (USP), X-ray emission spectroscopy, X-ray photoemission spectroscopy (XPS), electron-energy-loss spectroscopy (EELS), Auger-electron spectroscopy (AES) and some methods such as pseudopotential density-functional theory.[11, 27–30]. In theory, the energy difference between the HOMO (highest occupied molecular orbitals) in the valence band and the LUMO (lowest unoccupied molecular orbitals) in the conduction band gives the band gap value as seen on Figure 2.6. It can be useful to get a rough approaching on the electronic structure of molecule, but in order to get the exact value for optical band gap, the optical matrix elements in the valance and conduction bands that takes role in transition process should be taken into account as well. [31] With smaller diameters, the band gap energy increases and the energy band narrows in nanoparticles. For TiO_2 nanosheets, it is found that the band gap is increasing with decreasing dimensions. It is also mentioned that the lower edge of the conduction band for the same TiO_2 nanosheets was approximately 0.1 V higher and the upper edge of the valence was 0.5 V lower that of bulk anatase. [32]

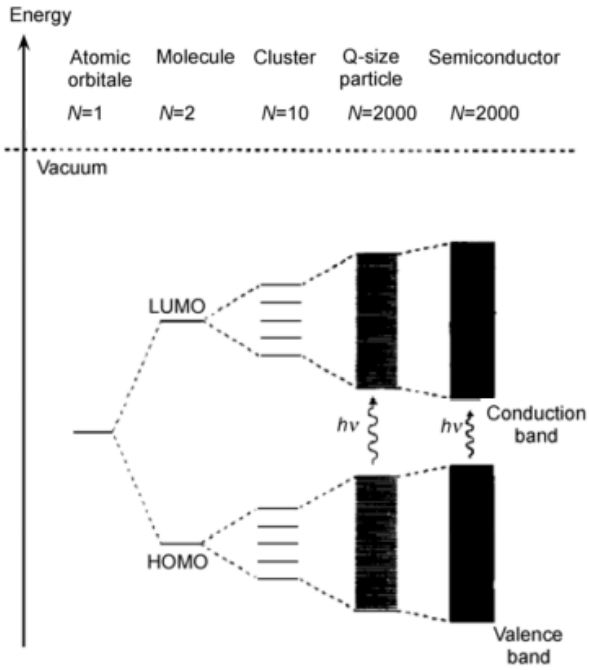

Figure 2.6 Molecular orbital model for particle growth of N monomeric units. The spacing of the energy levels (i.e. density of states) varies among systems

In a thermodynamically approach, some enthalpy analysis are carried out for three phases of TiO_2 nanoparticles. Figure 2.7 shows the comparison of enthalpy values versus surface area with respect to crystal morphologies. From the graphic it can be seen that anatase nanoparticles are more stable with increasing surface area. Rate and direction of the transition of the phases to each other are mainly depend on the temperature. [33]

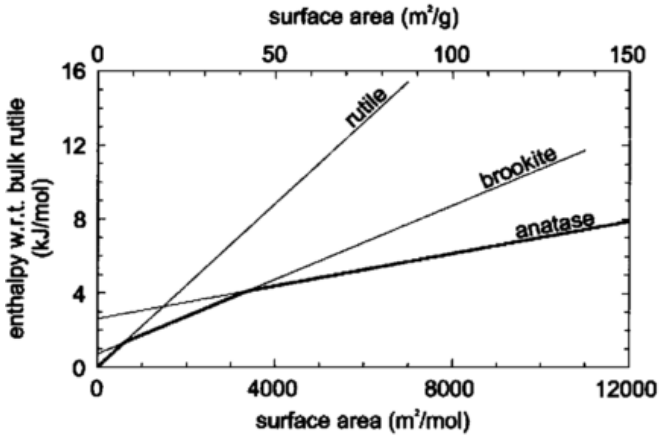

Figure 2.7 Enthalpy of nanorcrystalline TiO_2 [34]

2.1.3 Chemical Structure of TNT

Like all other TiO_2 nanoparticles, TNT's are started to get much interest from researches in last ten years. Figure 2.8 shows both the upward trend in publications in only TNT and TNT's with keyword *solar cell*. One of the results is that the works in nanotube area is expanding exponentially among the years. Nearly half of the nanotube researches are based on solar cells and it is also increasing rapidly. It is obvious that not only the energy demand of the earth forces scientists to find a sustainable and eco-friendly options, but only the promising features of TiO_2 nanoparticles, especially the nanotubes. They also provide higher control on chemical and physical behaviour because of controllable producing parameters. Declining dimensions also contribute great change in electronic properties due to the factors such as quantum size effects, strong contribution of surface reconstruction or surface curvature. These impacts can also promote the reaction/interaction between a device and the surrounding media, thereby making the system more effective by means of kinetics, or even allow for entirely novel reaction pathways. [4]

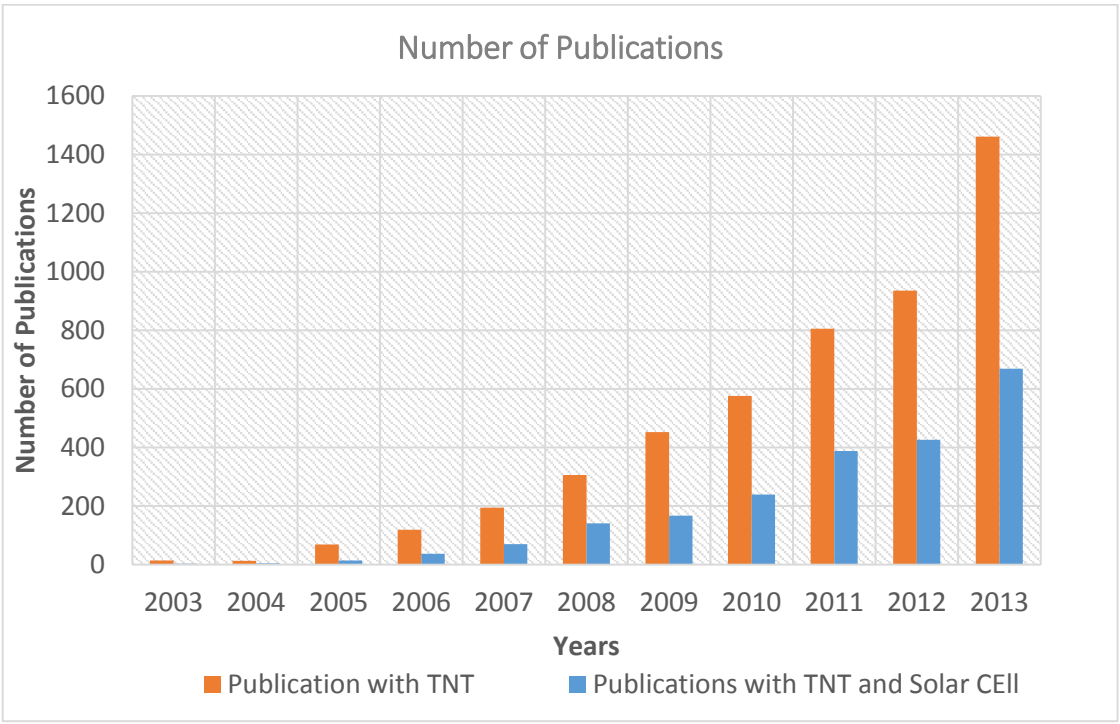

Figure 2.8 Number of publications with keywords "solar cell" and "TNT"

TNT's are more favoured for various of applications mostly on account of their high surface area-to-volume ratio (SA:V). They can be considered as rolled thin layers of TiO_2 into different tube frameworks. According to experimental data, they can be produced by different methods and can display divergent morphologies. Firmly, TNT's can be considered as single or multi-walled cylindrical, scroll-like or polycrystalline conglomerates of NCs also displaying side wall ripples or smooth walls. [35] . Multiwall TNT's are mostly consist of 2 to 5 layers with average layer distance of 0.78 nm. [36] Control of fabrication parameters has enabled variation of pore size from 5 to 350 nm, outer diameters from 8 to 256 nm, wall thicknesses from 3 nm to, while still a discernible wall 34 nm, large specific surface area (up to 478 m^2/g) and pore volume (up to 1.25 cm^3/g) and tube-to-tube spacing from adjacent to microns. [37, 38]. Length of the tube can be reach up to micrometers.

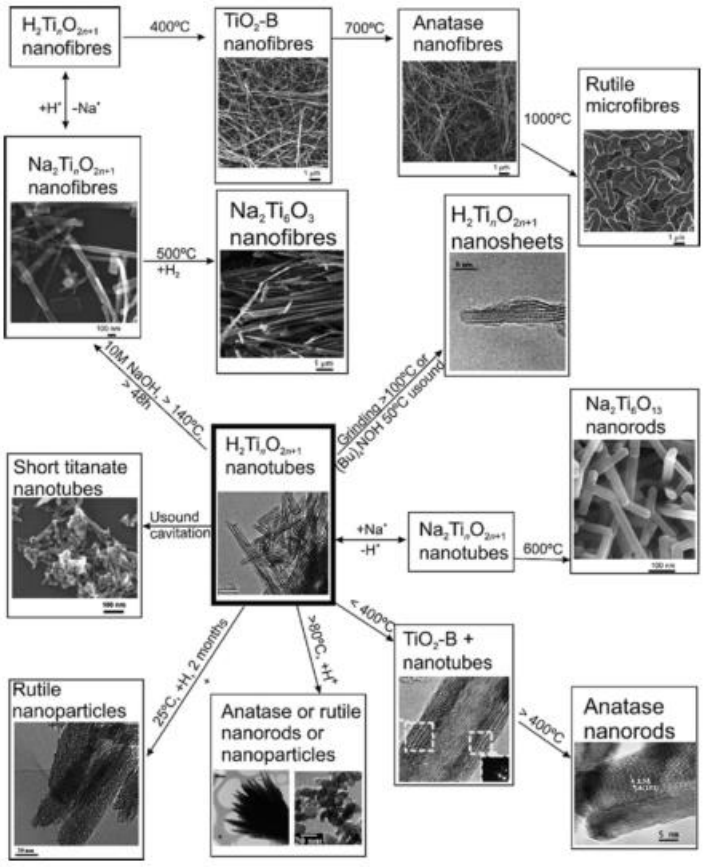

Figure 2.9 Chemical and structural transformations of titanate nanotubes and nanofibers [39]

2.1.4 Fabrication Methods of TNT

There have been three major methods in order to produce TNT's: Templating, anodic oxidation and hydrothermal synthesis. Formation steps of TNT's vary depending on the way of production. A rough comparison between these methods can be seen in Table 2.2. [36] Detailed study will be held in next chapters.

Table 2.2 Comparison of typical synthesis of TNTs

Synthesis method	Advantages	Disadvantages	Internal diameter/ length (nm/μm)
Template method	Controlled scale of nanotubes via different templates practical application	An increase in the cost of materials and long-term instability	2.5-6000/0.05-200
	More desirable for practical application	Complicated fabrication process	
		Tube morphology may be destroyed during fabrication process	
Anodic oxidation	More desirable for practical applications	Mass production is limited	20-110/0.1-2.4
	Ordered alignment with length-to-diameter radio	The utilization of highly toxic solvent such as HF	
	Feasible for extensive applications		
Hydrothermal synthesis	Simple route to obtain nanotube morphology for large scale production	Highly expense of fabrication apparatus and difficult separation of TiO_2 array film substrates	3-10/50-500
	A number of modifications can be used to enhance the attributes of titanium nanotubes	Long reaction duration is needed Highly concentrated NaOH must be added	
	High cation-exchange capacity and length-to-diameter ratio	Difficult in achieving uniform size Thermal unstable	

Production techniques can be divided two broad categories as, self-directed and template-assisted. Self-assembly method consist of both anodization and hydrothermal routes and provides a more direct means to the arrays. On the other hand template-assisted method brings opportunity to have more consistent control over dimensions of TNT such as intertube spacing, wall thickness and length. [40] Figure 2.10 shows the timeline of techniques for fabrication of TNT's.

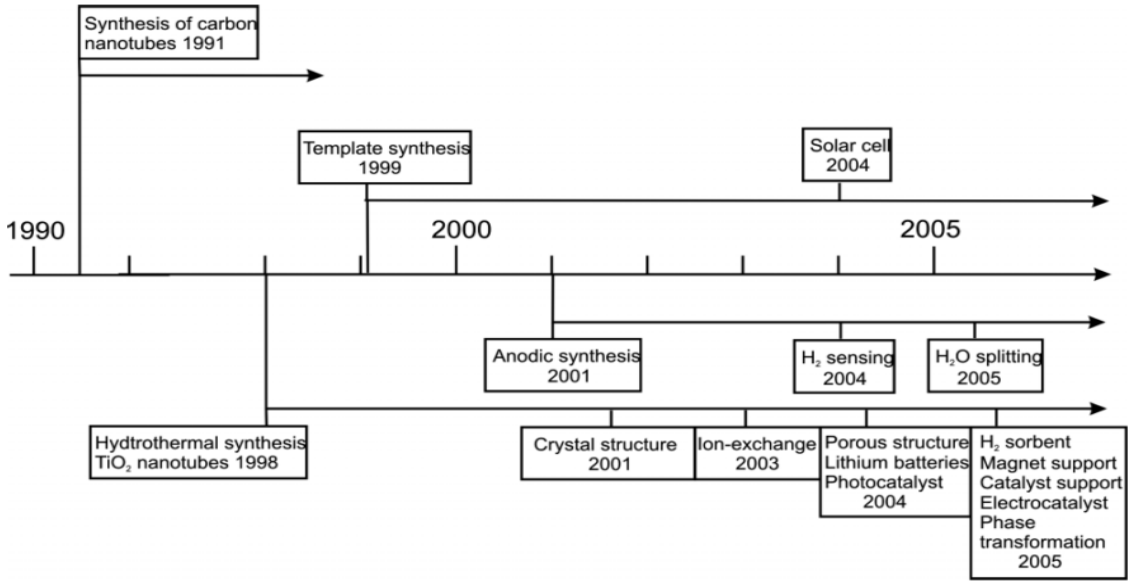

Figure 2.10 Simplified timeline describing the development of TiO_2-related nanotubular structures [41]

Template Assisted Method

Template-assisted method uses the structure properties of well-known materials (templates) in order to build new materials with similar morphology by using different methods including re-active deposition, dissolution, atomic layer deposition etc. By reason of bearing a well-ordered structure, it has been widely used to produce free-standing, nearly perfectly ordered or non-oriented nanowires, nanorods or nanotubes. These oriented structures are in additionally stated as *arrays*. [42]

From chemical point of view, the preparation of TNT's by chemical templating method generally involves controlled sol-gel hydrolysis of titanium ion contained solutions in the presence of templates. Figure 2.11 shows a rough diagram for synthesis steps.

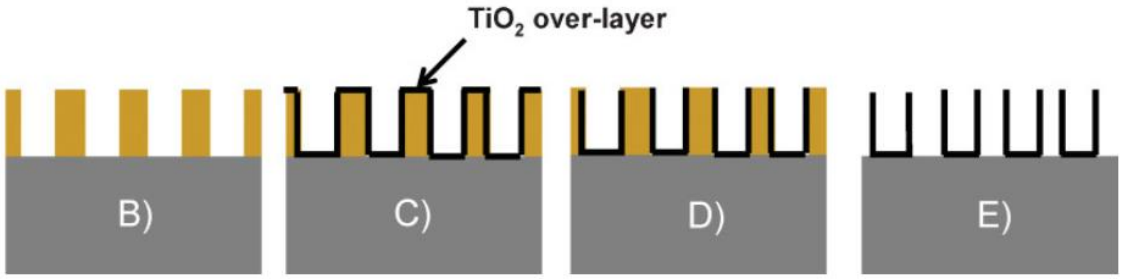

Figure 2.11 Schematics of A) the sequential and repeated chemisorption/hydrolysis reactions in a typical LALD cycle and B-E) the formation of TiO_2 nanotubes by depositing in AAO templates prepared on substrates TIP presents titanium (IV) isopropoxide

Features of nanotubes are directly connected to the properties of used template. Qualifications such as pore or channel size, size distribution and density of pores, morphology, and type of the material must be ensured by the template material. Furthermore some extra requirements are also desired to secure certain characteristic. Initially, template material should be compatible with reaction medium, like being insulated for a system that using electrochemical deposition. It also should be chemically and thermally inert during synthesis and following processing steps, if not template-directed synthesis is being used. Depositing solution must wet the pore walls and synthesis way should start from pore surface and proceed inwardly. At the end of the process, the template should be suitable for easy split-up. [42]

The most commonly used and commercially available templates are anodized alumina membrane (AAM)[43] and radiation track-etched polycarbonate (PC) membranes [44]. Other membranes have also been used, such as nanochannel array on glass [45], radiation track-etched mica, mesoporous materials, porous silicon by electrochemical etching of silicon wafer, zeolites and carbon nanotubes. Bio-templates are also explored for the growth of nanowires and nanotubes, like Cu, Ni, Co, and Au nanowires. [42] There are also a group of self-assembled organic surfactant template molecules that have been used for the same propose. Among the organic templates used for TiO_2 nanotube synthesis are the organogel of trans- (1R,2R)-1,2-cyclohexanedi(11-aminocarbonylundecylpyridinium)[46] and dibenzo-30-crown-10-appended cholesterol[47] the hydrogel of tripodal cholamide-based materials and lauryla- mine

hydrochloride surfactant. Other examples of specialized templating agents include tobacco mosaic viruses or precipitated platinum salts. [41]

Anodic aluminium oxide (AAO) are the most commonly used for template- synthesis of TNT's. Like other nanoporous oxide layers, AAO is also produced by anodization of aluminium sheets. The route consist electrochemical oxidation of metal substrate (such as aluminium) under constant potential. Anodization process can be divided into two main routes as mild and hard. Combination of these methods are known as "two-step anodization" and widely used to get desired structures. Table 2.3 shows the morphologic and chemical comparison of the processes. [48] Usually mild anodization results with narrower pore sizes comparing to hard anodization as shown in table.

Table 2.3 Comparison of mild and hard anodization methods

	Mild Anodization	**Hard Anodization**
Proportionality constant between the anodization voltage (V) and the interpore distance (d_{int})	2.5 – 2.8 nm V^{-1}	2 nm V^{-1c}
Porosity (P)	%10	%3.3-3.4
Impurities in chemical composition of alumina	High	Low
Color	Transparent	Bright yellow
Appearance [49]	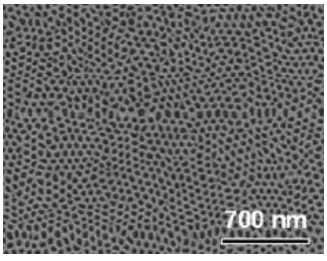	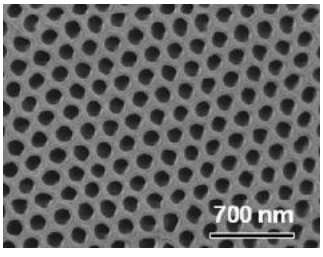

Fabrication process of AAO usually deals with a pure aluminium film as anode and a counter inert cathode material such as platinum. Acids are used electrolyte solution and

constant or pulsed voltage is applied to system depend on the morphology that is desired. The type of the acid solution and electrochemical potential are the most the most important parameters on morphology of AAO, particularly on its cell size (interpore distance) and pore diameter in porous layer. Some of the well-known acid solutions are shown in Figure 2.12. [50]

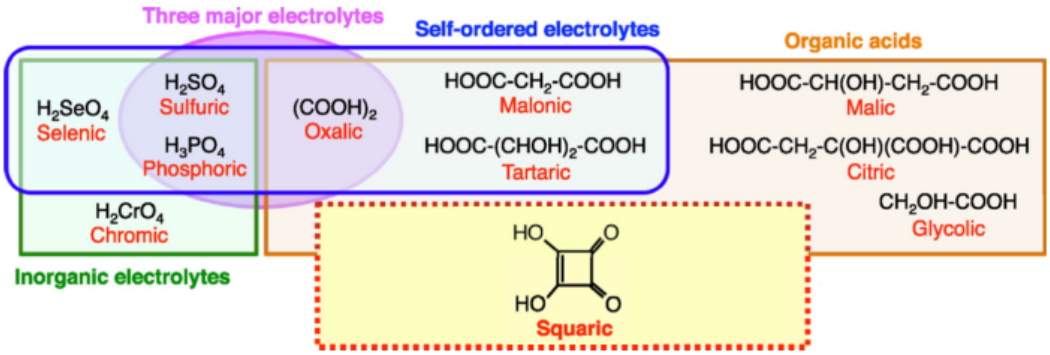

Figure 2.12 Acid solutions used in anodization method

The pores of AAO templates generally ordered in a hexagonal array. The pore density can be achieve up to 1011 pores/cm^2. Inner size of the pores ranges from 10 nm to 100 μm. Physical stability and chemical inertness enable AAO to be preferred for fabrication of nanoarrays. Furthermore, nearly perfect cylindrical and well-ordered pores with uniform diameter also provide a convenient way of producing highly dense and ordered nanoscale structures. Dimensions of desired nanotube or nanorod can be tuned by varying the fabrication conditions of template. This provides more flexibility in controlling shape of last product comparing the other fabrication methods of TNT. Another advantage of using AAO is its rigidity and resistance to high temperatures. By this, nanorods or nanotubes can be densify complete before the template starts deforming.

Some advanced geometries can be obtained by using different solutions or varied voltage pulses. Figure 2.13 shows a hybrid template that produced by combination of mild and hard anodization methods. [48]

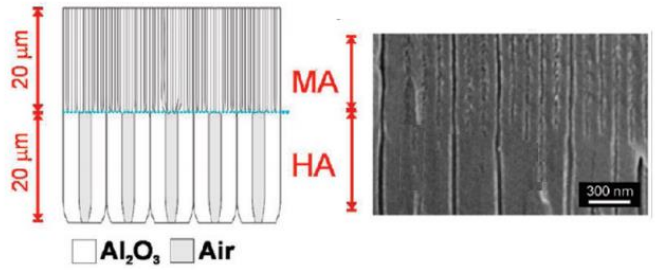

Figure 2.13 Schematic cross-section side view describing the general structure of TNT's (c) SEM image of the bottom side view (HA side) of the different types of TNT's

Some other techniques such as lithography or thermal evororator deposition can be also used to get specific shapes of templates. Figure 2.14 shows a combination of different shapes of AAO's. The aim of the research is to analyse the effect of shape of TNT's on DSSC yield. [51]

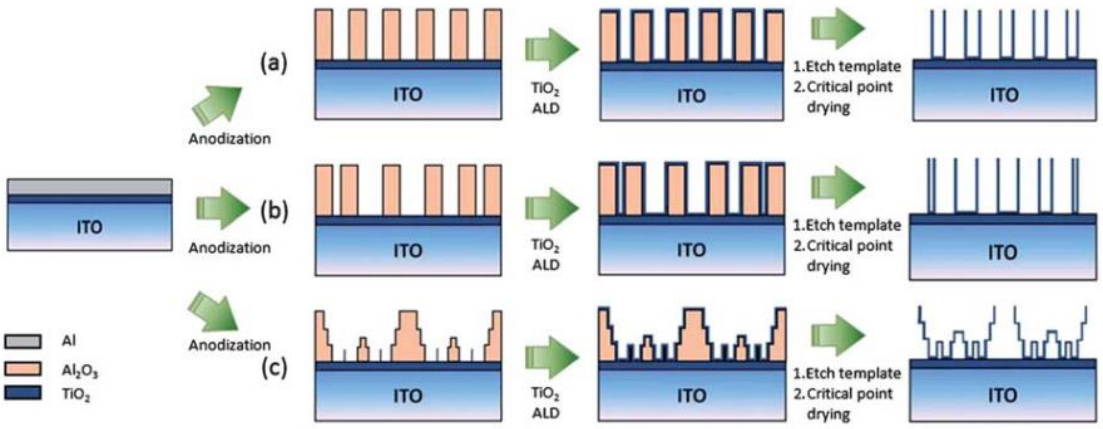

Figure 2.14 a) Near-perfect ordered PAA template by step and flash imprint lithography (SFIL)-based method. method.b) Dimension and morphology controlled PAA template by controlled anodization yielding 1D single branched and c) 3D multi-tiered branched template

In like matter, AAO's on some other substrates such as Si wafer are also synthesized successfully. These improvements are especially important for increasing the yield of solar cells. Figure 2.15 shows the fabrication steps of such material composed of Si substrate and alumina. [52] First, a pure Al-layer was grown on a Si wafer by thermal evaporator deposition (Figure 2.15.a). Then an anode is connected to the Al layer, while the cathode was a Pt rod for the first anodization being carried out for 80s in 0°C 0.5M H_2SO_4 solution at 25 V to be able to oxidize only part of the AAO film. This process

resulted in the regular pore array of hemispherical bottom structure but with uneven height at the upper part of the AAO film (Figure 2.15.b). The removal of this first AAO film was done in 1h in a mixture of 1.8 wt. % chromic acid and 6 wt . % phosphoric acid (Figure 2.15.c). Then the second anodization was carried out for 800 seconds until the total oxidation of remaining Al-layer at the bottom under same condition as the 1st anodization (Figure 2.15.d). Then 0.1 M H_3PO_4 solution was applied (Figure 2.15.e) for 1 h not only for the pore widening but also for the final removal of the hemispherical structure at the bottom of the pore columnar structure. This yielded a porous AAO film with a flat bottom as seen in Figure 2.15.f

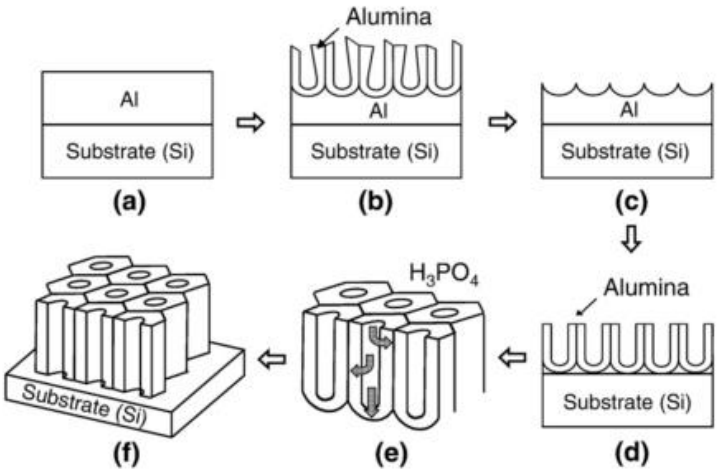

Figure 2.15 Schematic process of flat bottom porous AAO film sample. (a) Al deposition on Si substrate, (b) 1st anodization, (c) 1st alumina removal, (d) 2nd anodization, (e) pore widening, then (f) AAO film without the bottom structure is achieved

After getting the template ready, synthesis step of TNT's can be carried out by following different methods such as sol-gel, atomic layer deposition, electrodeposition. Main steps of each method are showed in Figure 2.16.

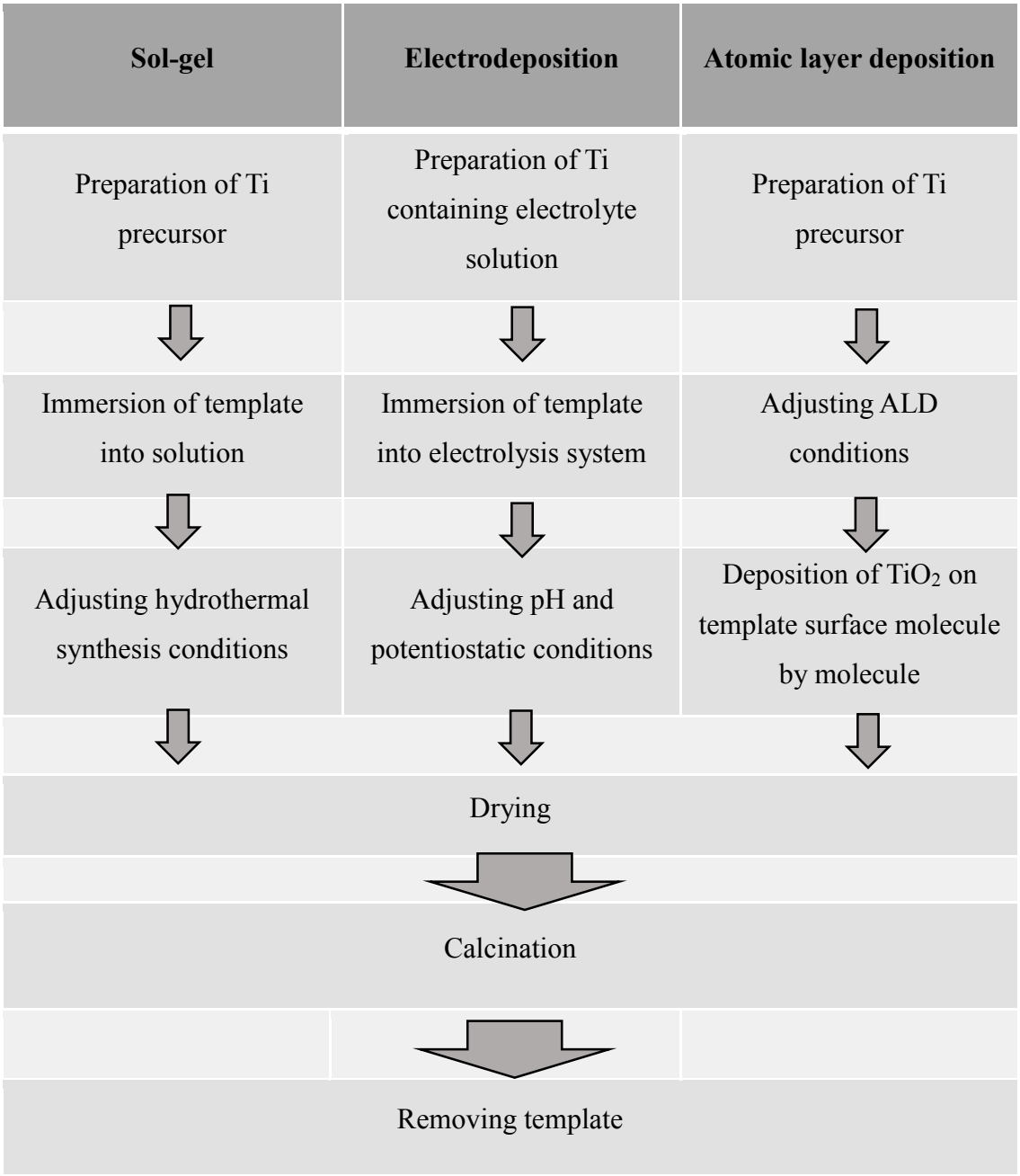

Figure 2.16 Comperative pathway of each production method for TNT

- **Sol-Gel Process**

The sol-gel process is a wet-chemical technique primarily for the fabrication of metal oxides from a chemical precursor solution. Since the deposition is uniform on the entire surface of a substrate in a sol-gel process, desirable complex structure can be obtained by using a proper substrate. For example, nanotubes of a large variability of materials can be deposited into the pores of AAO membranes.

The process simply starts by the preparation of TiO_2 sol solution. For this aim, titanium compounds such as TTIP dissolved in a suitable solvent such as ethanol, acetyl acetone or aqueous solvent mixtures. After getting a desired sol, pre-washed template material dipped into the solution and keep it for a certain time. After the nanotubes are formed, template is dried and calcinated for a relatively long time, usually overnight. After getting the desired crystal structure for nanotubes, template material is removed with a solvent such as diluted phosphoric acid.

As well as the macro properties of template material, it is also important to have proper micro characters for a desired product. Molecular structure, for example, is one of the biggest parameters that effect last product. Table 2.4 shows the internal diameter the TiO_2 nanotubes depends on precursor, template molecule and the reaction conditions for sol-gel combined template assisted method.

Table 2.4 Morhological properties of TNT's produced by the sol-gel method in the presence of templating agents

Precursor	**Template**	**Conditions**	**Nanotube diameter (nm)**
Ti $(OiPr)_4$	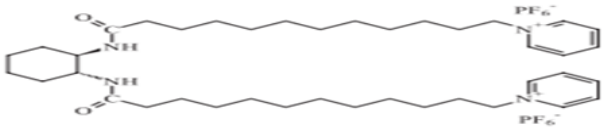	25°C, ethanol, NH_4OH	50-300
Ti $(OiPr)_4$		25°C, 1-butanol, benzylamine	500
Ti $(OBu)_4$	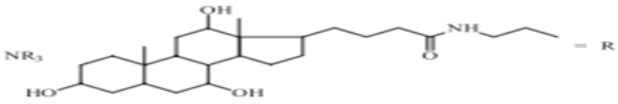	25°C, ethanol, CH_3COOH, H_2O	4-7
Ti $(OBu)_4$	$CH_3(CH_2)_{11}NH_2.HCl$	25−40°C, H_2O	1800-6000
Ti $(OiPr)_4$	Tobacco mosaic viruses	25°C, ethanol	20
Ti $(OBu)_4$	$[Pt(NH_3)_4](HCO_3)_2$	25°C, ethanol	100
Ti $(OiPr)_4$	Porous Alumina	25°C, pressure impregnation	60-70
TiF_4	Porous Alumina	60 °C, HCl	2.5-5
Ti $(OiPr)_4$	Porous Alumina	25°C, ethanol, CH_3COOH	120-140

- **Atomic Layer Deposition**

One of the most common supplementary methods for template-assisted technique is atomic layer deposition (ALD). The route simply relies on pulsing of the precursor which is in gas or vapour phase onto the substrate surface, and followed by chemisorbtion or reaction on substrate surface. Since the control has supplied by the reaction on surface, with a proper adjustment of the experimental conditions, film thickness, wall diameter, length and width of the materials can be precisely controlled in Angstrom or monolayer level. Furthermore, due to operating in a cyclic process and can produce uniform and conformal layers at atomic scale. The control of thickness obtained by the number of cycles. The self-limiting feature of ALD prompts to perfect step coverage and conformal deposition on high aspect ratio structures such as nanotubes. [53–56]

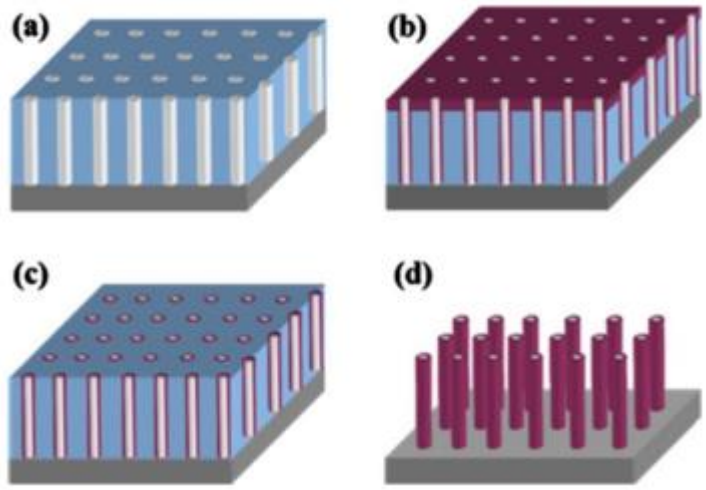

Figure 2.17 Illustration of the production process of TNT arrays: (a) AAO is produced on a Si substrate; (b) TNT arrays are deposited using ALD; (c) the TiO_2 layer is removed from the top surface (d) self-aligned TNT arrays after the removal of AAO

When using with AAO templates, ALD provides a deposition of almost perfect thin films. From perspective of TNT's, regularly arrayed thin-walled structures or unique geometries can be obtained. In additionally, growth on such substrates such as Si can also be achieved by this combined routes. [57] Figure 2.17 shows the production process of TNT's on Si substrate by using AAO-ALD combined technique. First, AAO is produced on Si substrate. Then Ti precursor such as $TiCl_4$ solution, added into reaction system with deionized water. Deposition conditions and number of cycles are being set in order to

reach desired TNT structure. After the synthesis is over, tubes are washed with water, therefore TNT's are get as covered AAO nanopore surfaces as a thin film to form tubes and top surface. In order to get tube formation, polishing step is being applied as shown in Figure 2.17(c). Finally, the specimen is soaked into diluted base solution (mostly NaOH) to remove AAO.

Figure 2.18 shows the corresponding SEM images.

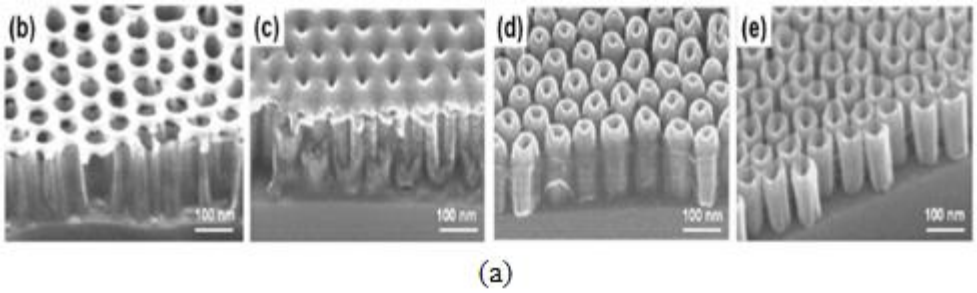

Figure 2.18 (a) Schematic of the process to fabricate highly ordered freestanding TNT arrays. Cross-sectional SEM images of (b) the Nanoporous template with a mean pore diameter of 53 nm and a thickness of 200 nm, (c) after ALD of 20 nm-thich TiO2 thin films on the Nanoporous template (d) followed by CF4 RIE to remove the overlayeres on the top surface of the template, and (e) highly uniform and densely packed freestanding TNT arrays with Wall thickness of 20 nm after calcination to completely remove the organic template

- **Electrodeposition**

This is the least common used techniques among the three of mentioned so far. The process mostly comprises of immersing the template into electrolysis medium which contains a titanium precursor as well as the electrolyte solutions.

Wang et al. successfully produced well ordered TNT's by this method. In experiment part, they carried out electrodeposition at 25^{o}C, using a three-electrode potentiostatic system with a saturated calomel electrode (SCE) as a reference electrode and a platinum plate as a counter electrode. The deposition was executed under potentiostatic conditions with the potential range between 0.8 and 1.0 V. The electrolyte contained 0.1M $TiCl_3$ in 1 L of deionized (DI) water. The pH was maintained at 2.0 by adding a few drops of 2M Na_2CO_3. In all cases, the electrolyte was freshly prepared prior to each deposition. After the deposition, the nanotubes in the AAO template were rinsed with double distilled water, and finally dried in air at room temperature. The samples were then heated at 500^{o}C

for two hours under N_2 atmosphere. To obtain the specimen for SEM and TEM, the samples were dissolved in a 4M NaOH solution at room temperature. Figure 2.19 shows the analysis results.

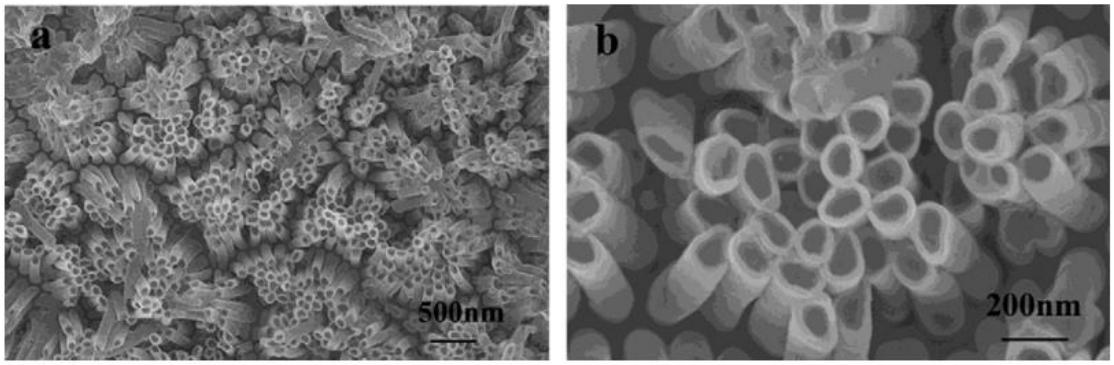

Figure 2.19 SEM images of TNT's

Electrochemical oxidation is a well-known technique that has been used for different kind of aims for long years. Mainly it is used for creating protective or decorative oxide layers of a metallic surface. The procedure consist of conducting item of the anodization connected to the positive terminal of a dc power supply and immerged into electrolytic solution which it has role as anode. Platinum is the most commonly used cathode electrode but there are also other materials such as rod and carbon. The operation starts when power is applied. Electrons are forced from the electrolyte to the positive anode. That results surface metal atoms exposed to oxygen ions within the electrolyte. That touching atoms react and become a part of the oxide layer. There are two options for the leftover electrons. They may travel among the power source and return to the cathode or if the conditions are satisfied they can react with hydrogen ions and the produce hydrogen gas that bubbles.

Anodization of titanium is not a new invention as well. Historically it is utilized mostly for colouring processes, especially for jewellery industry. During this coloring process, the oxide that is formed is generally barrier type film. [58] In 1999 Zwilling et a. firstly reported the self-ordered TiO_2 nanostructures by a simple electrochemical anodizing process in a fluoride electrolyte. [59] Today it is clearly known that, there are briefly five different morphologies can be occur possibly by anodization process as shown in Figure 2.20. Depending on the reaction conditions, metal electropolishing (I), compact anodic

oxides on substrates (II), self-ordered oxides (nanotubes or nanopores) (III), disorganized oxide nanotubes (IV) and ordered nanoporous layers (V) can be produced. [4]In nanotube formation point of view only process III is useful for well ordered structures. The main parameter that causes this situation is solubility of oxide compound in different electrolyte solutions. When oxide compound less likely to dissolve in solutions such as slightly alkaline of neutral electrolytes, oxide barrier layers tend to grow. Otherwise, if oxide forms and then rapidly dissolves, such as acidic electrolytes with fluoride and chloride ions, porous oxide layers tend to grow. [38]

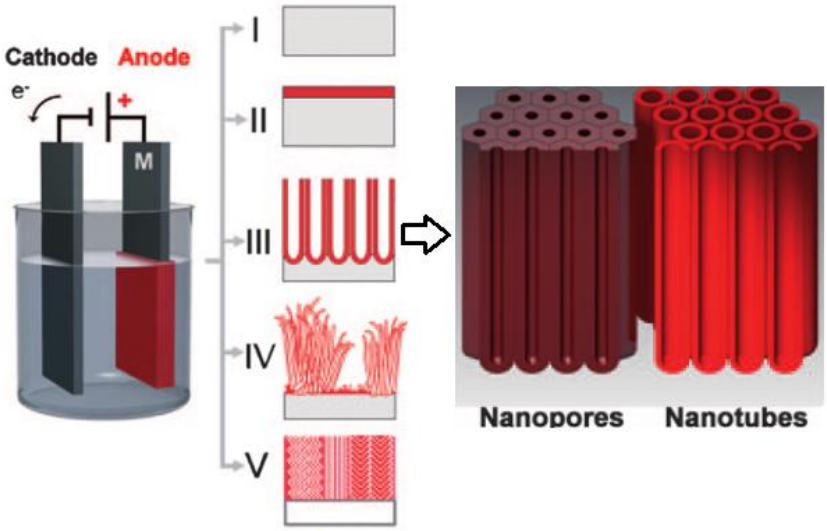

Figure 2.20 Electrochemical anodizing process for TNT production

Figure 2.21 shows evolution process for TNT's under constant anodization voltage. When anodization starts, a thin layer of oxide forms on the titanium surface (a). Dissolution of the oxide causes small cavities in the layer (b). This makes the barrier layer at the bottom of the pits relatively thin which, in turn, increases the electric field intensity across the remaining barrier layer resulting in further pore growth (c). The entrance of the pore does not affected by electric field assisted dissolution and so remains relatively narrow, while the electric field distribution in the curved bottom surface of the pore causes pore widening, as well as deepening of the pore. The result is a pore with a scallop shape [140, 146]. As the Ti–O bond energy is high (323 kJ/mol), in the case of TiO_2 it is reasonable to assume that only pores having thin walls can be formed due to the relatively low ion mobility and relatively high chemical solubility of the oxide in the electrolyte, hence un-anodized metallic portions can initially exist between the pores. As the pores grow deeper

the electric field in these protruded metallic regions increases, enhancing field assisted oxide growth and oxide dissolution, hence simultaneously with the pores well-defined inter-pore voids start forming Figure 2.21. Thereafter, both voids and tubes grow in equilibrium. The nanotube length increases until the electrochemical etch rate equals the chemical dissolution rate of the nanotube top surface. After this point is reached the nanotube length will be independent of the anodization duration, as determined for a given electrolyte concentration and anodization potential. [38]

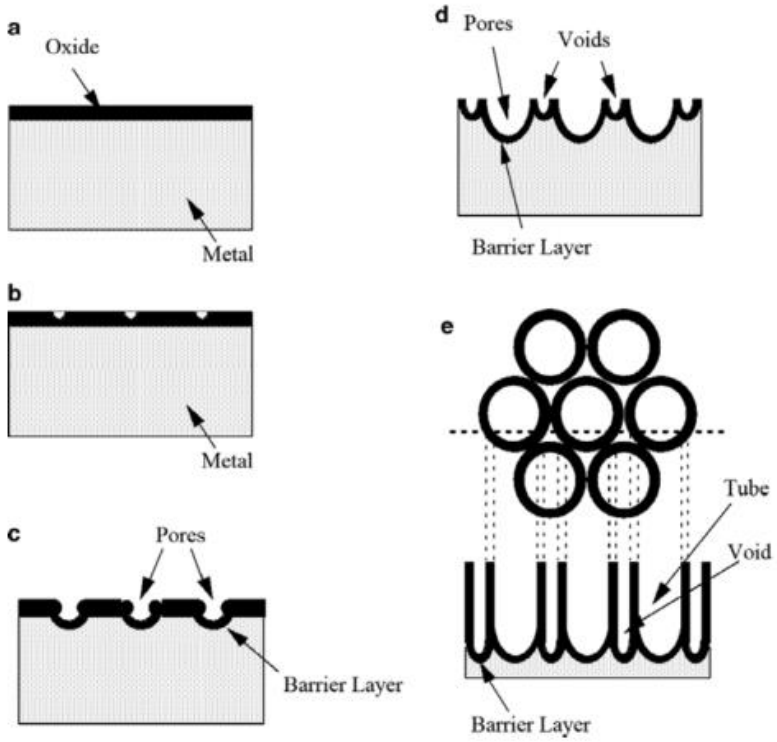

Figure 2.21 Schematic diagram of nanotube evolution at constant anodization voltage; (a) Oxide layer formation, (b) pit formation on the oxide layer, (c) growth of the pit into scallop shaped pores, (d) the metallic region between the pores undergoes oxidation and field assisted dissolution, (e) fully developed nanotubes with a corresponding top view

There are numbers of studies on producing TNT's in this method because it has many advantages such as, giving opportunity to control pore size, achieve good uniformity and being able to scale up into large areas at low cost. By using a pure titanium alloy, metal impurities can be easily introduced also. [60]

Usually commercially available titanium foils are used as anode material. These foils mostly has %99 purity and consist other trace elements such as Al and Mg. [61]

By optimizing conditions, high quality self-organized TNT's, such as short and rough TNT's, tapered andconical-shaped TNTs, smooth and high-aspect-ratio TNT's, transparent TNT's, free-standing and open-ended TNT's, and TNT's with a submicrometer size in diameter can be obtained. [62] In application point of view, highly ordered TNT's produced by this method, exhibited excellent properties such as photocatalytic activies, due to their high-oriented uniform nanotube architecture and the rapid transfer of the photogenerated holes to the surrounding electrolyte and the extended electron lifetimes in the nanotubes. [63]

Although there has been a great diversion in dimensions of TNT's due to the reaction conditions, mainly it can be said that, TNT's that produced by anodization process usually have wall thickness ranges from 5 to 30 nm, the pore size from 20 to 350 nm, the length from 0.2 to 1000 μm's and length/outer diameter ratio from 10 to 20.000.

Some physical and chemical properties of TNT's such as geometry, surface properties, photocatalytic activities etc are strictly depend on the reaction conditions like anodization time, voltage value, potential ramping speed, temperature, cathode material, roughness and purity of the Ti foil used, solvent, water content, electrolyte pH, viscosity, conductivity, some other organic additives and in additionally some parameters related to electrolyte composition such as ionic concentration. Beyond synthesising conditions, calcination time and temperature also effect has a great effect on the last product, especially on crystal structure. [64]

Electrolyte preference is the most important parameter on TNT's by far. To produce a proper solid product, it is essential to use electrolytes that oxide forms faster than it dissolves, because metal oxide partially dissolves almost in any electrolyte. [38] According to various of authors [64] [58], TNT's produced via anodic oxidation can be divided into four categories, so called *generations*, by depending on the electrolyte. Table 2.25 shows the basic characteristics of these classes. [64][38, 58, 62] Figure 2.22 shows the typical SEM images of the generations.

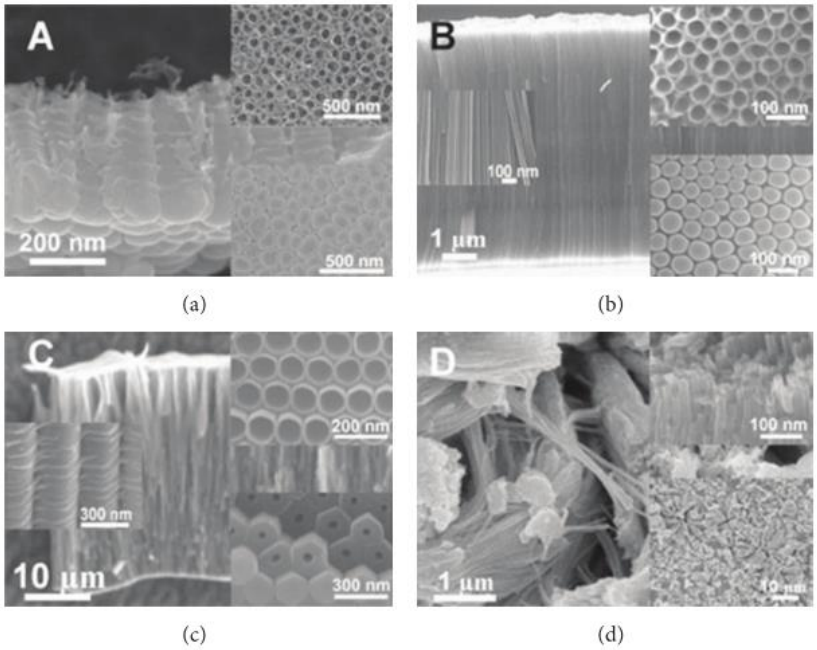

Figure 2.22 Different generations of TNT's

Table 2.5 Generations of TNT's produced by electrochemical method

Generation	Electrolyte	Example Electrolyte Composition	Conditions	Features of TNT's	Morphology	Main Factor
1st	Inorganic aqueous electrolytes (HF-Based electrolyte)	0.5wt%HF	1-25 V – 120 min	Poorly self-organized Ribbed Short	Length: 120-1000 nm Diameter: 10-120 nm Wall thickness: 13-27 nm	Potential, electrolyte
2nd	Buffered electrolytes (F^- - based electrolyte)	1M Na_2SO_4 + 0.1–1.0 wt% NaF 1M	20 V 10 – 600 min	Self organized Ribbed Rough wall with rings	Length: 0.5 – 1 μm Diameter: ~100 nm Wall thickness: ~10 nm	Potential, pH, time
3rd	Polar organic electrolytes (organic electrolyte containing F^- ions	0.5 wt % NH_4F + 0–5wt % H_2O in glycerol	20 - 60 V 13 – 216 h	Self organized Smooth Long	Length: 0.5 – 1 μm Diameter: ~100 nm Wall thickness: ~10 nm	Potential, water content, time
4th	Non-flouride-based electrolytes	0.01–3 M $HClO_4$	8-60 V 1 min	Smooth Ultra long Fine tuning of anodization conditions or multi-step aprrooach	Length: 30-1000 μm Diameter: 20-40 nm Wall thickness: ~10 nm	Electrolyte, time

The main branching in distinguishing mediums comes at aqueous and organic electrolytes. Most of the properties changes depending on the solution type. For fluoride using electrolytes, aqueous solutions are much more reactive than in organic element. This causes TNT's to grow shorter in water comparing to organic solution. Some examples of comparison are shown in Figure 2.23. It can be clearly noticed that the most remarkable difference between structures is the upper layer morphology. While TNT's produced in organic media tend to have open tops (mouth), the others tend to have closed scalloped tops. Furthermore, TNT's prepared in water indicates ripples on the side wall, whereas those grown in organic solutions can form with ripples or be smooth.

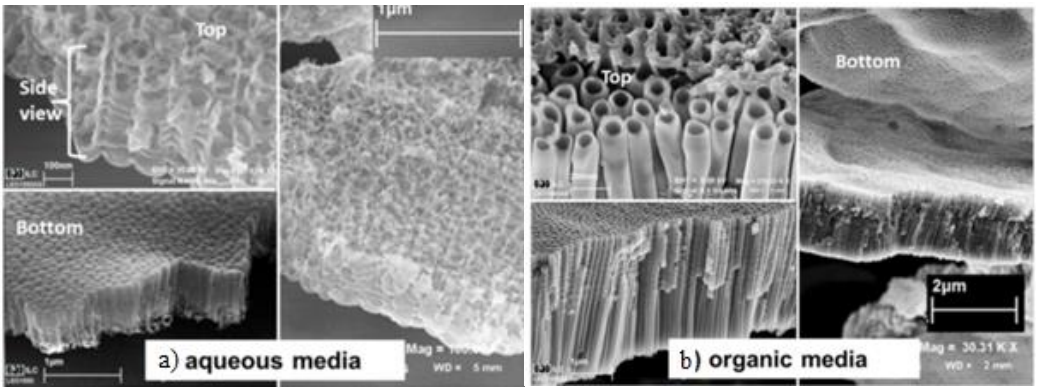

Figure 2.23 (a) TNT's produced in aqueous media (b) TNT's produced in organic media

Water media is the first researched medium for electrodeposition technique. Frontier studies only managed to produced 0.5 µm of TNT's due to the high chemical dissolution of TiO_2 in acidic electrolyte.[60][65][66] Later, longer TNT's have been produced by increasing pH values and using aqueous solutions of fluorine salts rather than HF. [72] [73] [74]

In an organic solution medium, any remaining or purposely added water plays the role as source of oxygen. The main reason of that fact is, the difficulty of getting oxygen from organic electrolytes, because the oxygen ion bonded to the carbon either by a single (C-OH) or a double bound (C=O). [67] Due to this fact, it is desired to have at least small amount of water (minimum ~%0.15 wt) in the medium to establish the oxidation. Another solution is to age the electrolyte. That provides solution to absorb moisture from environment. [58]

Other parameters such as pH, concentration, aging, anodization time, voltage etc should be optimized to get the desired product. The pH of anodization solution directly effects the electrolyte to dissolve forming oxide layer. In most cases greater dissolution values can be achieved in acidic mediums. That also expounds the reason of lowest dissolution of anodic oxide in presence of fluoride salts rather than hydrofluoric acid. Correspondingly, the concentration of fluoride ions should be kept low in order to minimize dissolution, but it also has to be at a level adequate to ensure TNT growth. It can be conclude that the optimum F^- concentration to obtain self-ordered TNT's is around %0.5 wt. The pH effect of F^- ions also must be taken into account. [140][141][142]

Ageing, reusing of the electrolyte, is also another important parameter for TNT growth, especially in organic solutions. It is generally observed that the electrical conductivity increases as a result of greater TiF_6^{2-} concentration due to formation in the previous anodization cycles that provides a lower chemical dissolution rate and greater water amount due to absorption moisture from environment.

Anodization voltage is usually applies in potentiostatic conditions, which means application of constant potential. Here the output parameter taken as anodization current. In some rare cases, galvanostatic growth, has been used in order to see the difference. It has been seen that it is more difficult to asset the desired morphology.

Voltage value is also depend on the electrolyte type. Normally, 5 to 30 V and 10 to 60 V for aqueous and organic electrolytes are used, respectively. The main effect of the voltage is its effect on electric field strength across the oxide, so it effects the movement of ions and finally wall thickness and inner and outer diameters.

Although there is a clear effect on reaction conditions, it is still hard to claim a district relation between anodization time and morphology, since it is still depend on the electrolyte type. For example, as one of the very early publications on TNT's, Gong et al tried producing four different TNT's for different anodization times (10 s to 8 min) and voltage values (3V to 20V) with 0.5 wt% HF solution as electrolyte. The first evidence is that the titanium oxide layer changed colour from purple to blue, green and red during the anodization process. It has been seen that as the voltage is increased, surface become particulate and then hollow, cylindrical, tubelike features appeared. (Figure 2.24) Similar

results has been taken at lower voltages, when 1.5 wt HF used. When they made crossed experiments they suggested that higher voltages needed to achieve the tube morphology in more dilute HF solutions. [60] Another more evident FE-SEM results for comparison of different voltage values can be seen in Figure 2.25. [68][68]

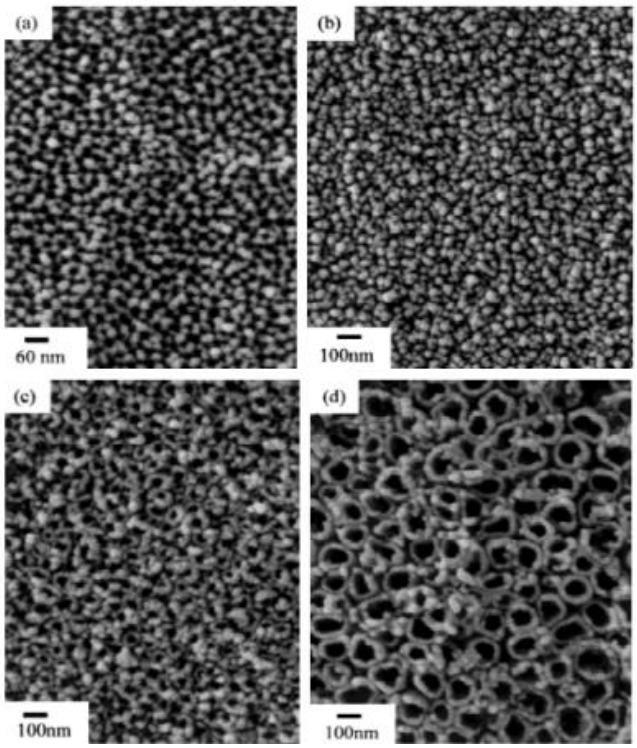

Figure 2.24 FE-SEM top-view images of porous TiO_2 films anodized in 0.5 wt% HF solution for 20 min under differen voltages: (a) 3 V, (b) 5 V, (c) 10 V and (d) 20 V

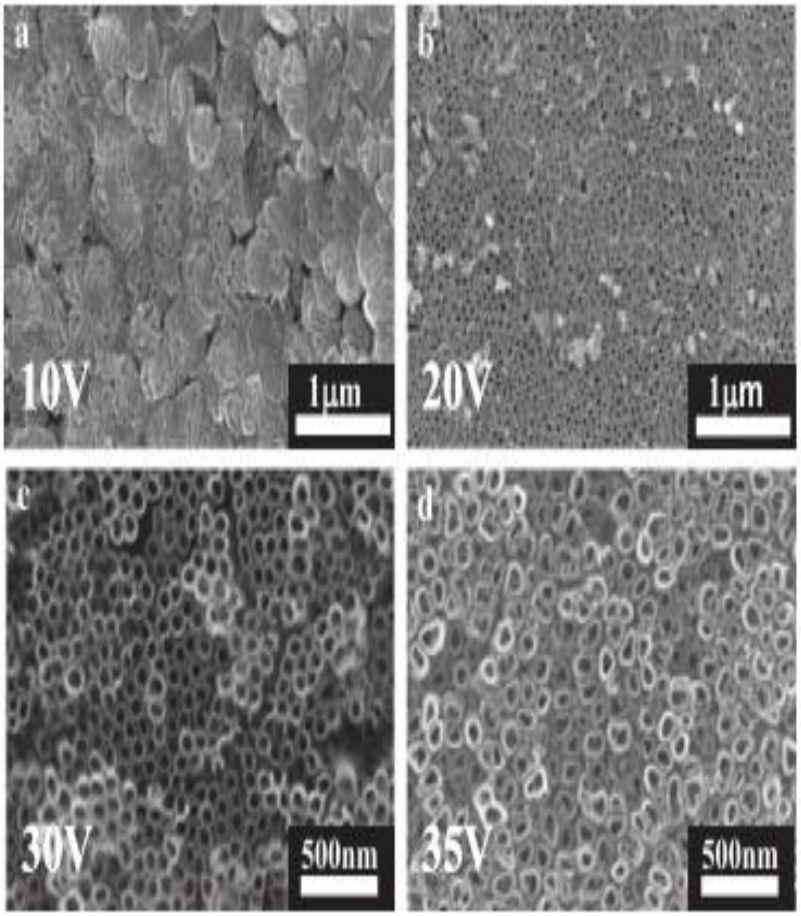

Figure 2.25 Morphology of titania film deposited under different voltages. (a) 10 V, (b) 20 V, (c) 30 V, (d) 35 V

Figure 2.26 also shows linear relationship between inner and outer diameters of TNT's versus potential value for certain reaction conditions. [69]

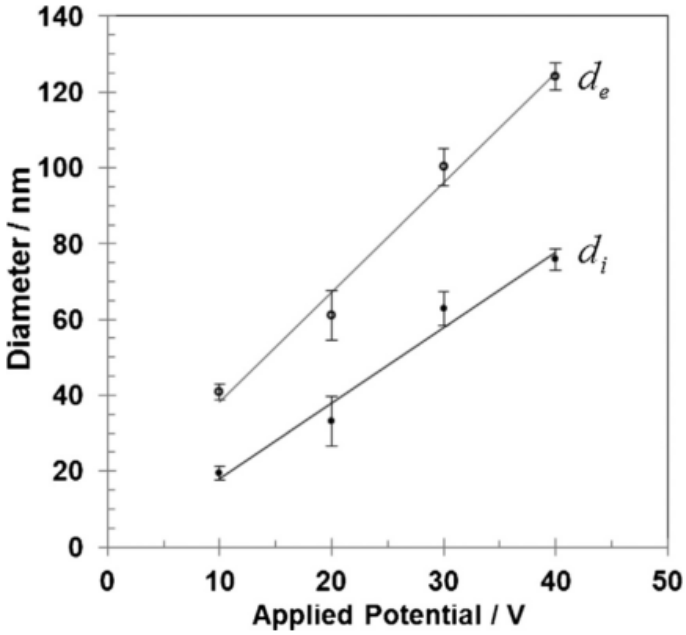

Figure 2.26 Linear relationship between applied potential and the internal (di) and external (de) diameter of TNT's.

As an opposite finding, Yin et al [70] found an inverse relationship between potenatial and diameters, for potentails higher than 100 V. Su and Zhou [71, 72] also observed that pore diameter of porous anodized nanostructrues drops when the applied potential exceed a critical value, which is determined by the electrolyte and has an influence on the dissociation of water, as well as the current density, and therefore on the porosity and the pore size of the film.

Anodization time is also another important parameter. Since the conditions are more aggressive in water medium, time needed for TNT growth is much more shorter comparing to organic medium. This results shorter tubes upto few micrometers in few minutes. After that, if reaction maintains for 30 min to 2 h, self-ordered and arranged structures can be obtained. On the other hand, completing anodization in organic medium is far more slower and dissolution phenomena are not as significant as in water. Owing to this, reaction times that reach from several hours to dates, enables obtaining TNT's longer than 100 μm. [73]

Furthermore, effect of time also depends on the electrolyte type. For example, for when HCl is used as electrolyte, it is found that the size of nanotubes does not change with time but at shorter anodization time, denser and organized nanotube films were obtained, while at longer anodization time the films became less dense and some parts of the film were dissolved. [74] On the other hand, Yoriya et al found that pore diameter and tube length increase with time when using EG or DEG electrolytes. [75]. In some cases, time effectiveness also depends on the pH value of the electrolyte. It can be said that, anodization time does not effective on length when using highly acidic electrolyte. [38] Figure 2.27 shows FE-SEM images of different TNT's produced by different anodization times with using 1.5 wt% HF solution.

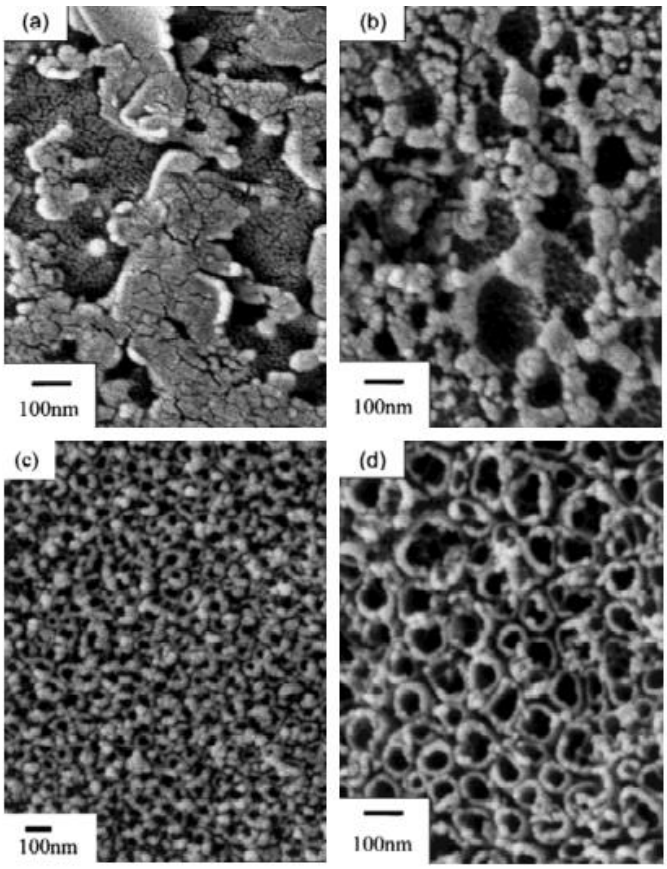

Figure 2.27 FE-SEM top images of porous TiO_2 films anodized in 1.5 wt% HF solution at 20 V for different times: (a) 10 s, (b) 30 s, (c) 120 s, (d) 8 min

One more equally important restriction is temperature. The dissolution rate of TNT's is directly depend on temperature. In normal circumstances, anodization takes place at room temperature (20-25˚C). At lower temperatures up to 2˚C, growth of tubes may be

inhibited.[154] In organic electrolytes, most fair temperature range is between 0 - 40˚C. [79]

Additionally, it is proved that the while diameter changes independently from temperature in aqueous medium, larger TNT's tend to grow in higher temperatures in organic medias. Main reason for that is leading the low temperature to higher viscosity values and reducing both ion migration and especially the dissolution of TiO_2 and Ti by F^- ions. [76]

Recently, there is an upcoming trend on search for new types of electrolytes, that produce nanotubes named as fourth generation. These electrolytes contain perchlorate, chloride or bromide ion or some acidic solutions like sulphuric acid instead of floruide ions or salts. This provides formation of disorganized nanotubes. Changing in flow mechanism inside the medium is the main reason causes this situation.

The process that is known as Rapid Breakdown Anodization (RBA) became one of the very widely used techniques for commercial TNT production, recently. The most significant advantage of this invention is that longer nanotubes up to several 100 micrometers can be obtained much more faster than other electrolytes, usually within few minutes. The main disadvantage is that the tubes are not well-defined regarding length distribution, not well-organized over larger surface areas, and they are hardly connected to the substrate. [4] That is why they are being used when low cost TNT's are desired by market. Figure 2.28 shows TNT's produced by RBA method.

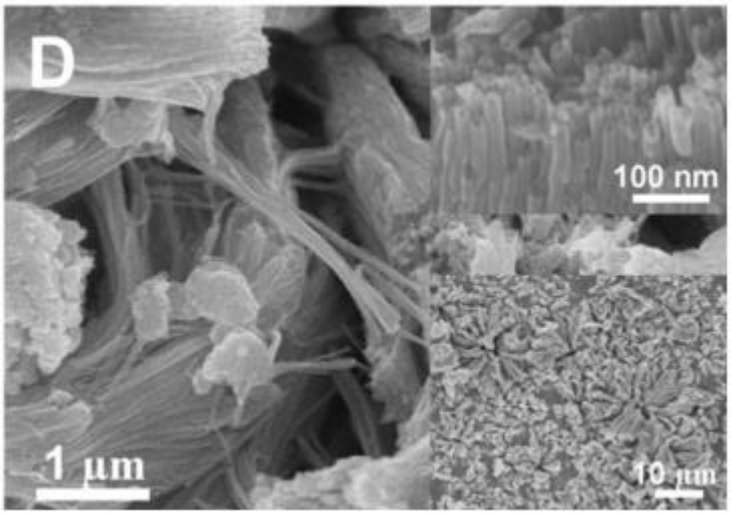

Figure 2.28 Tubes grown by a different approach: rapid breakdown anodization (RBA); these tubes grow in disordered bundles within seconds at comparably high anodic potentials

In summary, different electrolyte types provides different properties to anodic growth TNT's. The growth mechanism in presence of fluoride ions in aqueous media is determined by the difference between field-assisted oxidation and chemical and field-enhanced dissolution. [58] Fluoride ions supply high density of nucleation sites for the reactions. On the other hand, if water presence in medium, chemical dissolution is difficult to control and only short TNT's can be grown, while in contrast, chemical dissolution is suppressed in fluoride containing electrolytes and TNT's several tens of micrometer long can be obtained.

When it comes to non-fluoride electrolytes, RBA process is the dominant technique used by far. TNT's produced in that way appear to be interconnected by many TiO_2 nanoparticles, which may be crystalline or amorphous.

Table 2.6 summarizes the features of anodized TNT's growth in different electrolytes.

Table 2.6 Different regimes for anodized TiO_2 NTs growth. In aqueous electrolytes containing fluoride ions field-assisted and chemical dissolution processes are significant and only short tubes form. In organic media containing fluoride ions chemical dissolution is reduced and growth of long NTs by plastic flow is possible. The mechanism in fluoride free solutions is believed to be of a Rapid Breakdown Anodization (RBA) type.

F^- in aqueous electrolytes	i. NTs are formed, but of limited lenght (0.5 μm) ii. High density of nucleation sites. Pore nucleation due to F^- ions (and presence of water) iii. Growth process determined by chemical dissolution and field-enhanced dissolution/oxidation iv. Difficult to control chemical dissolution
F^- in organic electrolytes	i. Long NTs are formed. A small % of water is generally required as an oxygen soırce and to assist ionic migration and dissolution ii. High density of nucleation sites due to F^- ions (and small water content). Pore nucleation due to field-enhanced dissolution (i.e. chemical dissolution becomes relevant only for water content above a few wt%) iii. Growth process by 'plastic flow'
ClO_4^- /Cl^- /Br^- in aqueous electrolytes	i. Long NTs are formed, but are not self-organized ii. High density of nucleation sites due to water and presence of ClO_4^- /Cl^- /Br^- ions. High rate of formation. The process is initiated by localized anodic breakdown ii. Growth process by Rapid Breakdown Anodization (RBA)

Table 2.6 Continued

ClO_4^- /Cl^- /Br^- in organic electrolytes	i. NTs are formed, but are not self-organized ii. Sufficient density of nucleation sites provided by ClO_4^- /Cl^- /Br^- ions. The process is initiated by localized anodic breakdown. iii. RBA is poorly sustained by the electrolyte (current density too low) and the process soon stops iv. By increasing water content it is possible to form longer tubes. v. Self-organization is possible, particulatly in mixed (aqueous/ organic) solution, where the current density is sufficiently high. The mechanism behind delf organization is likely to be of a "plastic flow" type

One of the most popular used methods for producing nanoparticles is hydrothermal method. It is very substantial for its efficiency in growing bigger, purer, and dislocation-free single crystals. It is a widely known method since 1960s. Most of the studies have been performed for almost all inorganic species in a wide range of molecules starting from native elements to the most complex compounds for example oxides, silicates, germinates, phosphates, chalcogenides, carbonates and so on. Material with various properties such as piezoelectric, magnetic, optic, ceramic can be produced by this method. Furthermore, single or polycrystalline materials can also be prepared. [77]

The hydrothermal method can be described as a sub-branch of solvothermal method which basically carried out by using a solvent and a precursor in moderately high temperatures, typically from 100 °C to 1000 °C and pressure values between 1 atm to 10.000 atm. Different solvents such as methanol, 1,4 butanol or toluene can be used. [6] If the solvent is water, then the method is called "hydrothermal synthesis". When using aqueous conditions, the temperature usually kept below 374 °C that corresponds supercritical temperature of water. [78] In contrast, by using different organic solvents with higher boiling points, higher temperature values can be used, therefore it can be argued that the solvothermal method has better control than hydrothermal method, in terms of size and shape distrubition, as well as the crystallinity of the nanoparticles. [32] Solution composition, reaction time, reaction temperature, pressure, solvent properties, additives and aging time directly effects last properties such as grain size, particle morphology, crystalline phase, and surface chemistry. [6] Different geometries such as thin films, bulk powders, single crystals, and nano crystals can be produced varying such parameters. Furthermore, advanced crystal morphologies such as spheres (3D), rods (2D) and wires (1D) can also be produced. Figure 29, Figure 30 and Figure 31 shows the different morphologies of TiO_2 that produced by hydrothermal method. Because of this modifiability, a majority of the literature containing solvothermal synthesis has particularly interested in nano crystals. It also provides opportunity to produce thermodynamically stable and metastable states including novel materials that cannot be easily formed from other synthetic routes.

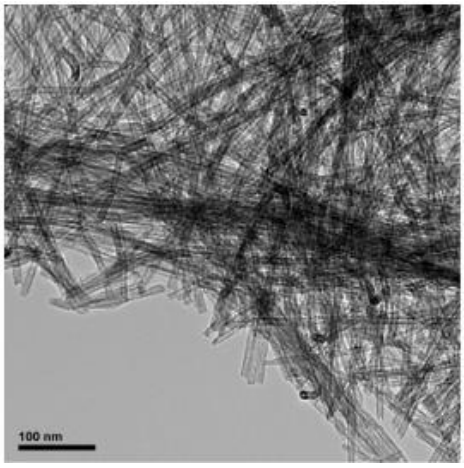

Figure 2.29 Web-like TiO_2 nanoparticles [79]

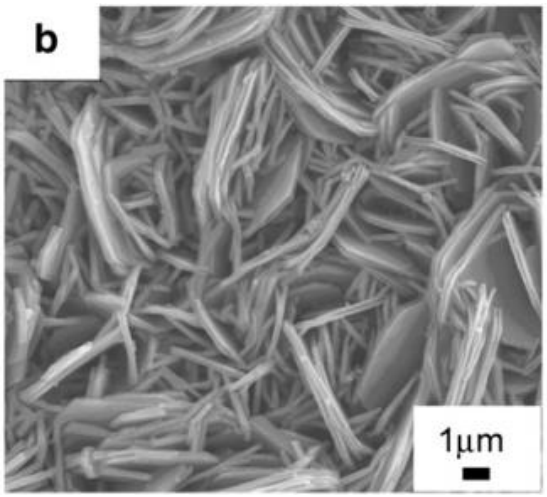

Figure 2.30 Shell-like TiO_2 nanoparticles [80]

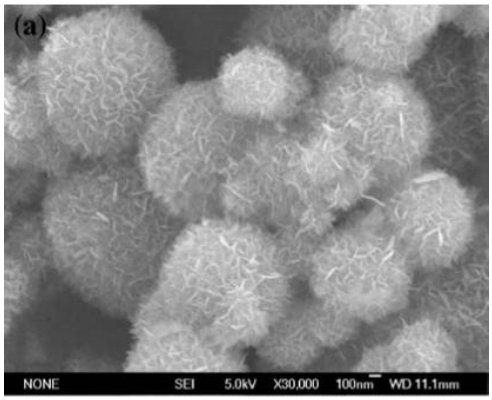

Figure 2.31 Flower-like TiO_2 nanoparticles [81]

Achieving a successful product via hydrothermal synthesis, is highly depend on the solubility of minerals in hot water under high pressure. The process usually carried out in autoclave, in which a nutrient feed into system along water. The internal pressure generated in the autoclave is governed by the operating temperature and the presence of the aqueous solutions in the autoclave. Between opposite ends of the growth chamber, a temperature gradient is maintained. While nutrient solute dissolves in hotter end, seed crystal deposits at the cooler end. A typical autoclave can be seen in Figure 2.32. The reactants are filled into Teflon vessel and autoclave is heated up to a certain temperature and set an autogenic pressure.

Choosing the right autoclave system is crucial for nanoparticle properties. There are some certain characteristic for autoclave to work properly. Firstly, it must be inert to acids, bases, oxidizing agents. Secondly, it must be resistant to corrosive materials. Thirdly, it must be easy to assemble and dissemble. In additionally, to get the desired temperature gradient, it must have a satisfactory length. It also must be leak-proof within the required temperature and pressure. Finally, it must be strong enough to bear high temperature and pressure experiments for long duration.

Figure 2.32 Hydrothermal equipment

From TNT production point of view, hydrothermal route is the most inexpensive and environment-friendly method because of its relatively low temperature requirement, being carried out in a closed aqueous system and almost non-polluting set up. Different

crystalline structures such as anatase, brookite, rutile and monoclinic can be obtained by differentiating reaction conditions.[82] There are three main steps of formation TNT's via hydrothermal route. i) generation of the alkaline titanate nanotubes, ii) substitution of alkali ions with protons iii) heat dehydration reactions in air. [83]

Figure 2.33 shows the steps for the formation of TNT's.

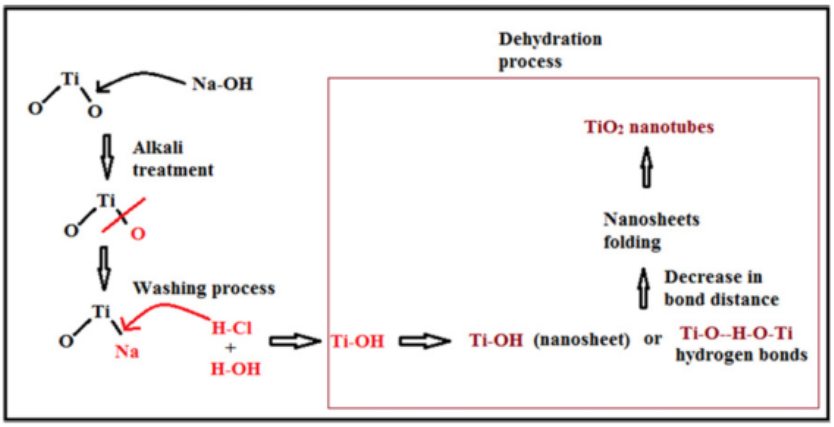

Figure 2.33 Formation mechanism of TNT using hydrothermal method [83]

Producing TNT's by hydrothermal synthesis consist of dissolving TiO_2 or its precursor in a concentrated aqueous solution of a base (mostly NaOH) to form a mixture. Afterwards the solution carried into an autoclave, in which the mixture can be converted to a nano-size crystallized tubular (titanate) structure. The typical hydrothermal temperature range is of 110–150◦C. Then by washing dilute acidic aqueous solutions subsequently, a high yield of nanotubular products can be achieved. [36] This method mostly consist long reaction times up to 24 hours and long washing times up to 12 hours. This is the biggest disadvantage of hydrothermal method.

The main control parameters are applied temperature, the type of Ti precursor or properties of TiO_2 if a bulk material is used at the beginning, the type of alkali solution, pH, reaction time.

- Effect of temperature

Temperature is the most effective parameter on TNT nucleation and growth. It is usually determined by considering alkali solution and reaction time. Many important properties such degree of crystallinity, yield, length, internal and external diameters, pore size and volume depend on temperature. Yield, length and crystallinity degree basically increases with temperature while others reach an optimum value.

The most used temperature range to obtain successful TNT's is between 100-200°C. [84] 90°C nanosheets do not transform into tubes effectively, and after 180°C nanoribbon occur instead of tubes, in presence of NaOH solution. [85] That is because of the lack of the thermal energy that required to curl-up the nanosheets into tubular structure due to high surface energy.[86].

Between the limits, 130°C is to be considered to give maximum internal diameter and specific surface area. That is why the most of the studies in literature are carried out between 130 and 150°C. For the temperatures lower than 130°C, Ti-O-Ti bonds tends to be less cleavage, which means the first stage of synthesizing TNT. On the other hand, after 130°C the lamellar structure of TiO_2, that means the intermediate stage of synthesizing TNT's, start to break. [87]

Another important consideration about temperature is reaction time. It has been found that at 130°C, when reaction time selected as 12h, a few nanotubes were observed when many of the products were nanosheet. When it is taken as 24h, most of the sheets transformed into nanotubes but there were still a few nanosheet exist. When waited for 36h almost %100 yield for nanotubes had been achieved. On the other hand, when working at 150°C, only 15h were enough to convert all sheets into tubes. [88] In Figure 2.34 the transformation from nanosheets to nanotubes with the effect of the time can be seen evidently.

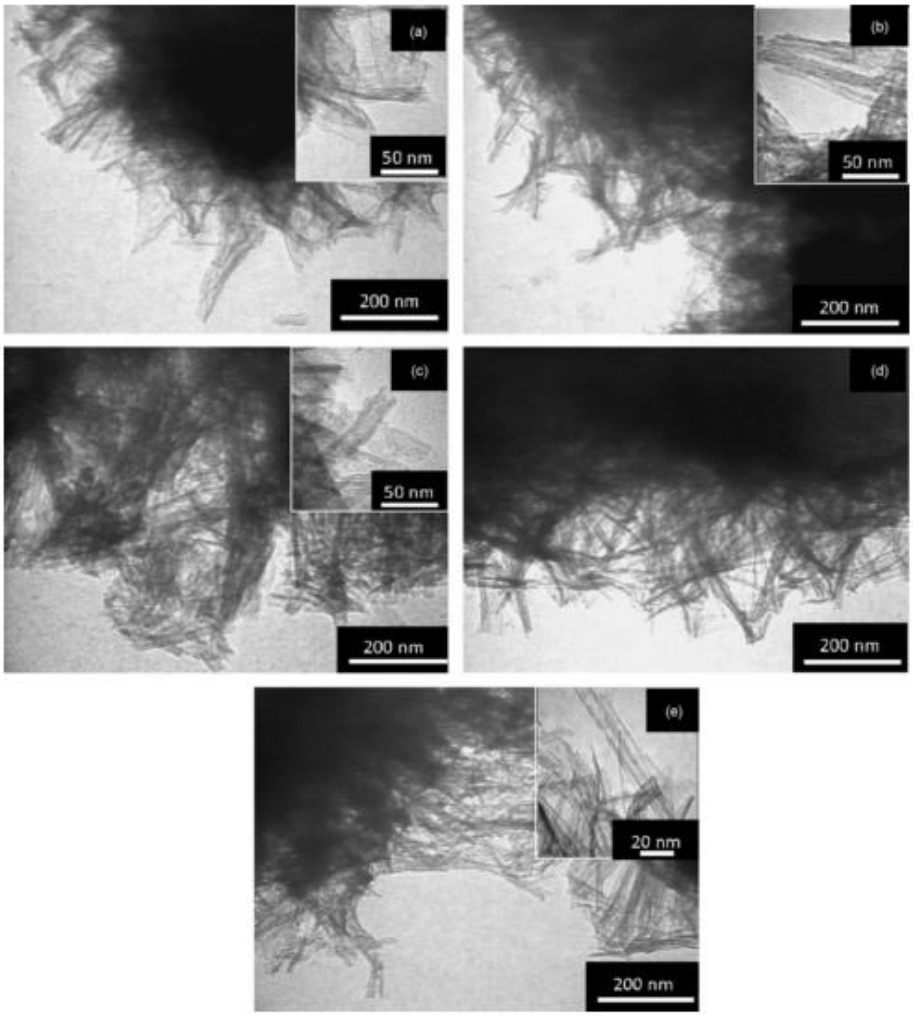

Figure 2.34 TEM images of TNT synthesized at different reaction time (a) 3h, (b) 6h, (c) 9h, (d) 15 h and (e) 18 h [the inset micrograph in (a) shows the presence of layered structures, (b) nanosheet structures were halfway curled up, (c) mixture of layered and tube structure and (e) tube-like structure][88]

- Effect of precursor

There are numerous of different precursor options in literature for hydrothermal method since it provides the opportunity to synthesize TNT's with different desired properties. The most common used examples are amorphous bulk TiO_2, anatase or rutile TiO_2, TiO_2 nanoparticles such as Degussa P25, lepidocrocite-type sodium titanate, molecular Ti^{IV} alkoxide, TiO_2 colloids, and Ti metal foil.

The last properties of TNT's such as crystal structure, chemical structure and thermal and physical stabilization values highly depend on the precursor used. It also effects the

reaction rate depend on the initial crystal morphology. When anatase TiO_2 is used, the TNT production reaction takes place in 0 degree kinetics and process carried out with high yield. When rutile Is used 2^{nd} degree of kinetics takes place and a slower process occurs. Furthermore, the surface area of the precursor is also important for yield and reaction rate.

- Effect of alkali solution

Select of alkali solution is considered in two different point of views. Firstly, the type of the compound and the concentration of the base solution. There have been different researches on different alkali solutions for hydrothermal synthesis. For example, the effect of NaOH, LiOH and KOH is investigated by Zhang et al, [89] . It has been found that TNT is only produced in presence of Na^+ ions. For the other cases, nanorods, nanoplates or other types of nanoparticles are being synthesized. Furthermore, due to the increasing solution rate of $Ti^{(IV)}$ ions, reaction rate and TNT production yield is also increased with the concentration of NaOH solution. Generally the concentration of NaOH changes between 5 to 20 M. Beneath these borders, reaction yield decreases dramatically. [90]

The morphological structure of the last compound is also effected by the alkali solution. With increasing $NaOH/Ti^{(IV)}$ ratio average inner diameter decreases while the surface area increase. In additionally, when $NaOH/Ti^{(IV)}$ decrease, nanoparticles tend to grow as nanorod shape rather than layered structure.[91]

As an interesting result, it has been found that when KOH and NaOH are used simultaneously, high yield of TNT production can be achieved in lower temperature degrees. For example, Bavykin and Walsh found that when working with 50:1 NaOH:KOH ratio, %100 yield occurred at 100°C. [39]

- Effect of HCl treatment

Acidic washing is another compelling step for formation mechanism of TNT's. According to Kasuga et al, acid treatment allays the electrostatic repulsion on surface and leads alteration of lamellar structures into nanotubes. In that step, the nanoribbons which have not been completely transformed into nanotubes also achieves complete conversion.[92–94] As a further theory, Tsai et al suggested that, while hydrothermal

process in progress Ti-O-Na and Ti-OH chemical bonds have been occur and if only an acid treatment is applied, Na^+ ions replace with H^+ ions to form Ti-O-H bonds which is essential for TNT morphology. This switch also effects surface charge and lead nanosheets to turn into tubes. [95]

Crystal structure also effected by the acid treatment. There have been numerous of studies showed that protonated titanate structures transforms into anatase in acidic medium. This conversion is directly proportional by the strength of acid. [95–100]

2.1.5. Application Areas of TNT's

TiO_2 molecule is being commonly used for years because its advanced properties such as high chemical stability, low-cost, non-toxicity, strong photocatalytic activity and high photo-electric conversion efficiency. [5]

Unusual geometry and unique properties of TNT's induces them to be very promising for many applications. Large surface area and high length/radius ratio distinguish TNT's between other TiO_2 nanoparticles. The most common application area of TNT's are photocatalysis and solar cells.

In the following pages, application of TNT's in solar cells and their use for photocatalytic properties will be explained.

Solar Cells

Increasing energy demand and search for cleaner energy systems led researchers to lean on alternative energy sources such as solar power. Currently, there have been three generations of solar cells invented. First generation solar cells are silicon based solar cells. They recently have highest conversion value, and constitute the %80 of the solar panels around the world. But they are still very expensive and have difficult production process. They also have a problem of losing some of their efficiency at higher temperatures. Second generation solar cells are thin-film solar cells. Low production cost and less material requirement are the most important advantages of this generation. Third generation solar cells are known as DSSC's and they will be explained detaily in the following pages.

TiO_2 particles have been investigating to be used in solar systems for more than 30 years. [101, 102] Most of these researches focuses on increasing solar cell efficiency. For example, it is now accepted that anatase TiO_2 not only has highest photocatalytic activity but it also shows the highest solar energy conversion efficiency. [103] There are also some physical limitations on usage of TiO_2 molecules. For example, one of the main challenges for photochemical applications is that the large band gap of TiO_2 making photo-induced reactions only possible at excitation <400 nm. For this reason there have been works targets reducing band gap by doping and dye-sensitization in order to get considerable efficiency for visible, thus solar, light. [104] It is now can be easily said that TiO_2 and dye combination is one of the most important in utilizing solar energy and can extend the absorption spectrum to the visible region. [5]

So far, TiO_2 nanoparticles are successfully emerged into photovoltaic systems. After establishing of the third generation solar cells, which is also known as Dye Synthesized Solar Cells (DSSC), by O'Regan and Grätzel in 1991 they have gained great interest by numbers of scientists. [105] Although the pioneer examples only achieved %7.9 efficiency, now there are papers which reports upto %15 efficiency. [105, 106] Figure 2.35 (a) compares the current efficiency data of different solar cell types from different producers. The most recent world record for each technology is highlighted along the right edge in a flag that contains the efficiency and the symbol of the technology. The company or group that fabricated the device for each most-recent record is bolded on the plot. Cell efficiency results are provided within different families of semiconductors: (1) multijunction cells, (2) single-junction gallium arsenide cells, (3) crystalline silicon cells, (4) thin-film technologies, and (5) emerging photovoltaics. Some 26 different subcategories are indicated by distinctive colored symbols. At the down side of the graphs (b) a clearer version of DSSC efficiency records can be seen.

The theoretical photoelectric conversion efficiency (PCE) limit of the DSSC, using a simple junction configuration, under standard test conditions (STC) is 32% according to Professor Michael Graetzel. A two level tandem DSSC embodiment could reach 46% efficiency under the same conditions. Higher PCE's reaching close to 40% can be achieved indoors or in diffuse daylight that has a low infrared light content [107].

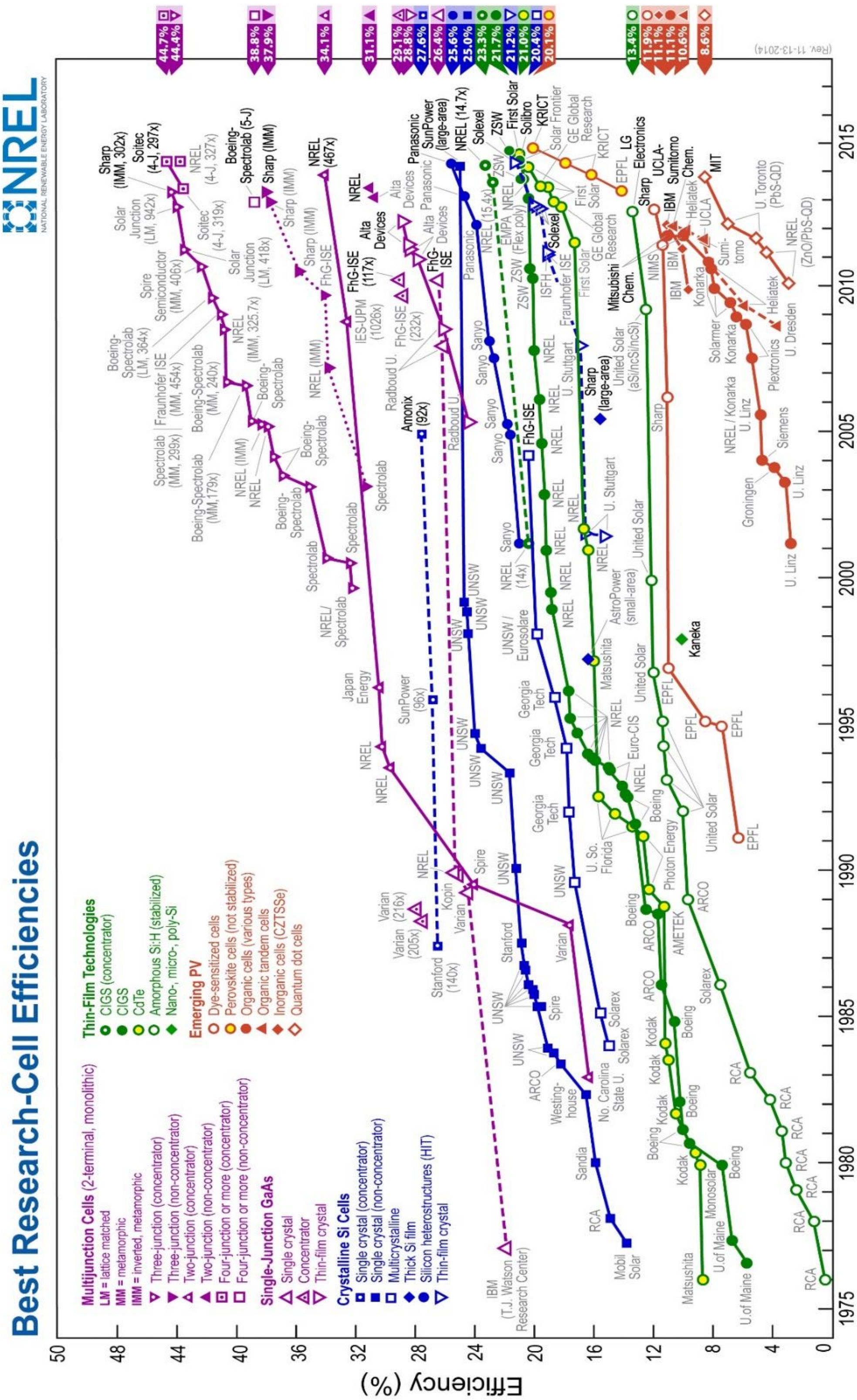

Figure 2.35 Solar cell efficiencies report 2015

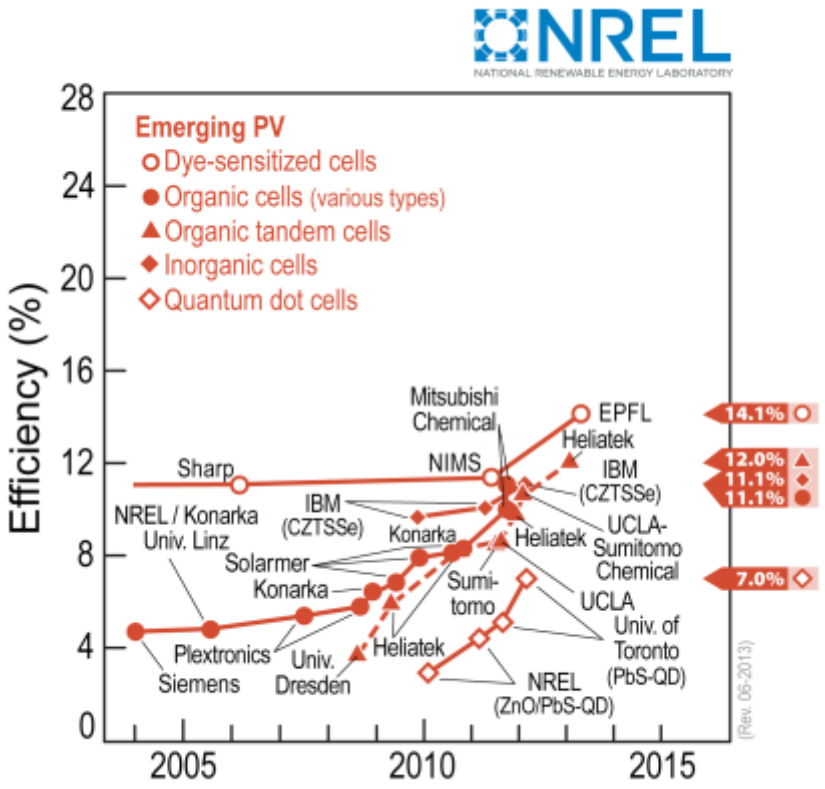

Figure 2.36 Photovoltaic cells efficiency chart [108]

The most widely used photoelectrode in DSSCs is porous TiO_2 films made from nanocrystalline TiO_2 particles which are deposited on conductive glass substrates.

A typical DSSC consist of different parts. An n-type (electron-conducting) semiconductor is coated on a conductive glass surface which acts as a transparent electrode. TiO2 layer covered by light-harvesting dye solution. An electrolyte solution, usually $I\text{-}I^{3-}$ (iodide–triiodide) redox couple filled into layers to produce a sandwich geometry.

When solar cell is under illumination, firstly, the dye sensitizer absorbs a photon (sun light) and produces a photoexcited-state of dye molecule (S*) (1). Then, the photoexcited dye (S*) injects an electron to the conduction band (CB) of TiO_2 (2). Afterwards, by donating an electron from the iodide ion I^- in the redox solution (if I-/I3- electrode is used), the generated oxidized dye (dye cation) is reduced back to its original neutral state; this process is usually called dye regeneration or re-reduction (3). The added electrons in CB move through the network of interconnected TiO_2 nanoparticles to arrive at the transparent conducting oxide (usually FTO) and then through the external circuit to the

counter electrode (usually Pt-coated glass). The iodide ion I− is regenerated by the reduction of triiodide ion (I3−) at the counter electrode through the donation of electrons from the external circuit (4) and then the electron flow cycle is completed. However, there are maybe some undesirable side processes: the electrons injected to the CB of TiO2 may reduce either oxidized dye (recombination) (5) or I3− in solution which is called dark current (6). These two processes (5) and (6) lower the short-circuit photocurrent density (Jsc) and the open-circuit photovoltage (Voc) of DSSCs, respectively. The recombination process (5) competes with the re-reduction of the oxidized dyes by I− (3). To generate greater Jsc and Voc, therefore, the electron injection (2) and the regeneration (3) processes must be much faster than those of the recombination (5) and dark current (6). [109]

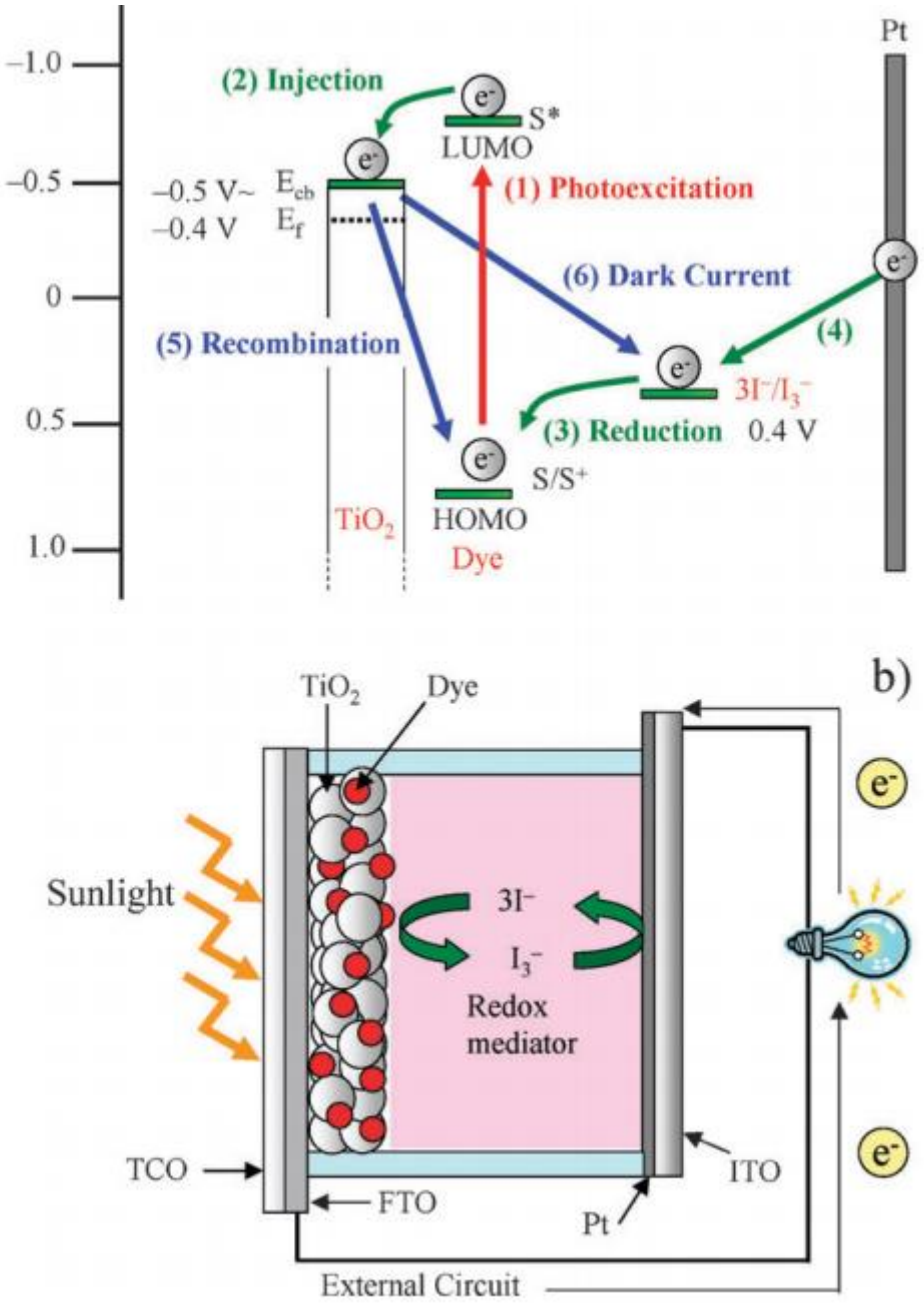

Figure 2.37 Diagrammatic illustration of (a) construction and (b) operation principle of DSSCs

The reasons that these solar cells mainly based on TiO_2 nanoparticles of their high efficiency, environmental-friendly production opportunity, being relatively low cost, non-toxic, stable and high production yield. [110, 111] Although they have well electron transport properties and good dye absorbance capacity due to large surface area, interconnected TiO_2 particles still not very favourable by researchers because of random connection. [55] After absorption of dye molecules on TiO_2 particles, a current is produced by the electron injection into the conduction band of TiO_2. Emerged electrons transport through the carrier molecules to reach the electrode layer. When using random ordered nanoparticles, gaps between structures acts as grain boundary leading to trapping and recombination of electrons. This phenomena reduces the efficiency of DSSC's by reducing the electron collection at the back contact as explained before. By applying TNT's into DSSC's, electron transportation capacity and charge separation efficiency is aimed to increase because of direct pathways of TNT's. These pathways helps charge transfer acceleration between interfaces. [5]

One-dimensional nanomaterials such as nanorods, nanotubes (especially electrochemical anodized TNT'S) differentiates from other TiO_2 nano particles because of their strong light-scattering effects and high surface-o-volume ratio which is important for solar energy conversion. The more the tubes get ordered and vertically oriented, the higher degree of electron mobility along the tube axis can be achieved. This will greatly reduce interface recombination and increase overall conversion efficiency. It also has a positive effect on dye-loading therefor efficiency per unit area of solar cell. Figure 2.38 compares transporting patways of electrons in TiO_2 nanoparticles and TNT's. [5] It can be easily seen that one-dimensional structure creates electrons a direct pathway and provides a high surface area by formation ordered tube shape.

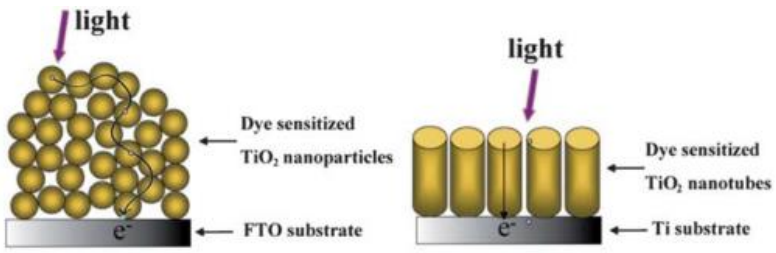

Figure 2.38 A comparison of the electron pathways through nanoparticle and nanotubular structured TiO_2 [5]

Photocatalytic Effect of TNT's

TiO_2 shows strong oxidizing photoactivity when irradiated by UV ray. When illuminated, TiO_2 molecules decomposes pollutants, malodours or other undesired contaminants usually made of organic compounds mostly into CO_2 and water as shown in Figure 2.39.

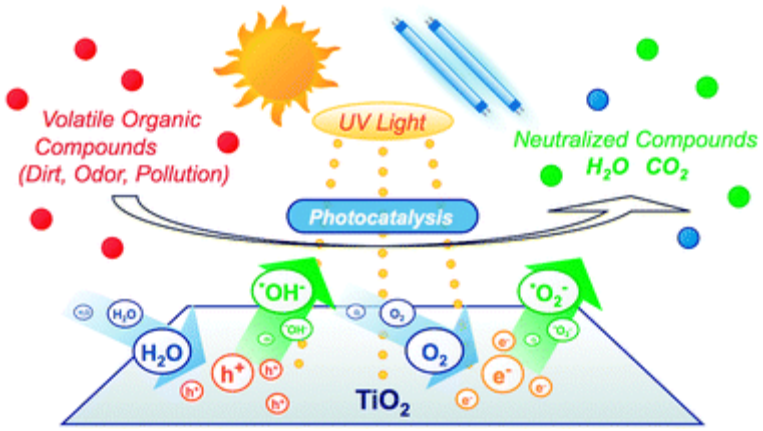

Figure 2.39 Photoactivity of TiO_2 molecule

As raw materials TiO_2 nanoparticles can be separated into two main categories: photocatalytic powders and photocatalytic sols. When they have processed, powder form can be transformed into granules, activated carbon/inorganic fiber honeycombs, dispersion (therefore paints and ceramic balls); on the other hand, sol can be transformed into coating materials as well as other kinds of ceramic balls. [112] TiO_2 photocatalysis usually used for deodorizing, air purification, anti-soiling or fog-proofing and anti-bacterial application. But it can be said that most of the studies targets on water treatment.

There have been some physical techniques used such as ultrafiltration, adsorption, biological treatment, coagulation and ion exchange on synthetic resins. [113, 114]. But they all have some kind of disadvantages like being expensive, ineffective, and selective to only some of the pollutants, creating more toxic materials, high operation costs and posing waste disposal problems of their own. [83]

Since discovery of photocatalytic effect of TiO_2 heterogeneous photocatalysis has been successfully used for treating of air and water by oxidation, decontamination, mineralization without generating harmful by products. [115, 116] It is also favourable because being relatively low-cost. [114]

Today catalytic effect of TiO_2 made it used in so many environmental application such as air and water purification, antibacterial protection, water disinfection, treatment of harmful gas emission and hazardous water remediation. [83] Nevertheless, ongoing researches mostly targets the low efficiency problem and optimization of catalytic parameters. After achieving generation of active charge carriers, these materials are expected to degrade more organic pollutions into harmless products in a more efficient way.

Like other application areas, physical and chemical structure of TiO_2 molecules directly influences the catalytic properties. Morphology, dimensions and crystallite phase are the most important physical parameters on photo catalytic performance. [117]. It has been proved that the larger surface area due to smaller particle size increases the photocatalytic efficiency of TiO_2 nanoparticles. [82]

As explained in solar cell applications, TiO_2 creates holes and electrons by irradiating light with higher energy than TiO_2's band gap energy (wave length < 380nm). These holes and electrons react with oxygen and hydroxyl ions, producing hydroxyl radicals and superoxide anions. Oxidation power of the chemicals are so strong that the chemicals decompose and eliminate organic compounds and NOx. A typical reaction mechanism can be seen in Figure 2.40.

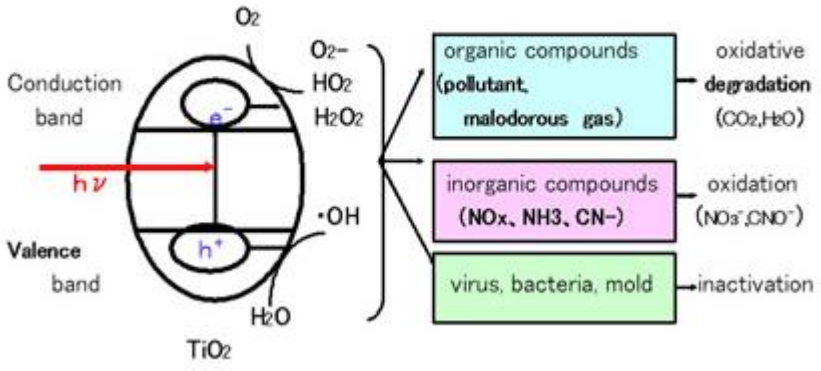

Figure 2.40 Typical reaction mechanism for TiO_2 particles

Studies show that efficiency of photocatalytic treatment systems based on three main parameters: i. activity of the photocatalyst, ii. type and power of irradiation source, iii. Surface area of photocatalyst or photocatalyst support. In that point of view, it can be suggest that, designing a treatment system which includes thin layer, photoactive materials that uses low powered and low cost irradiation sources (such as LEDs) could be really effective against VOCs or microorganisms. For possessing relatively high surface area and can be directly produced on the support material, TNT's meet mentioned requirements. They also provides photon absorption together with an extensive adsorption of reactant molecules on the surface. Other unique properties such as light conversion, improved ion diffusion capacity at the semiconductor-electolyte interface of enhanced electron percolation pathways made TNT's much more desired for catalytic reactions. [118, 119]

Photocatalytic properties of TNT's can be changed by dealing with production conditions like anodization time, applied voltage, temperature, Ti foil roughness, calcination parameters and electrolyte composition including fluoride concentration, solvent, water con- tent, pH, viscosity, conductivity, and organic additives. Therefore morphologic structure of TNT's change as well as the photocatalytic activity. [64]

CHAPTER 3

MATERIALS AND METHOD

3.1 Materials

3.1.1 Titanium Dioxide

In this study four different kind of TiO_2 source used as raw material in order to investigate the effect of titanium source. Each of them has the same molecular structure as can be seen in Figure 3.1.

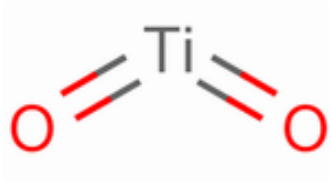

Figure 3.1 Molecular structure of TiO_2

i. Nano TiO_2

Nano TiO_2 as known Degussa P 25 or Aeroxide P25 is used in first raw with CAS number of 13463-67-7 and brand of Sigma-Aldrich. More technical properties can be seen in Table 3.1.

Table 3.1 Technical properties of Degussa P 25

Product Number	718467 (Sigma-Aldrich)
CAS Number	13463-67-7
Formula	O_2Ti
Formula Weight	79,87 g/mol
Assay	≥99.5% trace metals basis
Form	Nanopowder
Particle Size	21 nm (TEM)
Surface Area	35-65 m^2/g (BET)
Melting Point	1850 °C
Density	4.26 g/mL at 25 °C(lit.)
pH	3.5-4.5
Trace Metal Analysis	< 5000.0 ppm

ii. Anatase TiO_2

Anatase TiO_2 with CAS number of 1317-70-0 and brand of Sigma-Aldrich used as second raw material. Technical properties can be seen in Table 3.2.

Table 3.2 Technical properties of anatase TiO_2

Product Number	232033 (Sigma-Aldrich)
CAS Number	1317-70-0
Formula	O_2Ti
Formula Weight	79,87 g/mol
Assay	99.8% trace metals basis
Form	Powder
Melting Point	1825 °C
Density	3.9 g/mL at 25 °C(lit.)
Trace Metal Analysis	< 10000.0 ppm

iii. Rutile TiO_2

Rutile TiO_2 with CAS number of 1317-80-2 and brand of Sigma-Aldrich used as third raw material. Technical properties can be seen in Table 3.3.

Table 3.3 Technical properties of rutile TiO_2

Product Number	204757 (Sigma-Aldrich)
CAS Number	1317-80-2
Formula	O_2Ti
Formula Weight	79,87 g/mol
Assay	99.99% trace metals basis
Form	Powder
Density	4.17 g/mL at 25 °C(lit.)
Trace Metal Analysis	< 150.0 ppm

iv. Ultrasounded TiO_2

In order to investigate the effect of ultrasound on nanotube formation, pre-made TiO_2 samples have been used which has synthesized in previous studies.

In order to prepare these samples Riedel-de Haen brand TiO_2 raw materials exposed to ultrasonic homogenizer (Cole Parmar) with 750 W power. Ultrasound experiment set up has shown in Figure 3.2. 15 g of TiO_2 fed into 600 ml reactor filled with distilled water. Afterwards, while mixing with 800 rpm pace, ultrasound with %40 amplitude has been implemented for 1 hour. After that, ultrasounded solution has been centrifuged and, liquid phase has been decanted and TiO2 particles have been dried, grinded and used for nanotube synthesis.

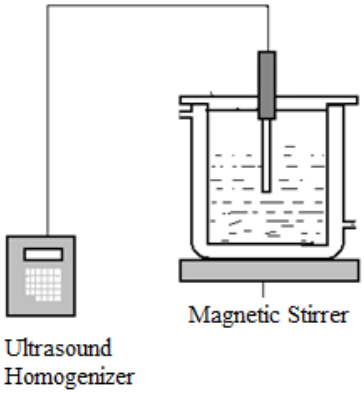

Figure 3.2 Ultrasound experiment setup

3.1.2 Alkali Solution

As mentioned before, alkali solution must be used in order to achieve TNT's when using hydrothermal method. In this study, in order to investigate the effect of molarity of alkali solution, we have used NaOH solution of 5M, 10M, 15M and 20M. Properties of NaOH pellets can be seen in Table 3.4.

Table 3.4 Technical properties of NaOH

CAS Number	1310-73-2
Product Number	1.064262.1000 (Merck)
Assay (acidimetric, NaOH)	>97%
Carbonate	<1%
Chloride	<0.1%
Sulphate	<0.1%
Heavy metals (as Pb)	<0.002%
Al	<0.002%
Fe	<0.002%

3.2 Method

3.2.1 Taguchi Method

Experimental design methods (or design of experiment (DOE) methods) are used in order to reduce number of experiments and to determine the most effective parameters on production properties. When it is needed to investigate the effect of too many parameters at the same time, it is essential to perform high numbers of experiments. It is not only waste of time for researchers but is also an expensive way. For example, when using factorial analysis method for a system of four factor with three levels, it is needed to perform 3^4=81 experiments. Similarly, number increases to 2^7=128 for a two-level, seven-parameter system. So it can be seen that the numbers are huge when not using a DOE method. It becomes nearly impossible when making real physical experiments in areas such as chemistry. In order to solve these problems and reduce number of experiments, Japon scientist Dr. Genichi Taguchi designed a method based on orthogonal series and standard tables which is called Taguchi method. These tables, which is called Taguchi Orthogonal Series, are symbolized by abbreviations such as L-4, L-9, L-16 etc, here numbers corresponds total experiment number in the table. Although deciding which table to use is not depend on rigid rules, it is determinant to take into account, number of parameters, levels of parameters and relations between parameters. In Table 3.5 common Taguchi arrays can be seen. [120]

Table 3.5 Taguchi design types

Series	**Number of Parameters**	**Level of Parameters**
L-4 (2^3)	3	2
L-8 (2^7)	7	2
L-12 (2^{11})	11	2
L-16 (2^{15})	15	2
L-32 (2^{11})	31	2
L-9 (3^4)	4	3
L-18 (2^1,3^7)	1	2
	7	3
L-27 (3^{13})	13	3
L-16 (4^5)	5	4
L-32 (2^1,4^9)	1	2
	9	4

After determining optimum conditions, it is always a good idea to perform affirmation experiment. Nevertheless, it is also possible to make a calculation about optimum condition results by using non-optimized condition data.

Taguchi describes two different route to make whole analysis. First, the standard approach which makes use of single study or an average of repeated studies with ANOVA analysis. Second, and highly recommended one for multiple parameter studies uses signal to nosie ratio S/N. The result gives the most appropriate conditions by spotting the differences in data.

Formulas for the calculation of the optimum conditions can be written as follow:

a. For larger is better:

Here, y goes to infinity and S/N ratio can be described as;

$$SN_L = -10log\left[\frac{1}{n}\sum_{n=1}^{n}\frac{1}{y^2}\right] \quad (3.1)$$

b. For smaller is better:

Here, y goes to zero and S/N ratio can be described as;

$$SN_S = -10log\left[\frac{1}{n}\sum_{n=1}^{n}y^2\right] \quad (3.2)$$

In both equation, *n* describes the number of repeated experiments and *y* describes the value of performance. If it is aimed to reach the maximum value, then the parameter levels which makes SN_L creates the optimum conditions. On the other hand, if it is aimed to reach the minimum value then, the parameter levels which makes SN_S creates the optimum conditions.

3.2.2 Experimental Method

In this research it is aimed to build a correlation between temperature, type of raw material, time, and concentration of NaOH solution and physical properties of TNT's for hydrothermal synthesis. Degussa P25, rutile and anatase bulk TiO_2, and ultrasounded TiO_2 used as different raw sources. The results were commentated by using Taguchi Optimization Method. Characterization of physical appearance determined by SEM analysis. Crystal structure investigated by XRD studies. Pore size and surface area values are determined by BET analysis.

Due to high temperature values used, oil bath reactor used with tailored Teflon reactor. First, alkali solution and TiO_2 raw material fed into the warm system. After waiting enough time (10h, 20h, 30h or 40h) sample collected from reactor. They have been cooled down, washed with HCl acid solution for 24h and then purified with distilled water. Each sample dried at 105°C overnight and collected in desiccator until analysis.

Determination of Orthogonal Experimental Design

In this study, four levelled-four parameter have been investigated. Table 3.6 and Table 3.7 shows the corresponding variables and orthogonal experimental system, respectively.

Table 3.6 Corresponding parameters for Taguchi design

Parameter	**Parameter Level**			
	1	**2**	**3**	**4**
Raw Material *(A)*	Degussa P25	Anatase	Rutile	Ultrasounded TiO2
Temperature *(B)* (°C)	100	120	140	160
Time *(C)* (hour)	10	20	30	40
Alkali Concentration *(D)* (mol/L)	5	10	15	20

Table 3.7 Levels of parameters of experimental setup

Number of Experiment	**A**	**B**	**C**	**D**
1	1	1	1	1
2	1	2	2	2
3	1	3	3	3
4	1	4	4	4
5	2	1	2	3
6	2	2	1	4
7	2	3	4	1
8	2	4	3	2
9	3	1	3	4
10	3	2	4	3
11	3	3	1	2
12	3	4	2	1
13	4	1	4	2
14	4	2	3	1
15	4	3	2	4
16	4	4	1	3

After designing the experiment table we only have to put on right values on right raw. For example, if we consider experiment 8, we have to choose Anatase TiO_2 (A-2), 160 (°C) (B-4), 30 hour (C-3) and have to use 10 M of NaOH solution (D-2). After substitute each cell by same logic, we can get the final Table 3.8.

Table 3.8 Real parameters and levels of experimental setup

Experiment Number	**Raw Material**	**Temperature °C**	**Time h**	**Alkali Concentration mol/L**
1	Degussa P25	100	10	5
2	Degussa P25	120	20	10
3	Degussa P25	140	30	15
4	Degussa P25	160	40	20
5	Anatase	100	20	15
6	Anatase	120	10	20
7	Anatase	140	40	5
8	Anatase	160	30	10
9	Rutile	100	30	20
10	Rutile	120	40	15
11	Rutile	140	10	10
12	Rutile	160	20	5
13	Ultrasound TiO_2	100	40	10
14	Ultrasound TiO_2	120	30	5
15	Ultrasound TiO_2	140	20	20
16	Ultrasound TiO_2	160	10	15

CHAPTER 4

RESULTS

In this chapter physical structure, surface characterises and crystal properties of TNT's will be presented. Taguchi analyses for each result will be carried out except XRD studies. This is because of getting non numeric results from XRD analysis.
A brief discussion will be made at the end of each subtitle but a comprehensive commentary will be made in Chapter 5.

4.1. Physical Structure

Physical appearance of TNT's characterized by Scanning Electron Microscope (SEM) (Zeiss - EVO® LS 10). For each sample, approximately twenty images under different magnification rates have been collected but four of most distinctive ones have been chosen and presented in this dissertation.

SEM results give the most important information about the success of production process. The morphologic structure, the type of the nanomaterial or the length and diameter of each tube could be determined by analysing SEM results.

Following pages will be show SEM images for each sample.

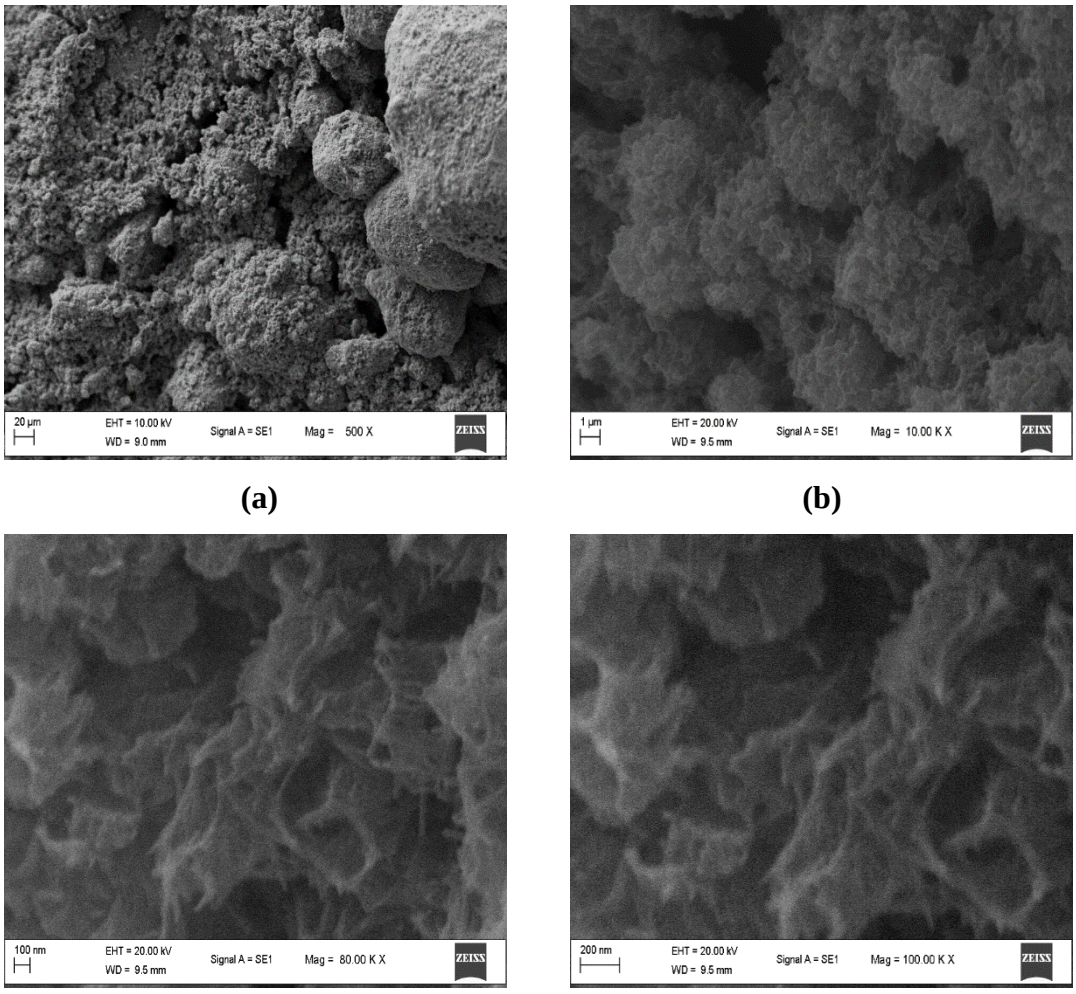

(a) **(b)**

(c) (d)

Figure 4.1. SEM images for sample (1) with different magnifications (a) 500 X, (b) 10.000 X, (c) 80.000 X and (d) 100.000 x

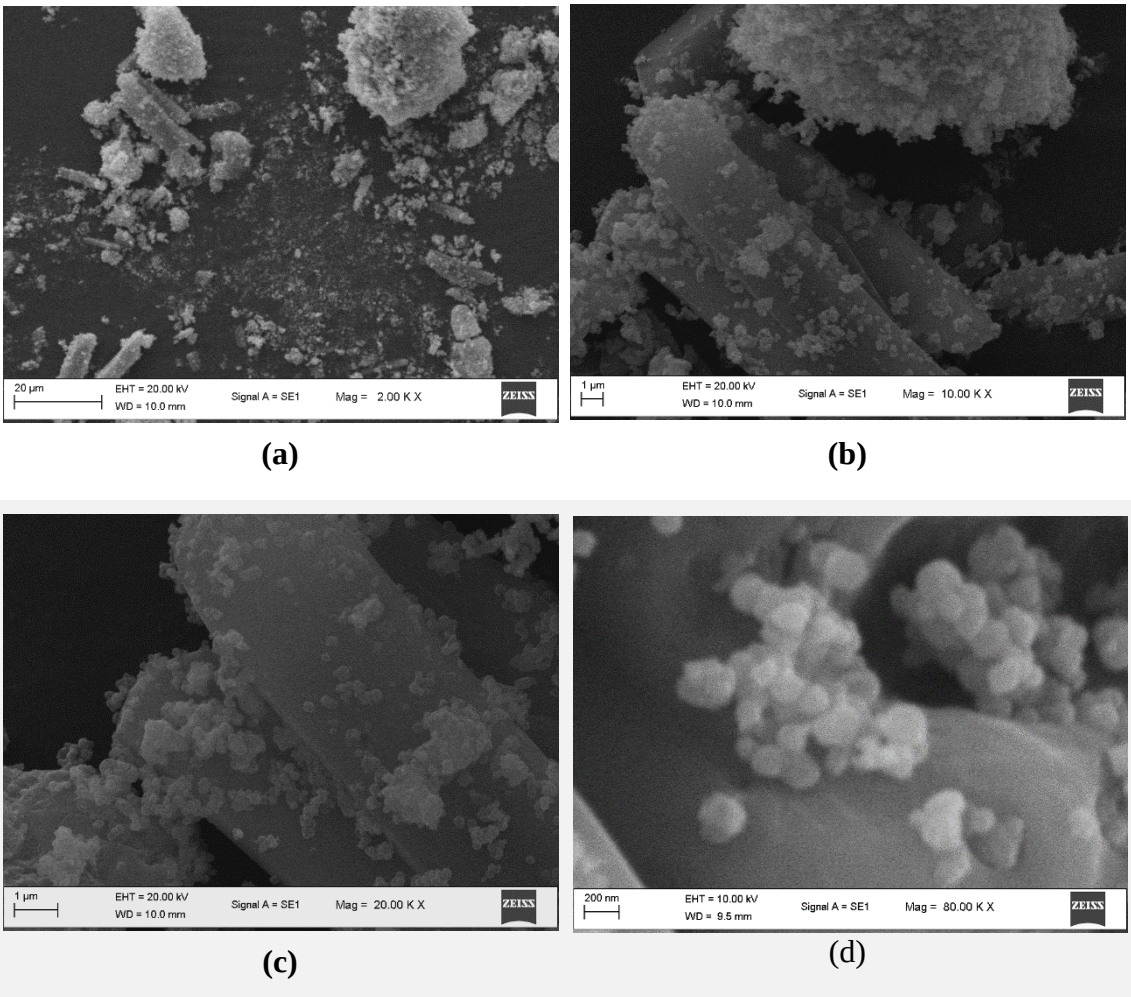

Figure 4.2 SEM images for sample (2) with different magnifications (a) 2.000 X, (b) 10.000 X, (c) 20.000 X and (d) 80.000 x

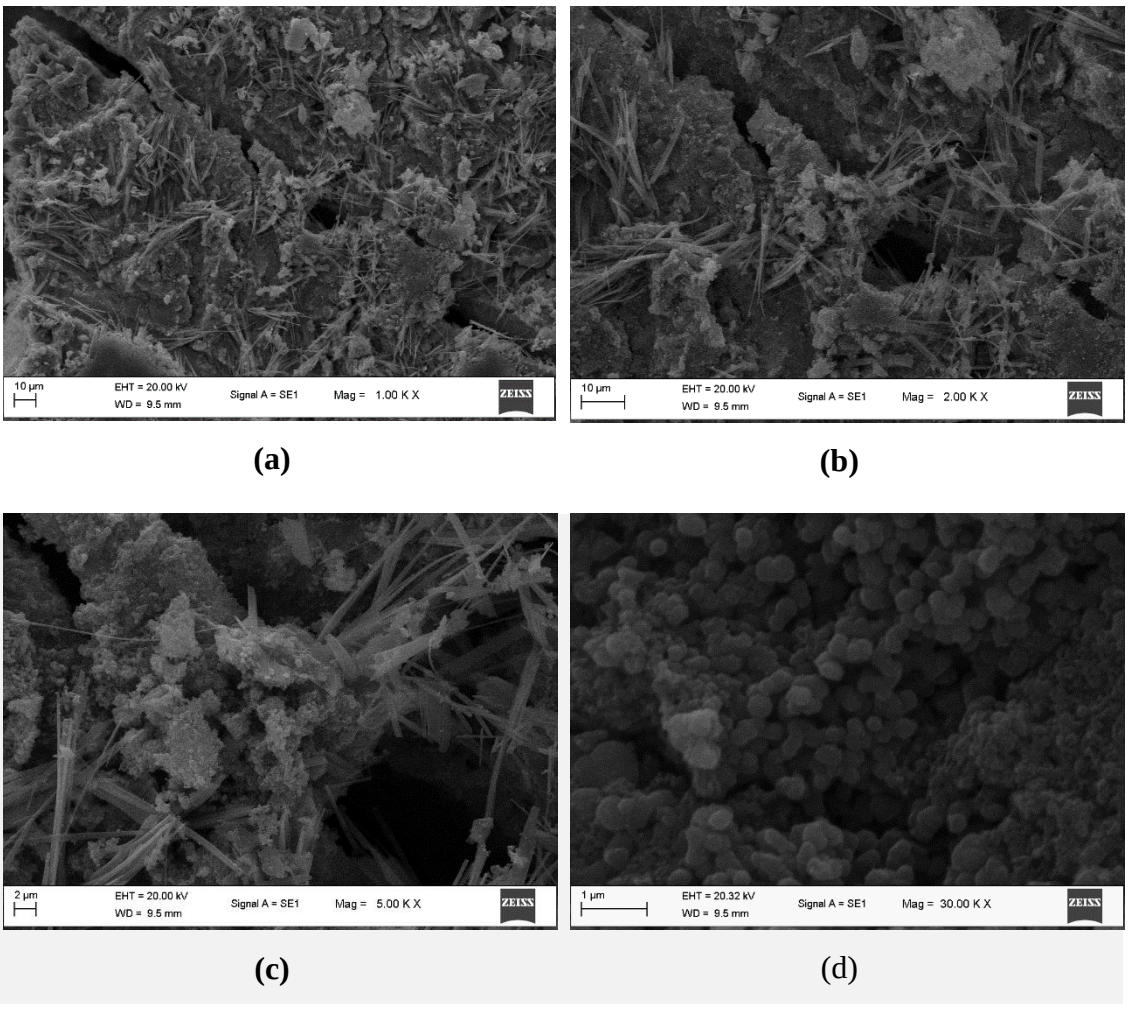

(a) **(b)**

(c) (d)

Figure 4.3 SEM images for sample (3) with different magnifications (a) 1.000 X, (b) 2.000 X, (c) 5.000 X and (d) 30.000 X

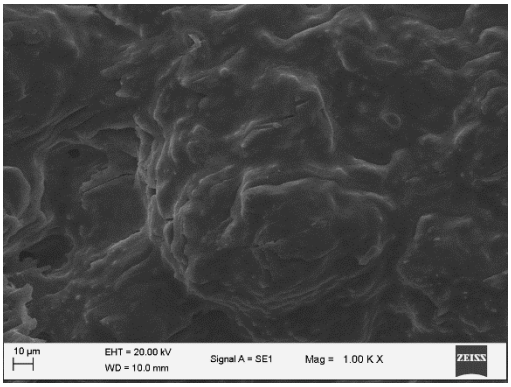

(a)

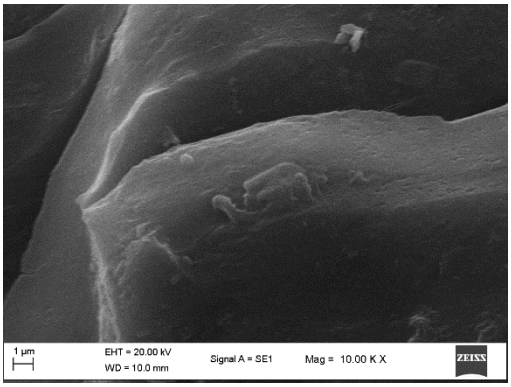

(b)

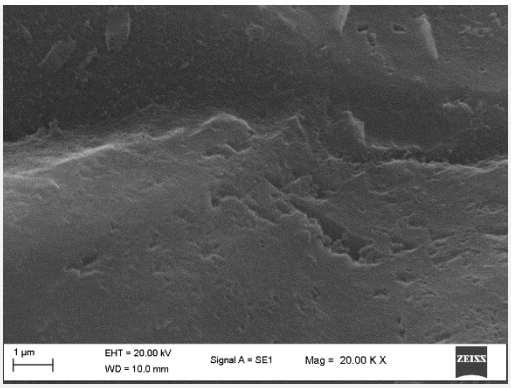

(c)

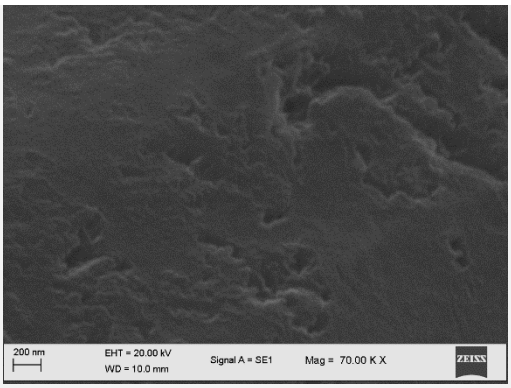

(d)

Figure 4.4 SEM images for sample (4) with different magnifications (a) 1.000 X, (b) 10.000 X, (c) 20.000 X and (d) 70.000 X

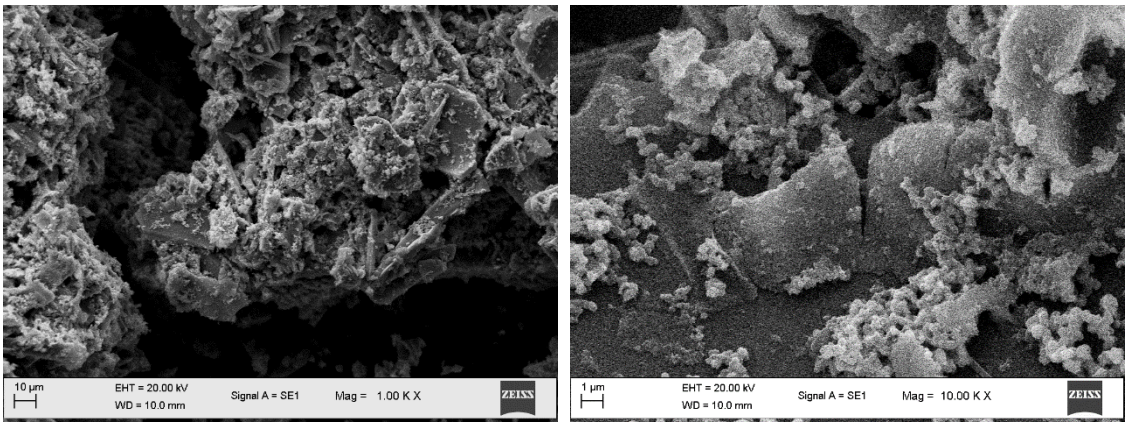

(a) **(b)**

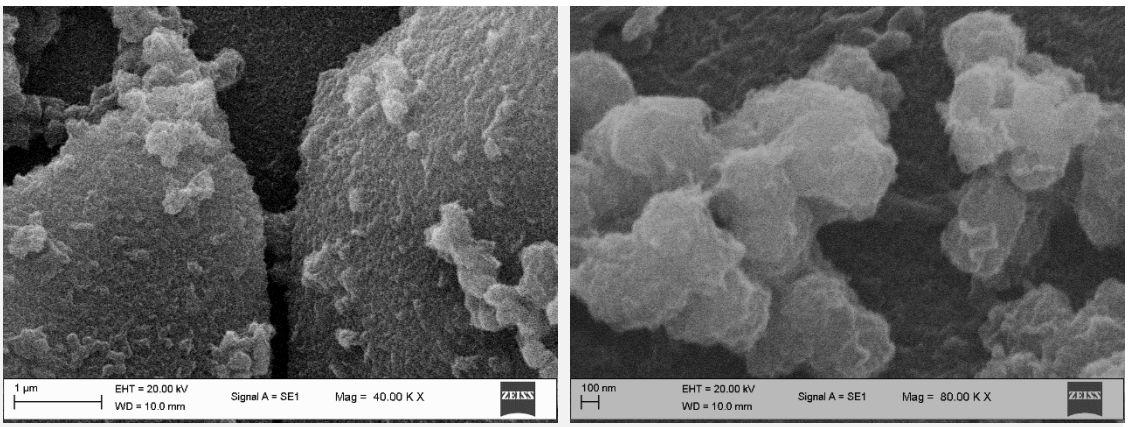

(c) (d)

Figure 4.5 SEM images for sample (5) with different magnifications (a) 1.000 X, (b) 10.000 X, (c) 40.000 X and (d) 80.000 X

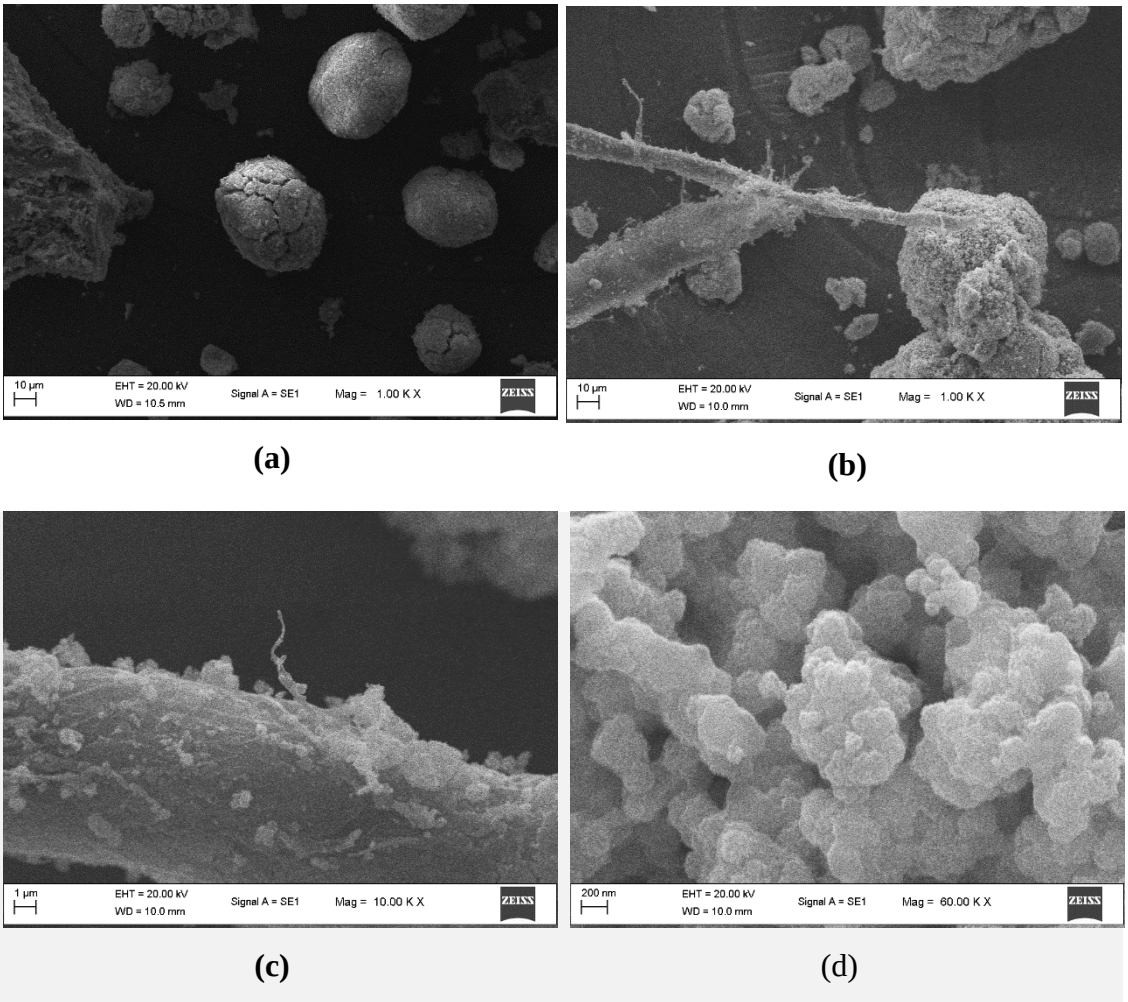

Figure 4.6 SEM images for sample (6) with different magnifications (a) 1.000 X, (b) 1.000 X, (c) 10.000 X and (d) 60.000 X

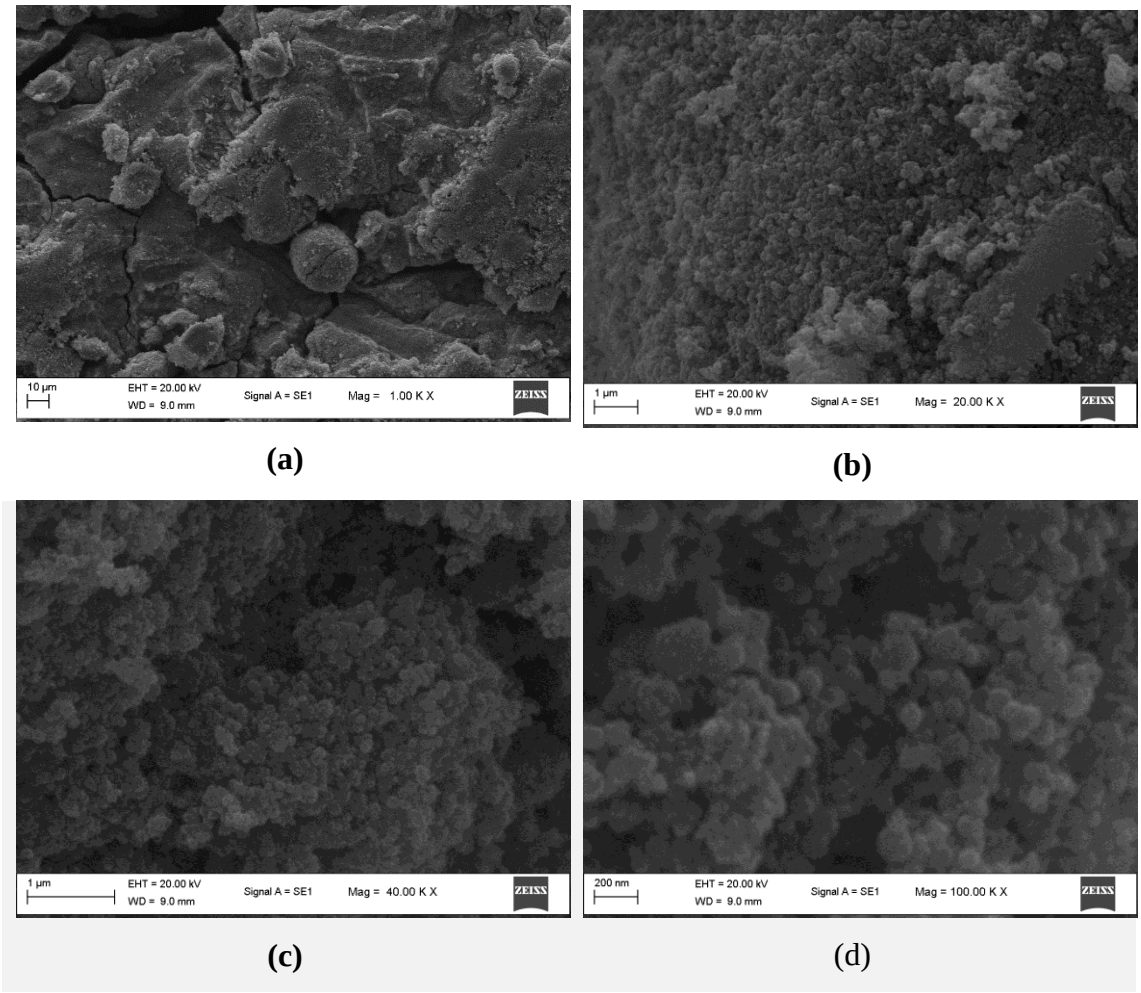

Figure 4.7 SEM images for sample (7) with different magnifications (a) 1.000 X, (b) 20.000 X, (c) 40.000 X and (d) 100.000 X

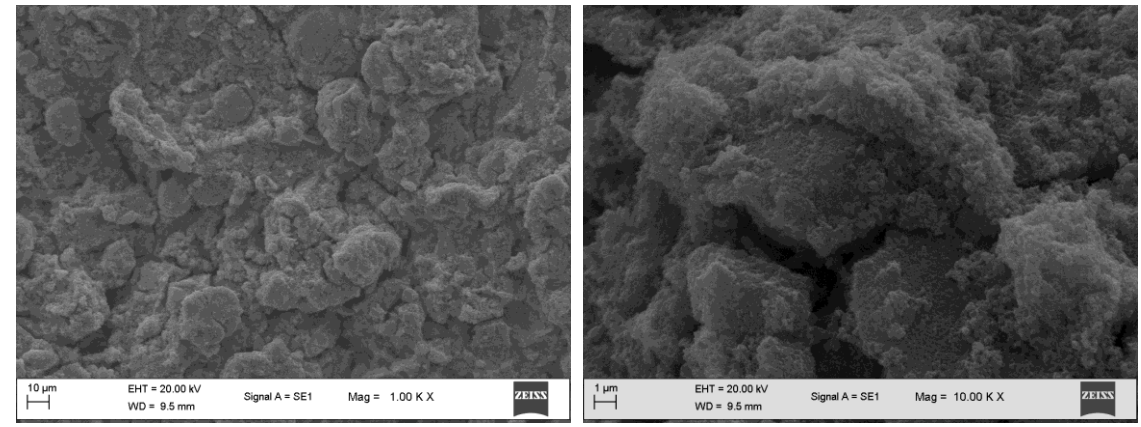

(a) **(b)**

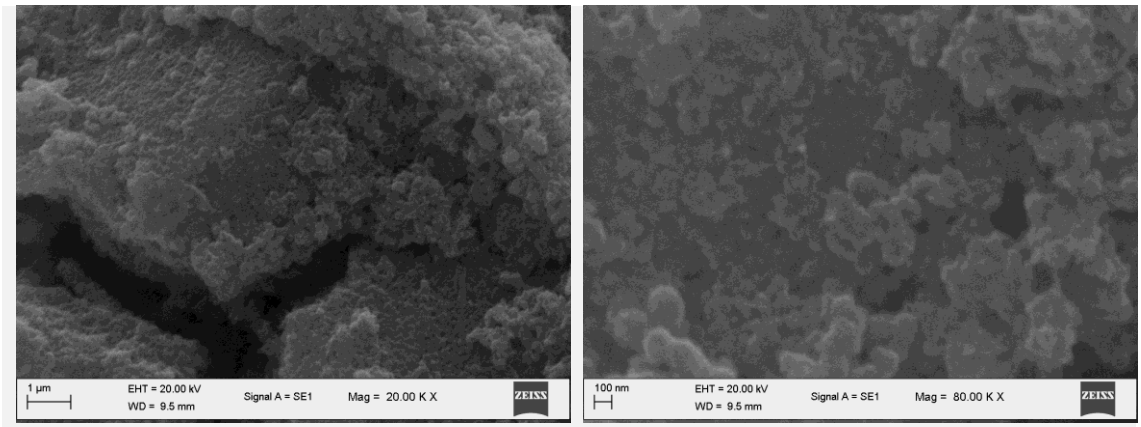

(c) (d)

Figure 4.8 SEM images for sample (8) with different magnifications (a) 1.000 X, (b) 10.000 X, (c) 20.000 X and (d) 80.000 X

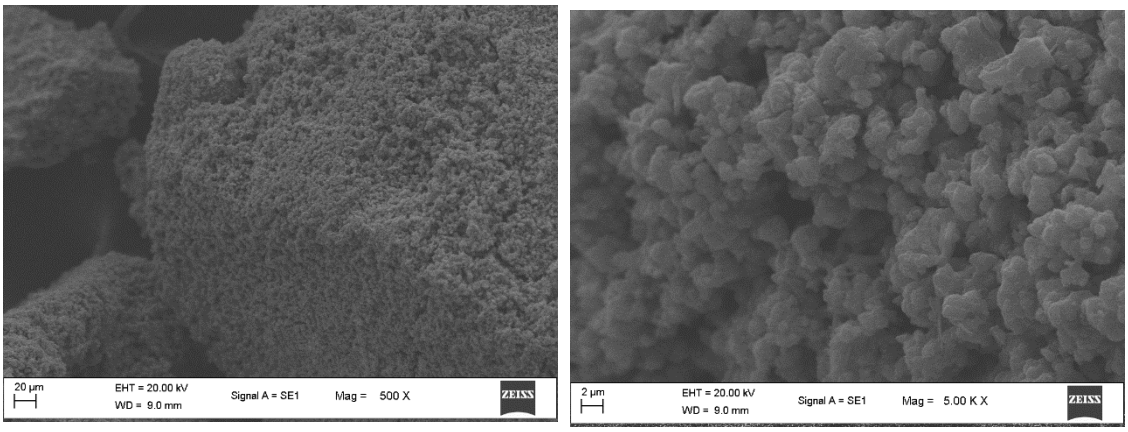

Figure 4.9 SEM images for sample (9) with different magnifications (a) 500 X, (b) 5.000 X, (c) 40.000 X and (d) 100.000 X

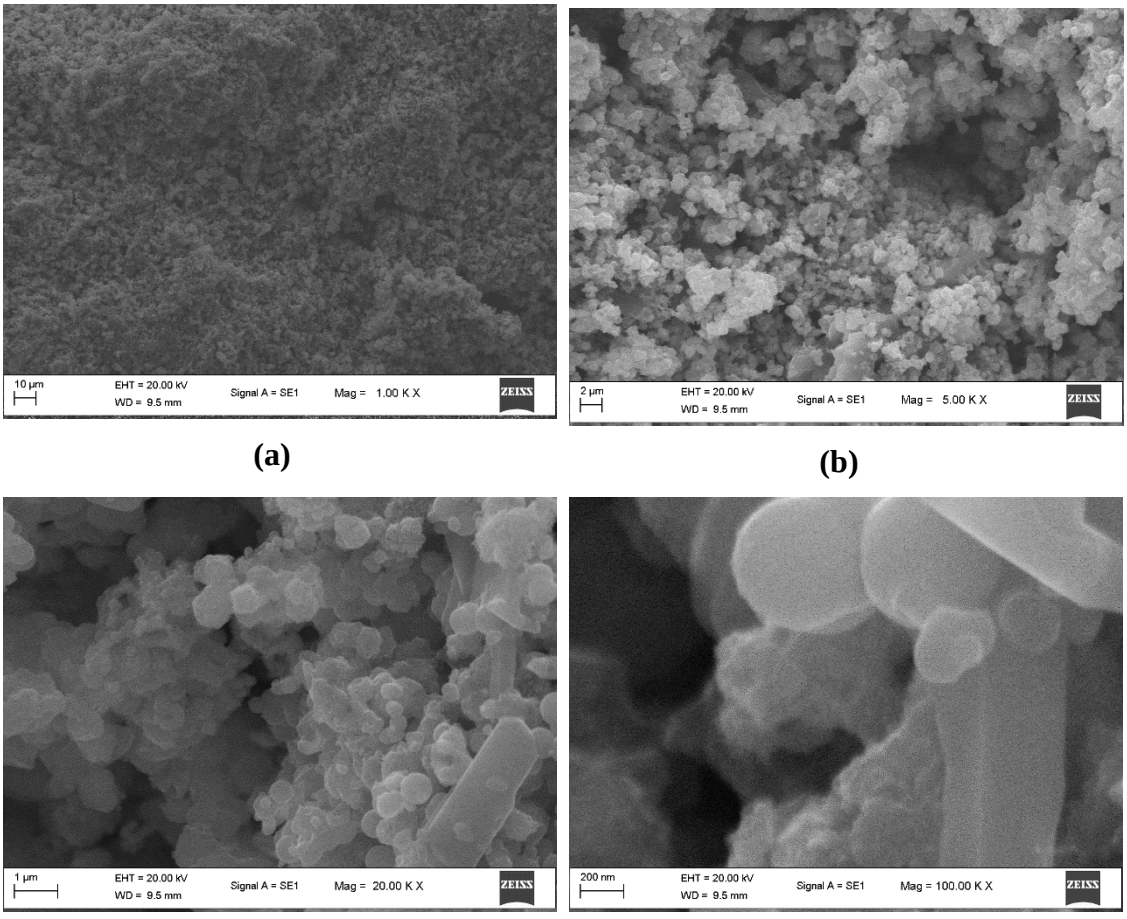

(a) **(b)**

(c) (d)

Figure 4.10 SEM images for sample (10) with different magnifications (a) 1.000 X, (b) 5.000 X, (c) 20.000 X and (d) 100.000 X

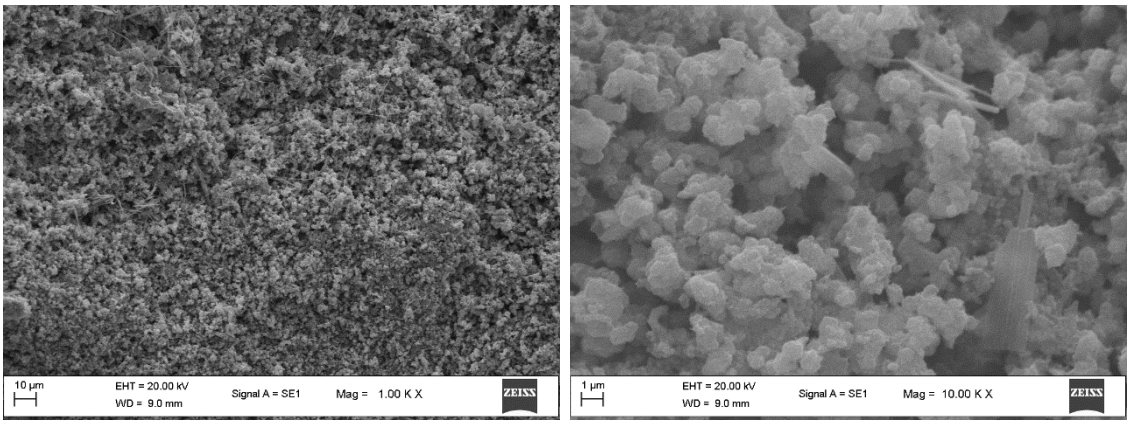

(a) **(b)**

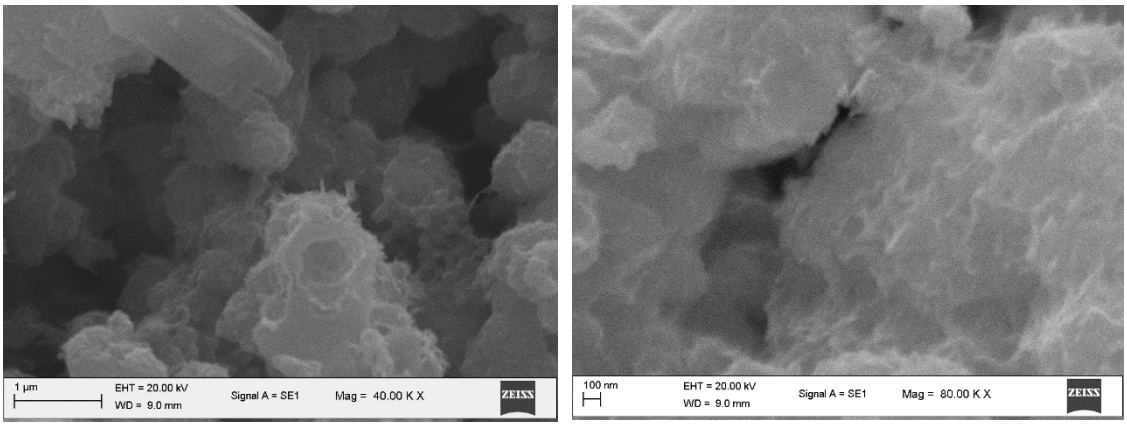

(c) (d)

Figure 4.11 SEM images for sample (11) with different magnifications (a) 1.000 X, (b) 10.000 X, (c) 40.000 X and (d) 80.000 X

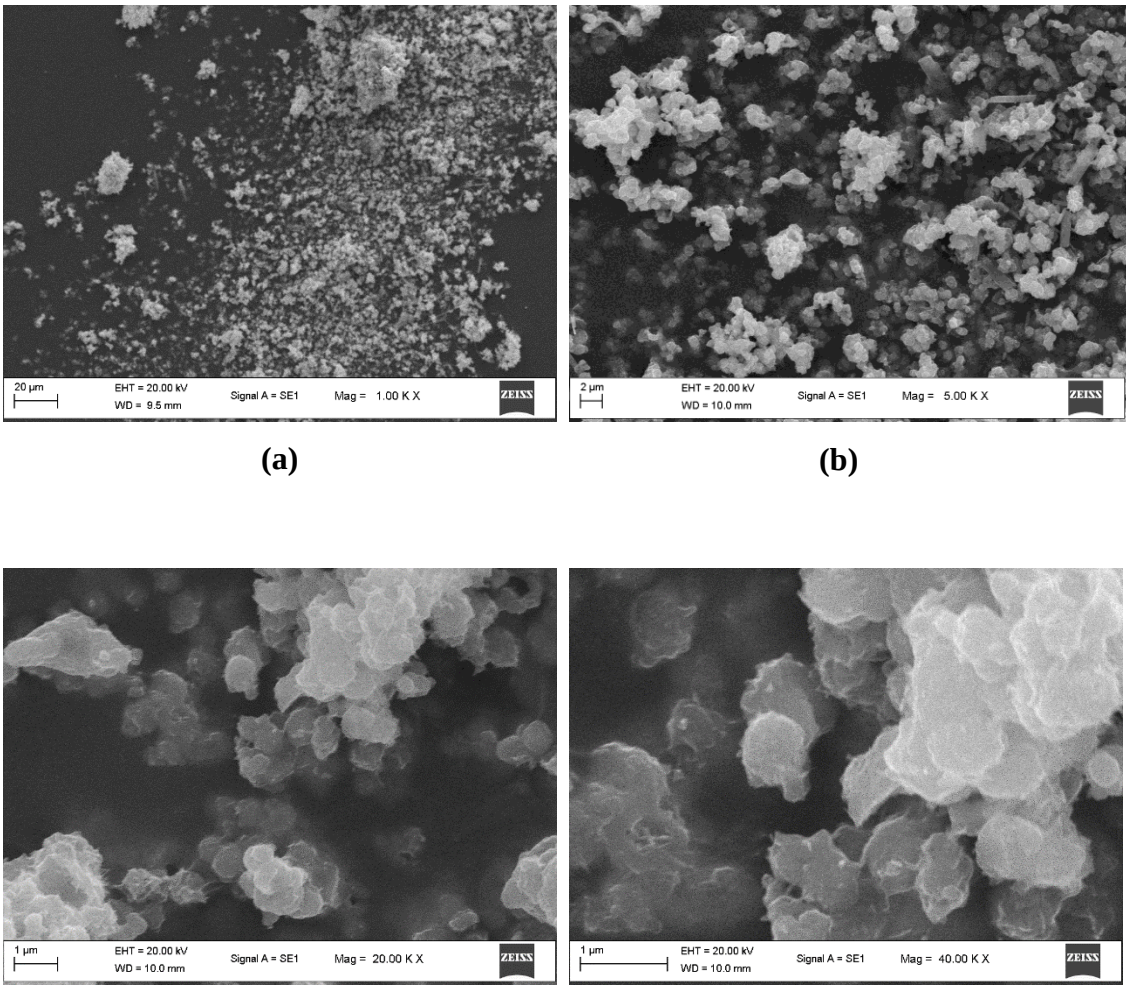

(a) **(b)**

(c) (d)

Figure 4.12 SEM images for sample (12) with different magnifications (a) 1.000 X, (b) 5.000 X, (c) 20.000 X and (d) 40.000 X

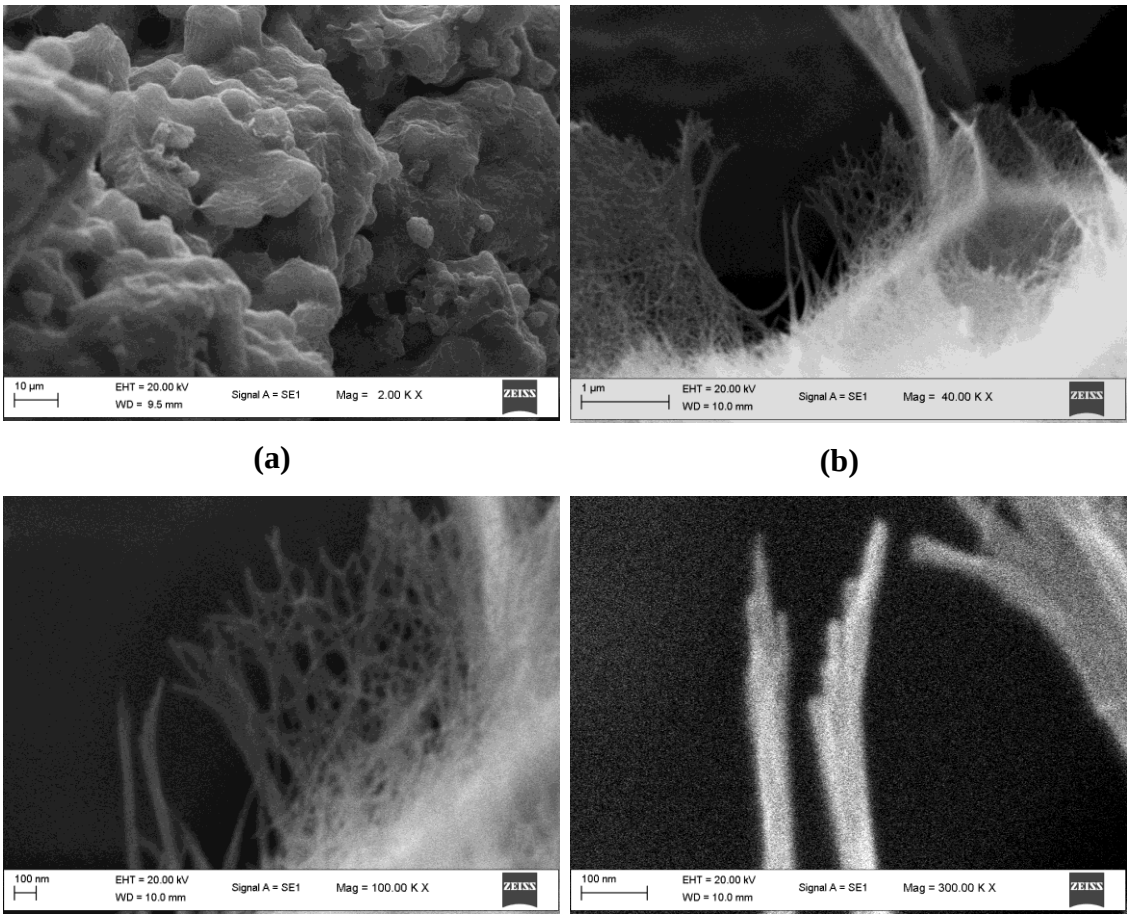

(a) **(b)**

(c) (d)

Figure 4.13 SEM images for sample (13) with different magnifications (a) 2.000 X, (b) 40.000 X, (c) 100.000 X and (d) 300.000 X

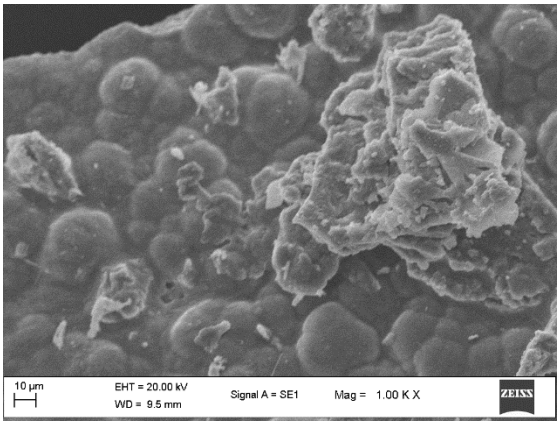

(a)

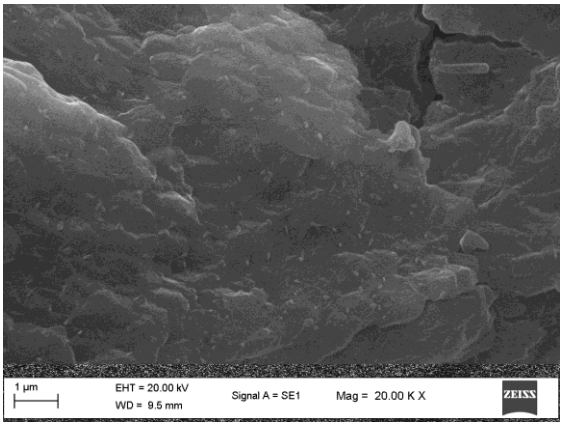

(b)

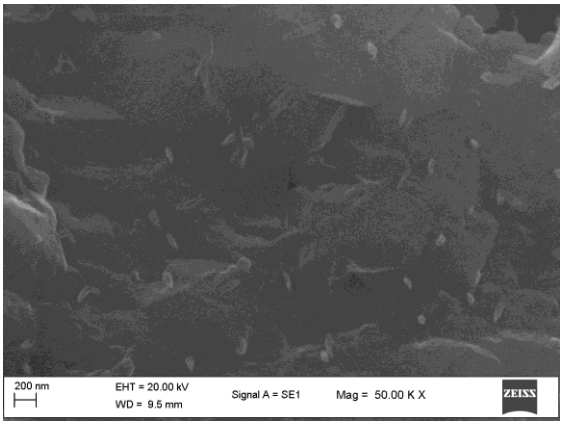

(c)

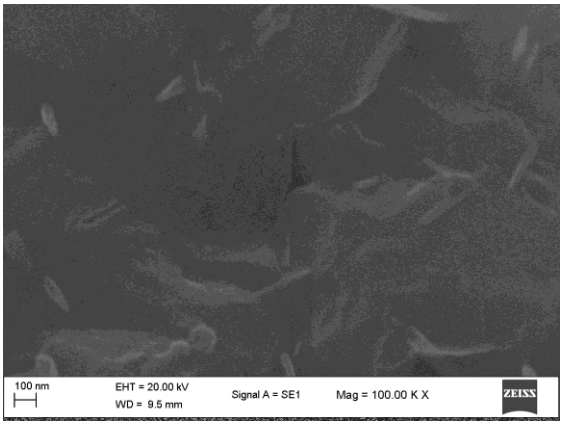

(d)

Figure 4.14 SEM images for sample (14) with different magnifications (a) 1.000 X, (b) 20.000 X, (c) 50.000 X and (d) 100.000 X

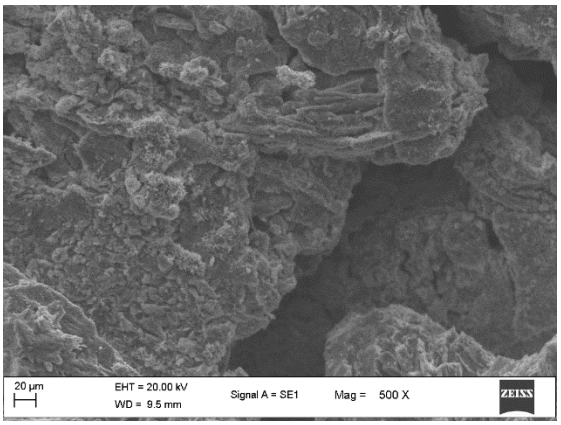

(a)

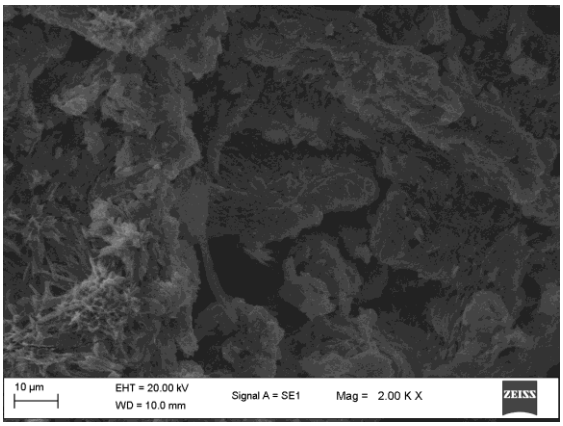

(b)

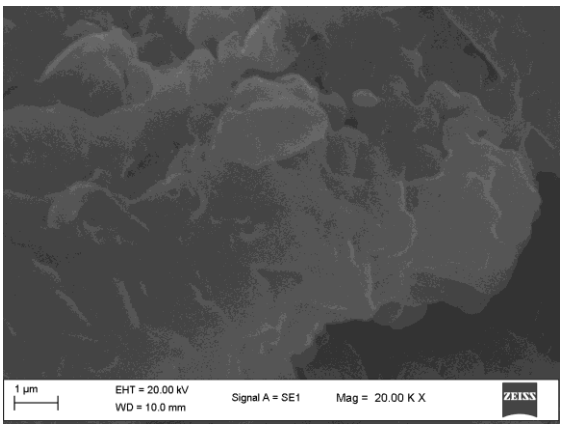

(c)

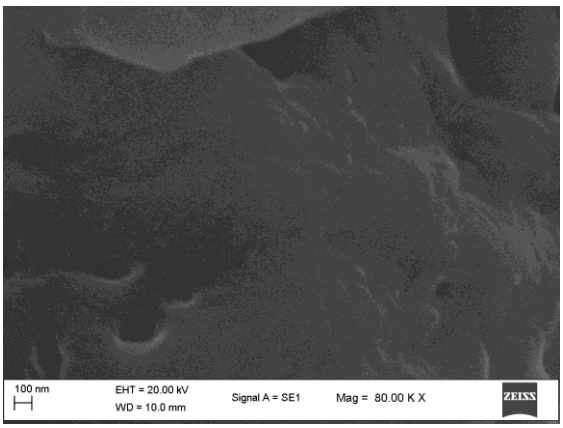

(d)

Figure 4.15 SEM images for sample (15) with different magnifications (a) 500 X, (b) 2.000 X, (c) 20.000 X and (d) 80.000 X

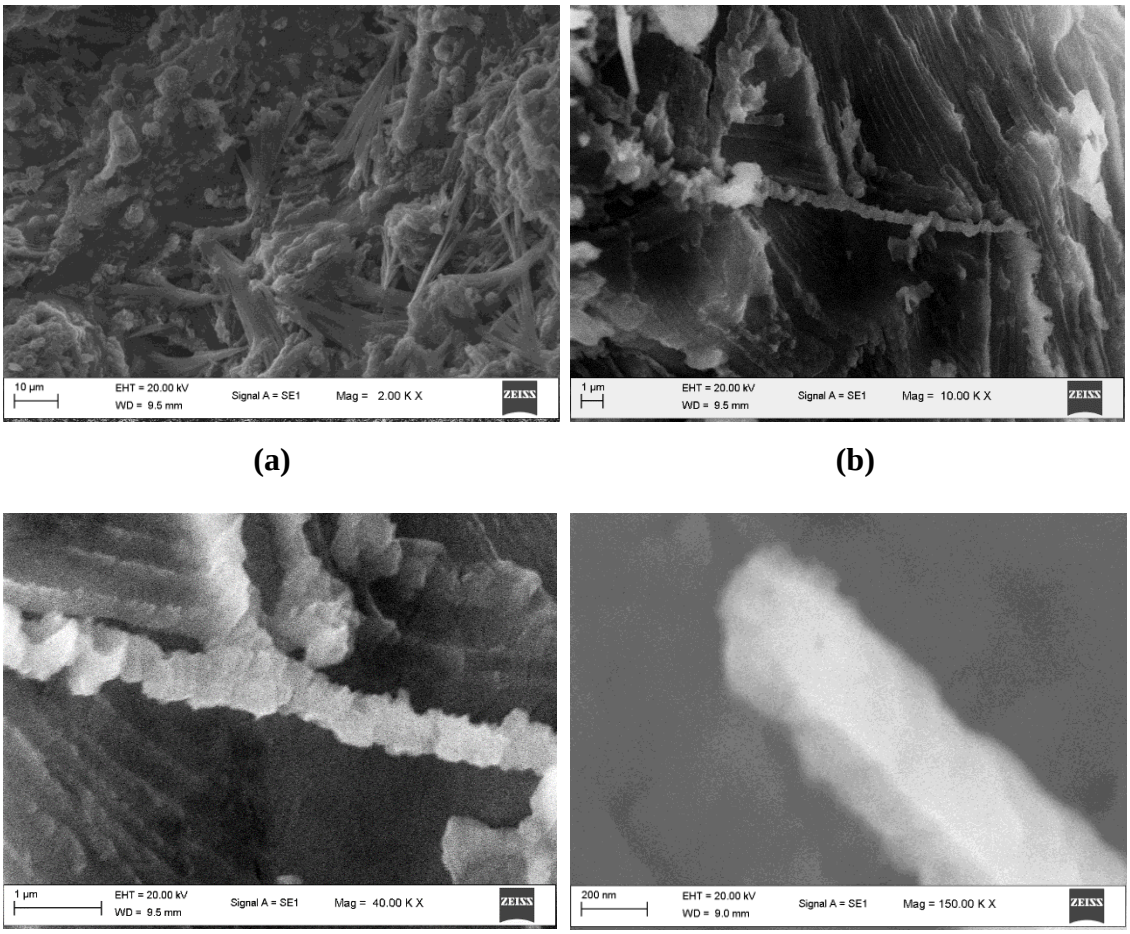

(a) **(b)**

(c) (d)

Figure 4.16 SEM images for sample (16) with different magnifications (a) 2.000 X, (b) 10.000 X, (c) 40.000 X and (d) 150.000 X

In order to apply Taguchi analysis, numeric values given for each sample by examining SEM images. For example, best TNT pictures are marked as 4 point for *perfect*, 3 point for *better* 2 point for *good* and 1 point for *poor*.

Optimum conditions determined by using Larger is Better S/N formula. Minitab software were used for all Taguchi calculations. Figure 4.17 shows effect of each parameter on SEM images.

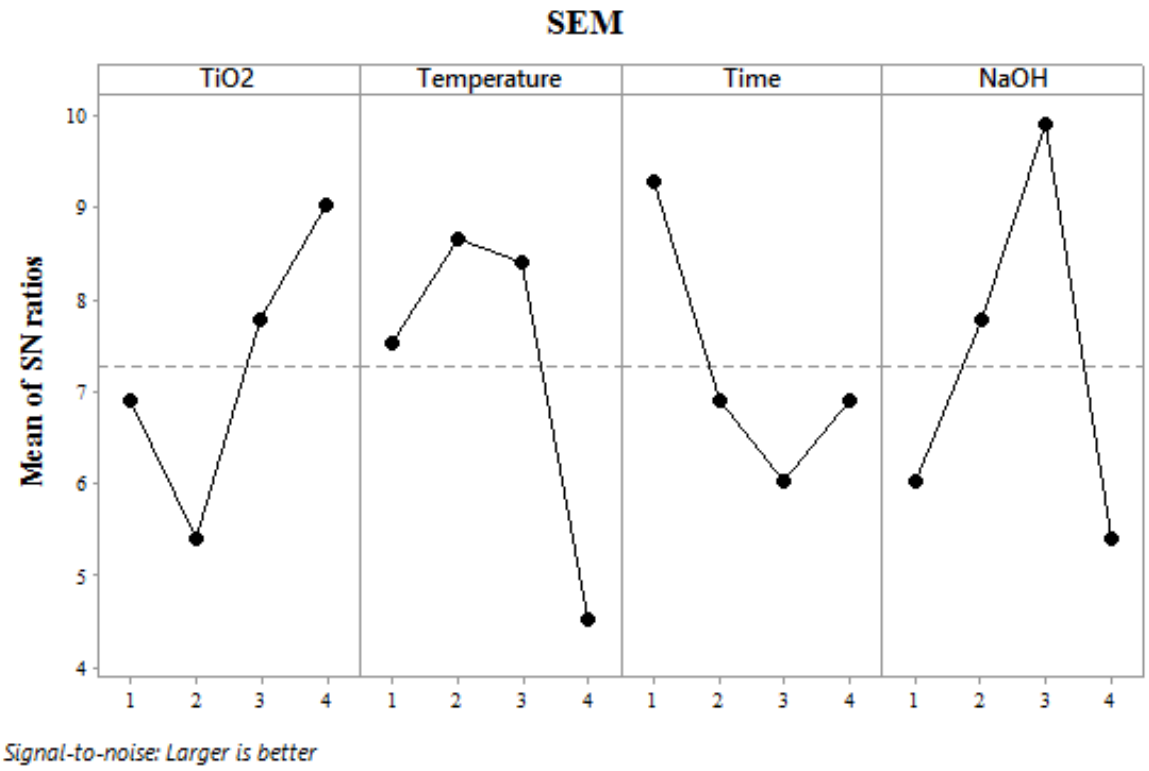

Figure 4.17 Taguchi analysis for TNT production by SEM images

Table 4.1 shows the optimum levels determined by Taguchi method. From the table it can be seen that level 4 TiO2 type, level 2 temperature value, level 1 time value and level 3 NaOH concentration value results the best TNT arrangement.

Table 4.1 Optimum levels for SEM images by Taguchi method

Parameter	**Level**
TiO_2 Type	4
Temperature	2
Time	1
NaOH Concentration	3

4.2. BET Analysis

BET analysis is carried out to discover BET surface area (m^2/g), pore sizes and pore volumes. (Micromeritics – ASAP)

BET surface area is another important parameter for DSSC performance, because it directly effect the dye loading capacity of TNT, therefore it is expected to be the high as much as possible.

Pore sizes or pore volumes are important because they have a great negative effect on electron carrying. Herewith, it is they are supposed to be minimum.

In the following subchapters BET surface area, pore size and pore volume results will be presented individually.

4.2.1 BET Surface Area

Table 4.2 and Table 4.3 show the results for BET surface area.

Table 4.2 BET surface area of raw materials

Raw Material Type	**BET Surface Area (m^2/g)**
Degussa P25	42,4761
Anatase	7,7038
Rutile	7,1037
Ultrasounded TiO_2	8,4620

Table 4.3 BET surface area of samples

Sample Number	**BET Surface Area (m^2/g)**	**Sample Number**	**BET Surface Area (m^2/g)**
1	90,8421	9	2,8528
2	11,8502	10	4,2360
3	18,8601	11	5,6907
4	4,3897	12	4,7866
5	7,3444	13	136,6948
6	211,1253	14	9,3652
7	16,4703	15	8,4006
8	10,1720	16	2,3691

It can be seen from BET surface area values that, Degussa P25 has already high surface area and other raw materials have almost identical surface areas. Therefore, BET measurements should be considered in this respect.

If we would like to analyse each raw material separately, we state following comments.

- For the samples 1-4 (which have been originated from Degussa P25), it can be seen that surface area inversely proportional with temperature, NaOH concentration and time. The decrease in surface area might be because of agglomeration.
- For the samples 5-8 (which have been originated from anatase TiO_2), it can be observed that sample 6 has the highest surface area. By considering SEM results and BET surface area together, it can be said that the most effective parameter is short time.
- For the samples 9-12 (which have been originated from rutile TiO_2) BET surface area has observed to be decreased for each sample comparing to raw rutile. Raw rutile has surface area of 7,1036 m^2/g. After the experiments BET surface area for rutile based samples ranged from 2,8528 m^2/g to 4,7866 m^2/g. That means

rutil materials tend to agglomerate under high temperature, high NaOH concentration and long time conditions.

- For the last four samples, (which is originated from ultrasounded anatase TiO_2 materials), 13 seem to have highest BET surface area. This result is thought to be due to low temperature.

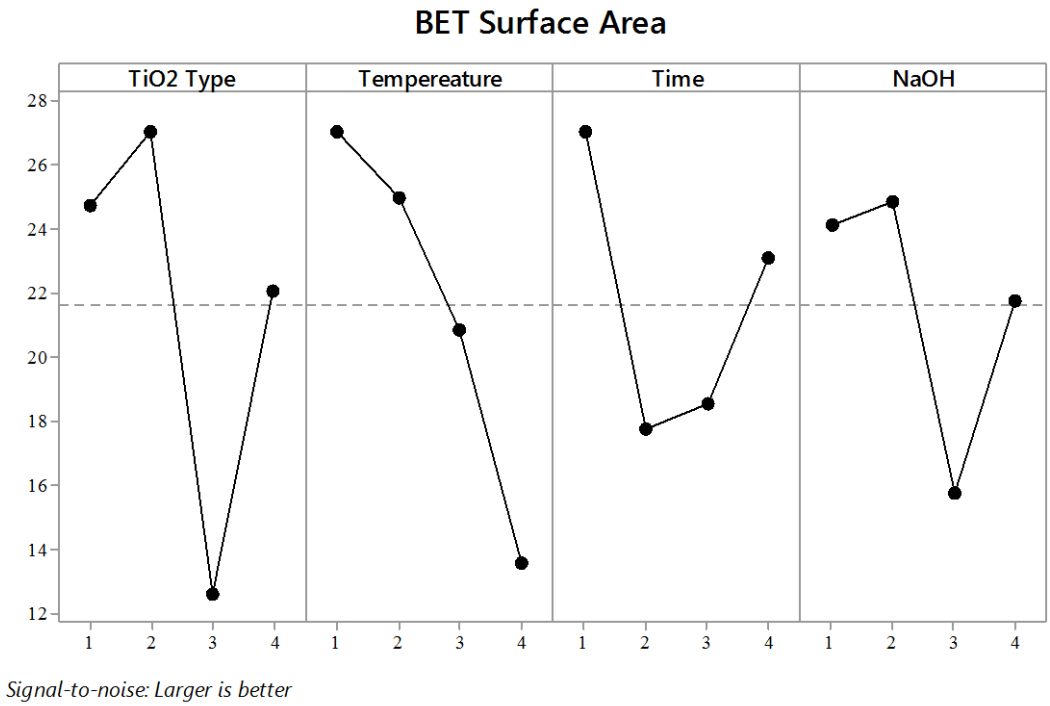

Figure 4.18 Taguchi analysis for BET surface area

For an overall comparison, Table 4.4 can be summarized. From the table it can be said that level 2 TiO_2 type, level 1 temperature value, level 1 time value and level 2 NaOH concentration value results the highest BET surface area results.

Table 4.4 Optimum levels for BET surface area by Taguchi method

Parameter	**Level**
TiO_2 Type	2
Temperature	1
Time	1
NaOH Concentration	2

4.2.2 Pore Volumes

Table 4.5 and Table 4.6 show the pore volumes of raw materials and samples, respectively.

Table 4.5 Pore volumes of raw materials

Raw Material Type	**Pore Volumes (cm^3/g)**
Degussa P25	0,1400
Anatase	0,02630
Rutile	0,0501
Ultrasounded TiO_2	0,0304

Table 4.6 Pore volumes of samples

Sample Number	**Pore Volumes (cm^3/g)**	**Sample Number**	**Pore Volumes (cm^3/g)**
1	0,2867	9	0,0107
2	0,0521	10	0,0150
3	0,1001	11	0,0226
4	0,0167	12	0,0149
5	0,0527	13	0,4462
6	0,1422	14	0,0477
7	0,0675	15	0,0430
8	0,0513	16	0,0139

When considering raw materials, pore volumes of Degussa P25, anatase, rutile and ultrasounded TiO_2 are ranged between 0,02630 to 0,1400 cm^3/g.

- For samples 1-4, (which have been originated from Degussa P25), pore volumes are changed irregular. It depends on the parameters of experiment. If we would

like to make an overall comment, it can be said that, temperature has found to be most effective parameter for this series.

- For samples 5-8 (which have been originated from anatase TiO_2), pore volumes are almost identical for 5, 7 and 8, while 6 has the highest volumes among the others in this series. The reason of this situation is thought to depend on the high concentration of NaOH. This result might be because of the large atomic volume of Na^+ ions.
- For samples 9-12 (which have been originated from rutile TiO_2), there is no significant effect of temperature, NaOH concentration or time on pore volume changing.
- For samples 13-16 (which have been originated from ultrasounded TiO_2), 14, 15 and 16 are almost identical while 13 has the greatest pore volume due to temperature.

Figure 4.19 shows the effect of each parameter by Taguchi analysis for pore volumes. As a difference from SEM analysis, smaller is better signal-to-noise ratio have been used to find out the level that makes pore volume smallest for each parameter.

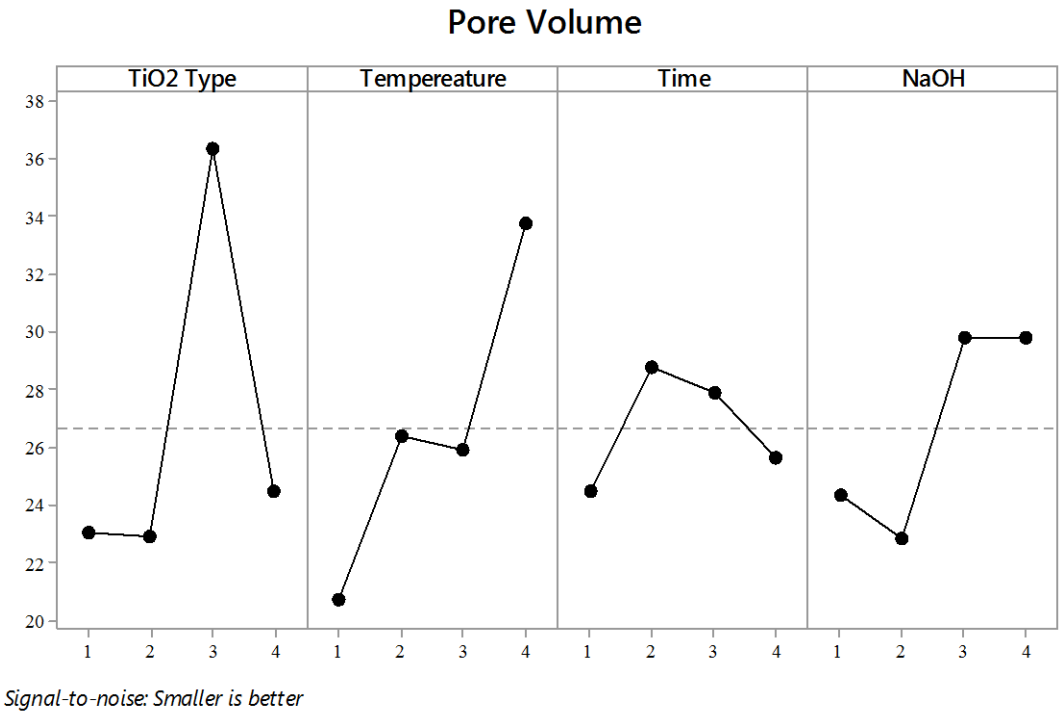

Figure 4.19 Taguchi analysis for pore volumes

For an overall comparison, Table 4.7 can be summarized. From the table it can be said that level 3 TiO_2 type, level 4 temperature value, level 2 time value and level 3 and 4 NaOH concentration value provides the smallest pore volume results.

Table 4.7 Optimum levels for smallest pore volume by Taguchi method

Parameter	**Level**
TiO_2 Type	3
Temperature	4
Time	2
NaOH Concentration	3,4

4.2.3 Pore Sizes

Table 4.8 and Table 4.9 show the pore sizes of raw materials and samples, respectively.

Table 4.8 Pore sizes of raw materials

Sample Number	**Pore Size (nm)**
Degussa P25	12,6032
Anatase	13,5152
Rutile	23,0976
Ultrasounded	14,3780

Table 4.9 Pore sizes of samples

Sample Number	Pore Size (nm)	Sample Number	Pore Size (nm)
1	12,62556	9	15,0556
2	17,60381	10	14,1847
3	21,23246	11	15,9287
4	14,7402	12	12,4892
5	28,7553	13	13,0403
6	2,6943	14	20,3944
7	16,9921	15	20,4981
8	20,1943	16	23,6200

Pore size is one of the most important control parameters for TNT production. In this study,

- For samples 1-4, (which have been originated from Degussa P25), the pore size shows irregular distribution. None of the parameters shows significant proportional effect on pore size.
- For samples 5-8 (which have been originated from anatase TiO_2), each sample except 6 are tend to have greater pore size than the raw material. For pore size value of sample 6 it can be said that short time and medium concentration values are the reason of having dramatic small pore size.
- For samples 9-12 (which have been originated from rutile TiO_2), four of the samples are showing obvious decrease. This is probably due to agglomeration of rutile based samples.
- For samples 13-16 (which have been originated from ultrasounded TiO_2), it can be said that all of the samples have increasing pore size except 13. For sample 13 long time condition might be the reason for having low pore size.

Figure 4.20 shows the effect of each parameter by Taguchi analysis for pore volumes. Similar to pore volume analysis, smaller is better signal-to-noise ratio have been used to find out the level that makes pore size smallest for each parameter.

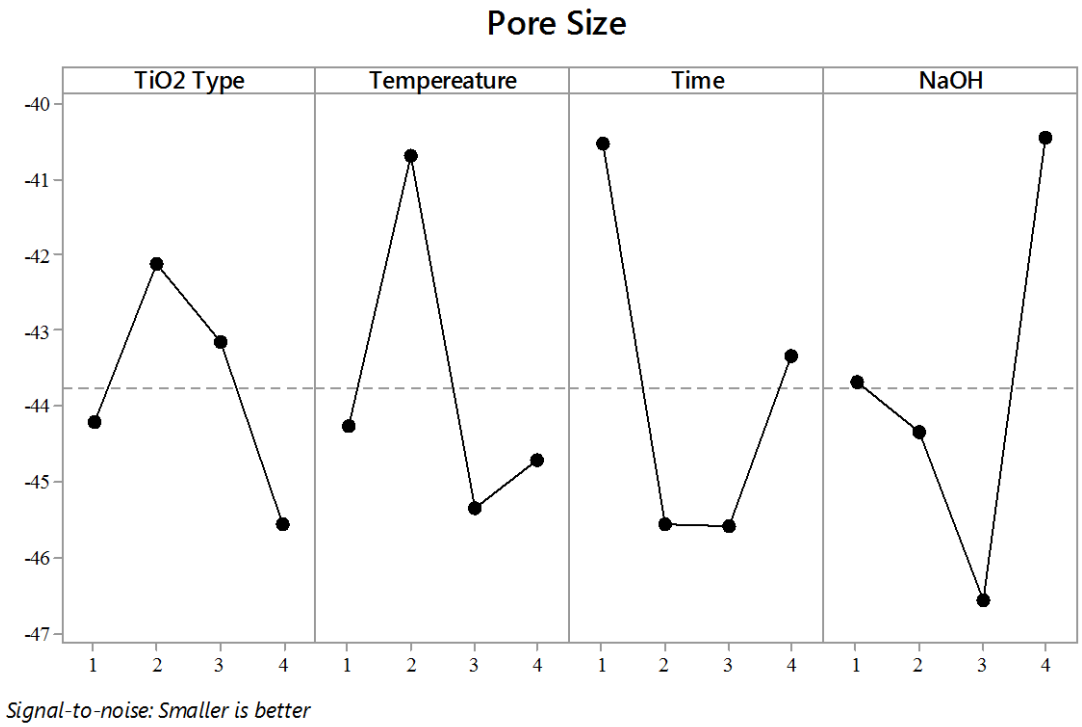

Figure 4.20 Taguchi analysis for pore sizes

For an overall comparison, Table 4.10 can be summarized. From the table it can be said that level 2 TiO_2 type, level 2 temperature value, level 1 time value and level 4 NaOH concentration value provides the smallest pore volume results.

Table 4.10 Optimum levels for smallest pore size by Taguchi method

Parameter	**Level**
TiO_2 Type	2
Temperature	2
Time	1
NaOH Concentration	4

4.3 Crystal Structure

Crystal structure of TNT's is another important parameter for DSSC performance. It is known that, it is most effected by temperature.

XRD measurements have been carried out in Chemical Engineering Department of Yildiz Technical University (Philips PANanalytical X-Ray Diffractometer). Results have been anlyzed with Xpert High Score Plus software.

In the following pages, bunched XRD results will be given that grouped by each raw material. Afterwards, one of the distinctive sample will be shown with corresponding crystal peaks in order to provide better understanding to overall graphs.

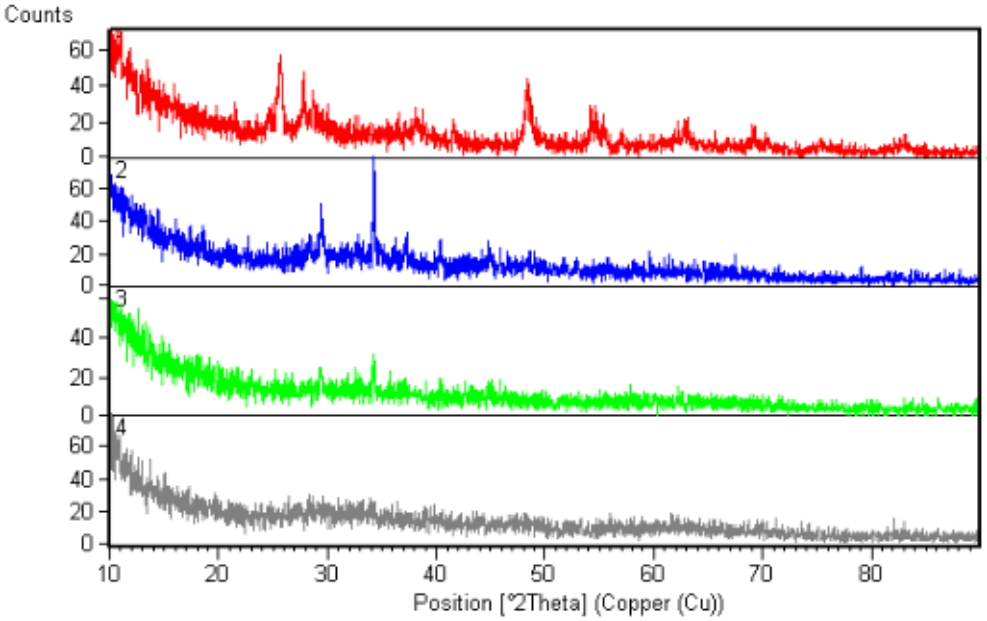

Figure 4.21 XRD Results for samples 1, 2, 3 and 4

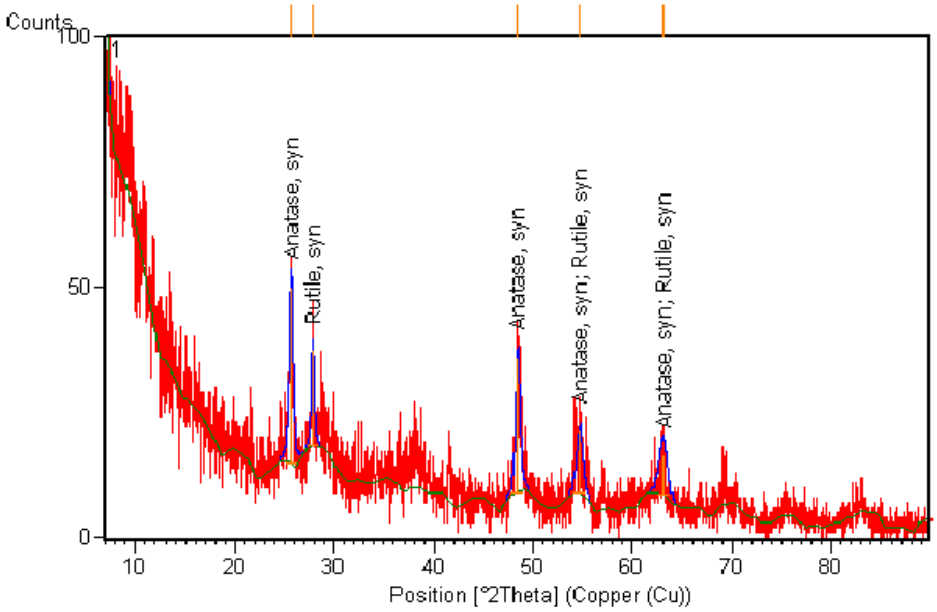

Figure 4.22 XRD Results for sample 1

For samples 1-4, (which have been originated from Degussa P25); it can be said that as temperature, reaction time and NaOH concentration increase, the structure changes from crystal to amorphous form.

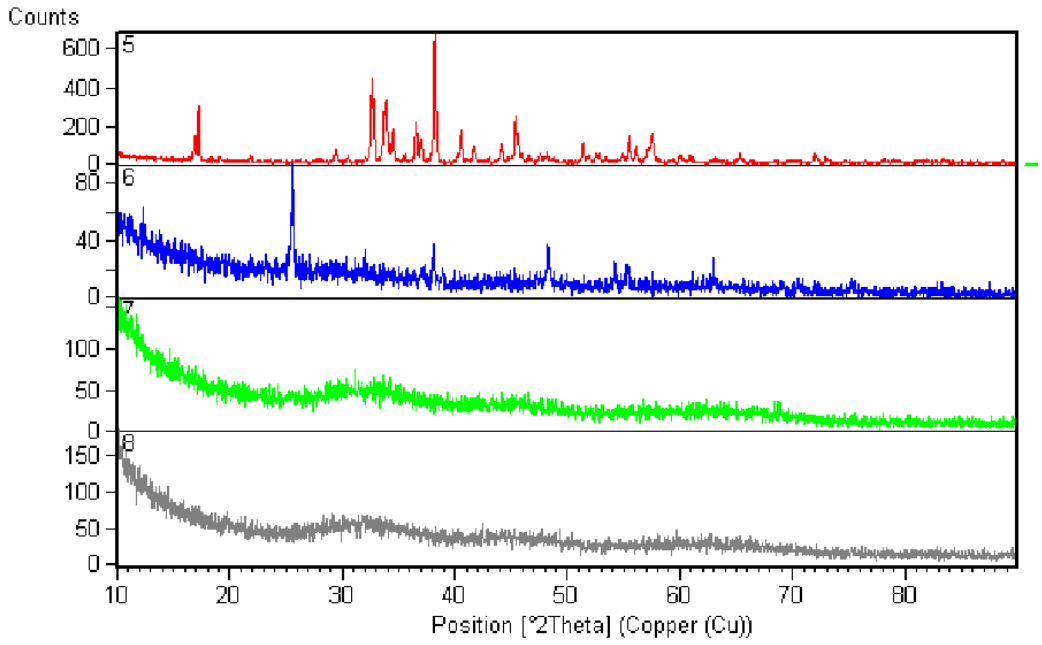

Figure 4.23 XRD Results for samples 5, 6, 7 and 8

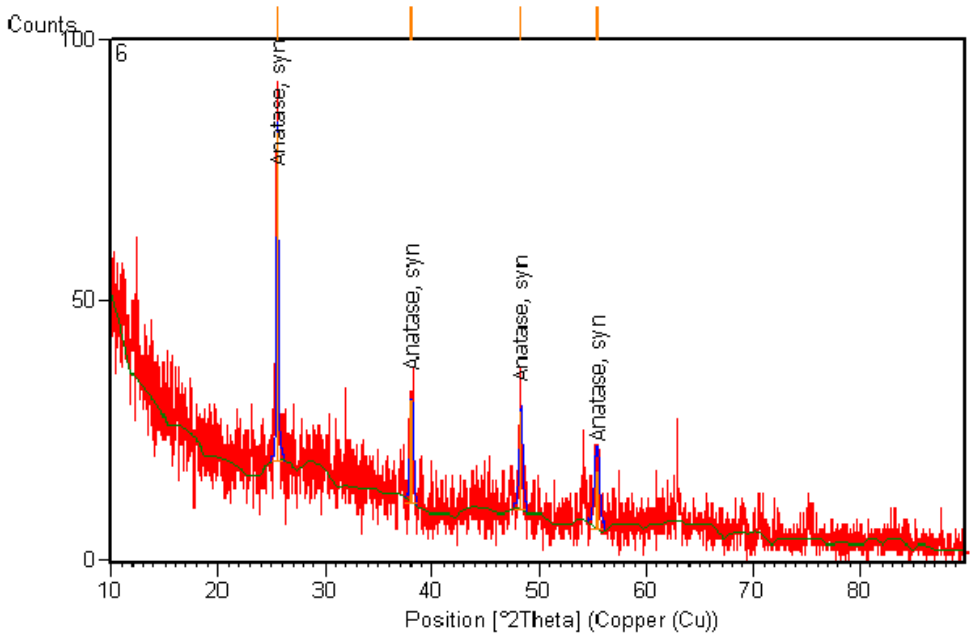

Figure 4.24 XRD Results for sample 6

- For samples 5-8 (which have been originated from anatase TiO_2), the dominant effect is found to be temperature and with increasing temperature crystal structure changes to amorphous form.

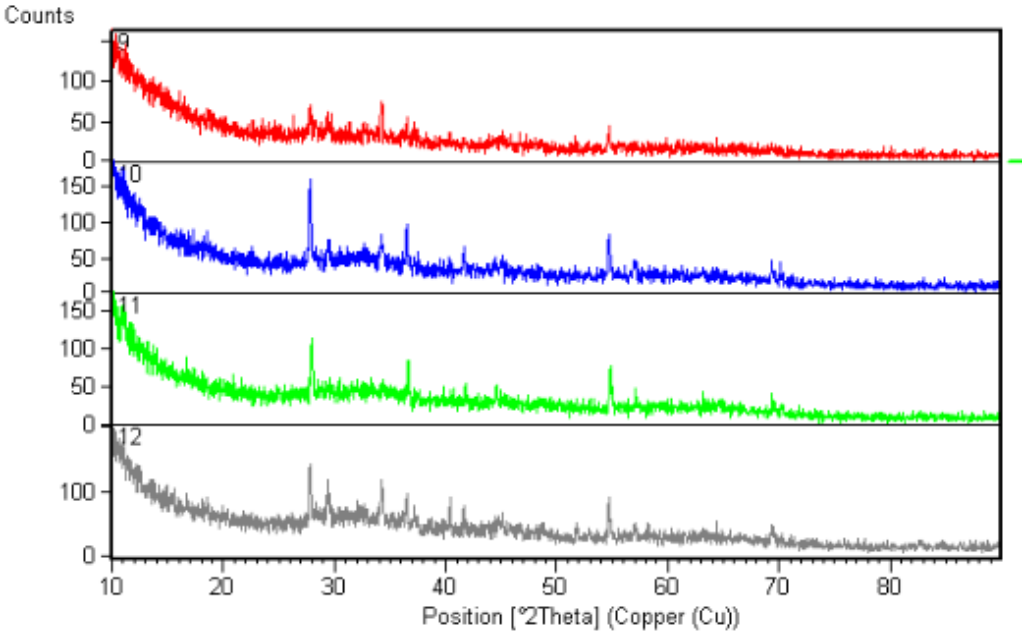

Figure 4.25 XRD Results for samples 9, 10, 11 and 12

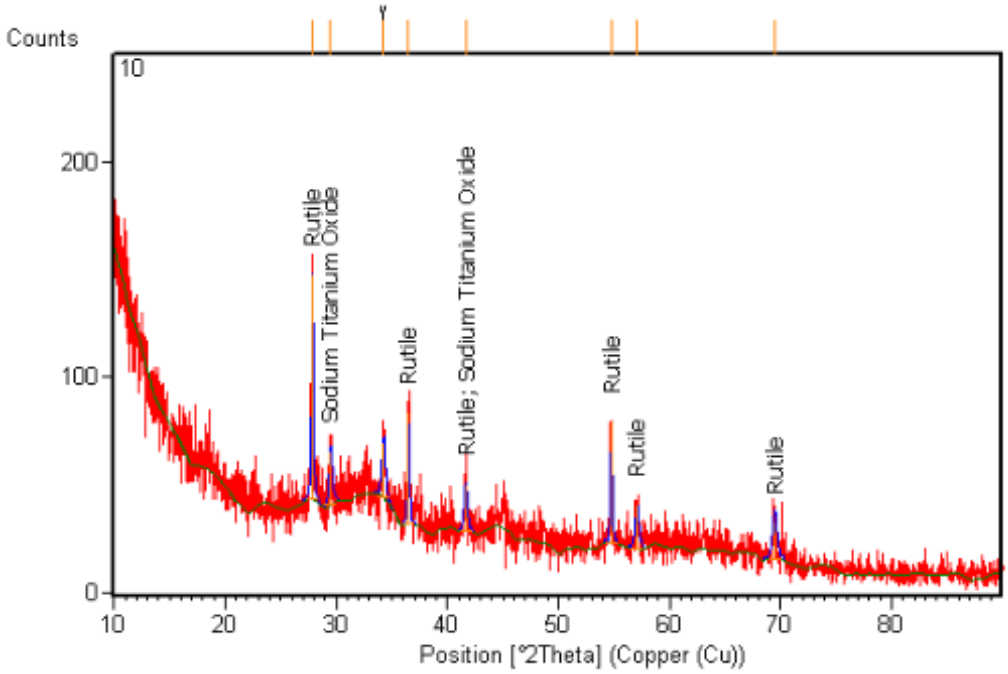

Figure 4.26 XRD Results for sample 10

- For samples 9-12 (which have been originated from rutile TiO_2), there is no clear change observed on XRD graphs.

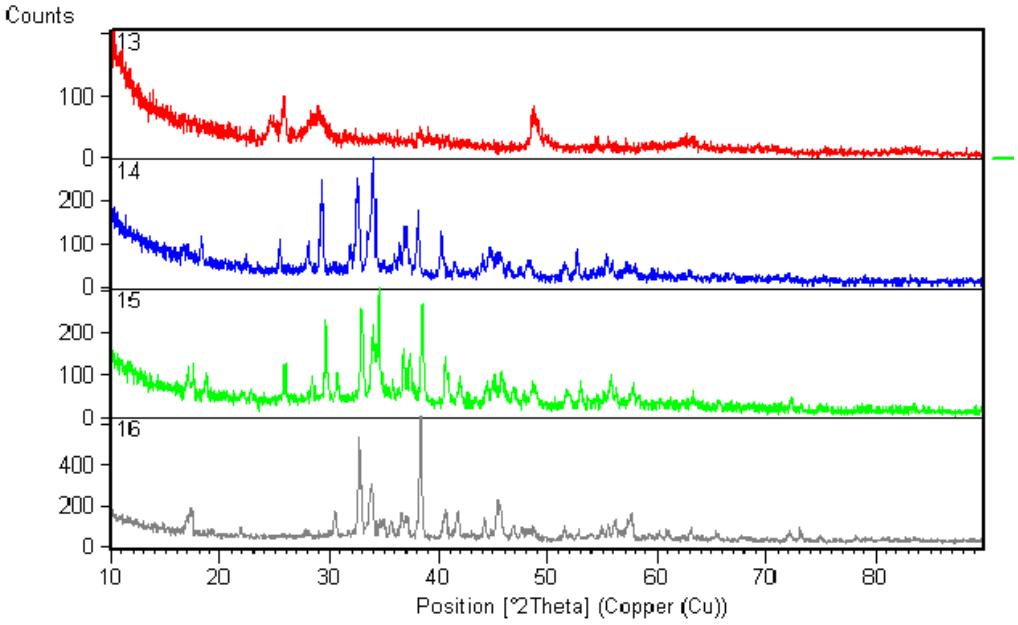

Figure 4.27 XRD Results for samples 13, 14, 15 and 16

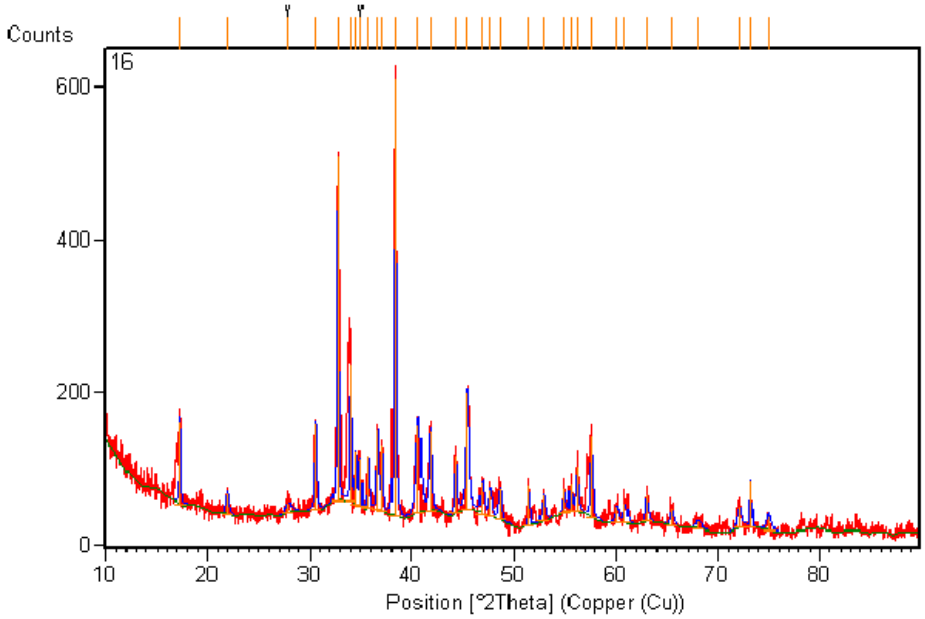

Figure 4.28 XRD Results for sample 16

- For samples 13-16 (which have been originated from ultrasounded TiO_2), as temperature increases and the reaction time decreases, the form of crystal structure changes from amorphous to crystal.

CHAPTER 5

DISCUSSION

Chapter 4 represents the results and primary commentaries for each analysis. Therefor this chapter will be consist overall comparison and discussion about the effective parameters on properties of TNT's and their application potential on DSSC's.

Taguchi analysis showed that each property has a different optimized experiment set. So, one must decide on which property is the most important one for the targeted application.

In the following paragraphs each analysis will be discussed separately.

- SEM results

They showed that ultrasounded anatase TiO_2 raw material has the best morphology. In previous studies it has been showed that photocatalytic properties of TiO_2 also gets better with ultrasound treatment. [121]

In literature, it has been known that the best TNT productions carried out between 100-200°C. It is also claimed that 130 °C is the best temperature as at lower temperatures, Ti-O-Ti bonds tends to be less flexible, so that TNT molecular structure will not be able form. And, after 130°C the lamellar structure of TiO_2, start to break. Therefore, it can be said that, our result about the best temperature which submitted as 120°C is very compatible with previous studies.

Morphological studies showed that time is inversely proportional with good TNT alignment until 30 h and it has a small improvement at 40 h. Long reaction times are the most repellent necessity in TNT production. In this study it has been claimed that 10h can be enough when choosing other parameters carefully. On the other hand, previous

researchers showed that, time is directly influenced by temperature. At higher temperatures, the shorter time may be enough to convert each layers into nanotubes. It is also coherent with our results.

Reaction rate of TNT formation has said to be increased by NaOH concentration. The linear climb in NaOH concentration graph has also proved that hypothesis. 15 M NaOH concentration has found to result best morphology.

- BET results

The highest surface area value has been observed in anatase samples according to Taguchi results. But when comparing numeric data, we can see that sample 6 has a great deviation and causes a pseudo rank to anatase. If we compare the other results without taking 6 into consideration, we can say that Degussa P25 samples has the highest surface area values due to their nanosized starting materials. Afterwards, ultrasounded TiO_2 follows Degussa P25. When pure anatase TiO_2 has 7,7038 m^2/g surface area, ultrasounded TiO_2 has 8,4620 m^2/g. It has been known that ultrasound has a positive effect on surface properties of TiO_2 materials. [121]

Temperature has directly negative effect of surface area, this is probably because of the curling up the layers of TiO_2.

Time has found to be giving best result for 10 h, like in SEM results. This is followed by 40 h.

NaOH concentration has found to be 10 M for the achieving highest surface area values.

- Pore volume analysis

Taguchi graphics are almost symmetrical with surface area graphs. Therefore, if surface area going to be considered, it should be noted that the results might be because of the porous structure and not because of the alignment of the tubes.

Rutile TiO_2 has the smallest total pore volume. This might me agglomeration, as in seen in SEM images. Afterwards, ultrasounded TiO_2 follows it, and it is also another good result for concluding ultrasounded TiO_2 is a good option for TNT production.

When temperature analysis carried out for pore volume, we can say that, pore volume decreases with time and has the smallest value at 160°C.

Effect of time on pore volume has an optimum value at level 2, 20 h. And finally, NaOH concentrations said to be have a narrow range of effectiveness, and 15 and 20 M of NaOH give the smallest pore volume.

- Pore size

Rutile TiO_2 samples have the smallest pore size. This result is again probably the agglomeration of rutile.

Pore size and temperature has no linear relationship, but has a peak value at 120°C. The other three temperature values results very close pore size values.

Time neither has not got a direct relationship with pore size. There is no significant change between 20h and 30h while it provides the smallest pore size at 10 h.

Finally, NaOH concentration is best for 20 M for pore size with a clear distance to other levels.

- XRD results

As it mentioned before in the thesis, there is no Taguchi analysis for XRD results, due to not having numerical values.

As an overall comparison, we can say that, crystallinity decreases with time, time and NaOH concentration. We can also say that, molecular structure involves Na^+ ions and long molecules occur in last ultrasounded series. This result also compatible with SEM results, because they give the most TNT-like structures for the same series.

Finally, for making a suggestion for the best option for TiO_2 that will use in DSSC, it might be said that, hydrothermal synthesis of TNT'S by using ultrasounded TiO2 with 120°C and 15 or 20 M NaOH for 10 h gives the best result. But it is also should be noted that not every sample has turned to TNT, this comments only made by the instrumental results.

REFERENCES

[1] Roper, L. D., Future World Energy, http://www.roperld.com/science/energyfuture.htm, Access Date: 10/05/2015.

[2] The Solar Spark, Renewable Energy, http://www.thesolarspark.co.uk/the-science/renewable-energy/, Access Date: 04/04/2015.

[3] PIRA (2015), International Market Report The Future of Titanium Dioxide Vol.44.

[4] Roy, P., Berger, S., and Schmuki, P., (2011), "TiO2 nanotubes: synthesis and applications.", Angewandte Chemie (International ed. in English), 50(13):2904–39.

[5] Yan, J., and Zhou, F., (2011). "TiO2 nanotubes: Structure optimization for solar cells", Journal of Materials Chemistry, 21(26):9406.

[6] Carp, O., Huisman, C. L., and Reller, A., (2004). "Photoinduced reactivity of titanium dioxide", Progress in Solid State Chemistry, 32(1-2):33–177.

[7] Merrsews, A., and Uniuersity, T. H., (1976). "The crystallization of anatase and rutile from amorphous titianium dioxide under hydrothermal conditions", American Mineralogist, 61:419-424.

[8] Gupta, S. M., and Tripathi, M., (2011). "A review of TiO2 nanoparticles", Chinese Science Bulletin.

[9] Zhang, H., and Banfield, J. F., (1998). "Thermodynamic analysis of phase stability of nanocrystalline titania", Journal of Materials Chemistry, 8(9):2073–2076.

[10] Grassian, V. H., (2008). "When Size Really Matters : Size-Dependent Properties and Surface Chemistry of Metal and Metal Oxide Nanoparticles in Gas and Liquid Phase Environments", 18303–18313.

[11] Mo, S.-D., and Ching, W., (1995). "Electronic and optical properties of three phases of titanium dioxide: Rutile, anatase, and brookite", Physical Review B, 51: 13023-13032.

[12] Lewis, A., Richardson, J. W., and Smith, J. V, (1987). "Structural-Electronic Relationships in Inorganic Solids : Powder Neutron Diffraction Studies of the Rutile and Anatase Polymorphs of Titanium Dioxide at 15 and 295 K", (5):3639–3646.

[13] Thomas, A. G., Flavell, W. R., Mallick, A. K., Kumarasinghe, A. R., Tsoutsou, D., Khan, N., Wiame, F., (2007). "Comparison of the electronic structure of anatase and rutile TiO2 single-crystal surfaces using resonant photoemission and x-ray absorption spectroscopy", Phys. Rev. B, 75:3510-5.

[14] Liu, M., Piao, L., Zhao, L., Ju, S., Yan, Z., He, T., Wang, W., (2010). "Anatase TiO(2) single crystals with exposed {001} and {110} facets: facile synthesis and enhanced photocatalysis.", Chemical communications (Cambridge, England), 46(10):1664–6.

[15] Merrsews, A., and Uniuersity, T. H., (1976). "The crystallization of anatase and rutile from amorphous titianium dioxide under hydrothermal conditions", American Mineralogist, 61:419-424.

[16] Zhifeng Liu, Chengcheng Liu, Jing Ya, and E. Lei, (2011). "Controlled synthesis of ZnO and TiO2 nanotubes by chemical method and their application in dye-sensitized solar cells", Renewable Energy, 36(4):1177–1181.

[17] Lazzeri, M., Vittadini, A., and Selloni, A., (2001). "Structure and energetics of stoichiometric TiO2 anatase surfaces", Physical Review B, 63(15):155409.

[18] Sanjinés, R., Tang, H., Berger, H., Gozzo, F., Margaritondo, G., and Lévy, F., (1994). "Electronic structure of anatase TiO2 oxide", Journal of Applied Physics, 75(6):2945.

[19] Commission, T., European, T., and Joint, C., (2011). "L 275/38", (June 2010):2010–2012.

[20] Number of journal papers with "TiO2" and "nanotube". http://www.sciencedirect.com/science?_ob=ArticleListURL&_method=list&_ArticleListID=813437715&_sort=r&_st=13&view=c&md5=ec9e2b0bed62edb3c2c4b32c720f5810&searchtype=a Access date : 04.05.2015

[21] Han, H., and Bai, R., (2009). "Buoyant Photocatalyst with Greatly Enhanced Visible-Light Activity Prepared through a Low Temperature Hydrothermal Method", Industrial & Engineering Chemistry Research, 48:2891–2898.

[22] Lu, N., Zhu, Z., Zhao, X., Tao, R., Yang, X., and Gao, Z., (2008). "Nano titanium dioxide photocatalytic protein tyrosine nitration: a potential hazard of TiO2 on skin.", Biochemical and biophysical research communications, 370(4):675–80.

[23] Zhang, T., You, L., and Zhang, Y., (2006). "Photocatalytic reduction of -chloronitrobenzene on illuminated nano-titanium dioxide particles", Dyes and Pigments, 68(2-3):95–100.

[24] Gandhi, V. G., Mishra, M. K., Rao, M. S., Kumar, a., Joshi, P. a., and Shah, D. O., (2011). "Comparative study on nano-crystalline titanium dioxide catalyzed photocatalytic degradation of aromatic carboxylic acids in aqueous medium", Journal of Industrial and Engineering Chemistry, 17(2):331–339.

[25] Bianchi, C. L., Gatto, S., Pirola, C., Naldoni, a., Di Michele, a., Cerrato, G., Capucci, V., (2014). "Photocatalytic degradation of acetone, acetaldehyde and toluene in gas-phase: Comparison between nano and micro-sized TiO2", Applied Catalysis B: Environmental, 146:123–130.

[26] Gnaser, H., Huber, B., and Ziegler, C., (2004). "Nanocrystalline TiO 2 for Photocatalysis", Encyclopedia of Nanoscience and Nanotechnology, 6:505-535.

[27] Wang, M., Guo, Y., Wang, Q., Zhang, X., Huang, J., Lu, X., Leng, Y., (2014). "Density functional theory study of interactions between Glycine and TiO2/graphene nanocomposites", Chemical Physics Letters, 599:86–91.

[28] Wu, H.-C., Lin, S.-W., and Wu, J.-S., (2012). "Effects of nitrogen concentration on N-doped anatase TiO2: Density functional theory and Hubbard U analysis", Journal of Alloys and Compounds, 522:46–50.

[29] Jha, P. K., Gupta, S. K., and Lukačević, I., (2013). "Electronic structure, photocatalytic properties and phonon dispersions of X-doped (X = N, B and Pt) rutile TiO2 from density functional theory", Solid State Sciences, 22:8–15.

[30] Shukri, G., and Kasai, H., (2014). "Density functional theory study of ethylene adsorption on clean anatase TiO2 (001) surface", Surface Science, 619:59–66.

[31] Hossain, F. M., Evteev, A. V., Belova, I. V., Nowotny, J., and Murch, G. E., (2010). "Electronic and optical properties of anatase TiO2 nanotubes", Computational Materials Science, 48(4):854–858.

[32] Chen, X., and Mao, S. S., (2007). "Titanium dioxide nanomaterials: synthesis, properties, modifications, and applications.", Chemical reviews, 107(7):2891–2959.

[33] Ye, X., Sha, J., Jiao, Z., and Zhang, L., (1997). "Thermoanalytical characteristic of nanocrystalline brookite-based titanium dioxide", Nanostructured Materials, 8(7):919–927.

[34] Hoffmann, M. R., Martin, S. T., Choi, W., and Bahnemannt, D. W., (1995). "Environmental Applications of Semiconductor Photocatalysis", Chemical Reviews, 95:69–96.

[35] Migas, D., Filonov, A. B., Borisenko, V. E., Skorodumova, N. V., (2014). Orientation effects inmorphology and electronic properties of anatase TiO2 one-dimensional nanostructures. II. Nanotubes1, Physical Chemistry Chemical Physics

[36] Liu, N., Chen, X., Zhang, J., and Schwank, J. W., (2014). "A review on TiO2-based nanotubes synthesized via hydrothermal method: Formation mechanism, structure modification, and photocatalytic applications", Catalysis Today, 225:34–51.

[37] Knauth, P., and Tuller, H. L., (1999). "Electrical and defect thermodynamic properties of nanocrystalline titanium dioxide", Journal of Applied Physics, 85(2):897.

[38] Gong, D., Grimes, C. A., Varghese, O. K., & Dickey, E. C., (2001), "Titanium oxide nanotube arrays prepared by anodic oxidation", 3331–3334.

[39] Bavykin, D. V., and Walsh, F. C., (2009). "Elongated Titanate Nanostructures and Their Applications", European Journal of Inorganic Chemistry, 2009(8):977–997.

[40] Foong, T. R. B., Shen, Y., Hu, X., and Sellinger, A., (2010). "Template-Directed Liquid ALD Growth of TiO2 Nanotube Arrays: Properties and Potential in Photovoltaic Devices", Advanced Functional Materials, 20(9):1390–1396.

[41] Bavykin, D. V., Friedrich, J. M., and Walsh, F. C., (2006). "Protonated Titanates and TiO2 Nanostructured Materials: Synthesis, Properties, and Applications", Advanced Materials, 18(21):2807–2824.

[42] Cao, G., and Liu, D., (2008). "Template-based synthesis of nanorod, nanowire, and nanotube arrays.", Advances in colloid and interface science, 136(1-2):45–64.

[43] Furneaux, R. C., Rigby, W. R., and Davidson, A. P., (1989). "The formation of controlled-porosity membranes from anodically oxidized aluminium", Nature, 337:147-149.

[44] Fleischer, R. L., Price, R. B., and Walker, R. M., (1969). "Nuclear tracks in solids.", Scientific American, 220:30–39.

[45] Tonucci, R. J., Justus, B. L., Campillo, A. J., and Ford, C. E., (1992). "Ngnochannel array glass.", Science (New York, N.Y.), 258:783–785.

[46] Kobayashi, S., Hanabusa, K., and Science, S. L., (2000). "Preparation of TiO 2 Hollow-Fibers Using Supramolecular Assemblies Seiji Shinkai Porous , nanostructured materials have attracted considerable attention because of their

potential ap- materials is quite difficult . Nanostructured inorganic cationic charge", (13):1523–1525.

[47] Jung, J. H., and Kobayashi, H., (2002). "Creation of Novel Helical Ribbon and Double-Layered Nanotube TiO 2 Structures Using an Organogel Template", (14):1445–1447.

[48] Santos, A., Montero-Moreno, J. M., Bachmann, J., Nielsch, K., Formentín, P., Ferré-Borrull, J., Marsal, L. F., (2011). "Understanding pore rearrangement during mild to hard transition in bilayered porous anodic alumina membranes.", ACS applied materials & interfaces, 3(6):1925–32.

[49] Lee, W., Ji, R., Gösele, U., and Nielsch, K., (2006). "Fast fabrication of long-range ordered porous alumina membranes by hard anodization.", Nature materials, 5(9):741–7.

[50] Kikuchi, T., Yamamoto, T., Natsui, S., and Suzuki, R. O., (2014). "Fabrication of Anodic Porous Alumina by Squaric Acid Anodizing", Electrochimica Acta, 123:14–22.

[51] Tan, L. K., Liu, X., and Gao, H., (2011). "Vertically standing, highly ordered, and dimension and morphology controllable TiO2 nanotube arrays via template-assisted atomic layer deposition", Journal of Materials Chemistry, 21(30):11084.

[52] Jung, Y. W., Byun, J. S., Woo, D. H., and Kim, Y. D., (2009). "Ellipsometric analysis of porous anodized aluminum oxide films", Thin Solid Films, 517(13):3726–3730.

[53] Leskelä, M., and Ritala, M., (2002). "Atomic layer deposition (ALD): from precursors to thin film structures", Thin Solid Films, 409(1):138–146.

[54] George, S. M., (2010). "Atomic layer deposition: an overview.", Chemical reviews, 110(1):111–31.

[55] Lee, J., and Jho, J. Y., (2011). "Fabrication of highly ordered and vertically oriented TiO2 nanotube arrays for ordered heterojunction polymer/inorganic hybrid solar cell", Solar Energy Materials and Solar Cells, 95(11):3152–3156.

[56] Gao, X., Chen, J., and Yuan, C., (2013). "Enhancing the performance of free-standing TiO2 nanotube arrays based dye-sensitized solar cells via ultraprecise control of the nanotube wall thickness", Journal of Power Sources, 240:503–509.

[57] Liu, C.-M., Chen, C., and Cheng, H.-E., (2011). "Growth Mechanism of TiO[sub 2] Nanotube Arrays in Nanopores of Anodic Aluminum Oxide on Si Substrates by Atomic Layer Deposition", Journal of The Electrochemical Society, 158(3): 58.

[58] Regonini, D., Bowen, C. R., Jaroenworaluck, a., and Stevens, R., (2013). "A review of growth mechanism, structure and crystallinity of anodized TiO2 nanotubes", Materials Science and Engineering R: Reports, 74(12):377–406.

[59] Zwilling, V., Darque-Ceretti, E., Boutry-Forveille, A., David, D., and Perrin, M. Y., (1999). "Structure and physicochemistry of anodic oxide films on titanium and TA6V alloy", Suface and Interface Analysis, 27:629–37.

[60] Gong, D., Grimes, C. A., Varghese, O. K., and Dickey, E. C., (2001). "Titanium oxide nanotube arrays prepared by anodic oxidation", 3331–3334.

[61] Omidvar, H., Goodarzi, S., Seif, A., and Azadmehr, A. R., (2011). "Influence of anodization parameters on the morphology of TiO2 nanotube arrays", Superlattices and Microstructures, 50(1):26–39.

[62] Huang, J., Zhang, K., and Lai, Y., (2013). "Fabrication , Modification , and Emerging Applications of TiO 2 Nanotube Arrays by Electrochemical Synthesis : A Review", International Journal of Photoenergy, 2013.

[63] Zhang, M., Lu, D., Yan, G., Wu, J., and Yang, J., (2013). "Fabrication of Mo + N-Codoped TiO 2 Nanotube Arrays by Anodization and Sputtering for Visible Light-Induced Photoelectrochemical and Photocatalytic Properties", Journal of Nanomaterials, 2013.

[64] Nischk, M., Mazierski, P., Gazda, M., and Zaleska, A., (2014). "Ordered TiO2 nanotubes: The effect of preparation parameters on the photocatalytic activity in air purification process", Applied Catalysis B: Environmental, 144:674–685.

[65] Varghese, O. K., Gong, D., Paulose, M., Grimes, C. A., and Dickey, E. C., (2003). "Crystallization and high-temperature structural stability of titanium oxide nanotube arrays", Journal of Materials Research, 18:156-165.

[66] Mor, G. K., Varghese, O. K., Paulose, M., Mukherjee, N., and Grimes, C. A., (2003). "Fabrication of tapered, conical-shaped titania nanotubes", Journal of Materials Research, 18:2588-2593.

[67] Kelly, R. G., Moran, P. J., Gileadi, E., and Kruger, J., (1989). "The passivity of iron in mixtures of propylene carbonate and water", Electrochimica Acta, 34(6):823-830.

[68] Wang, J., Wang, H., Li, H., and Wu, J., (2013). "Synthesis and characterization of TiO2 nanotube film on fluorine-doped tin oxide glass", Thin Solid Films, 544:276–280.

[69] Regonini, D., Satka, A., Jaroenworaluck, A., Allsopp, D. W. E., Bowen, C. R., and Stevens, R., (2012). "Factors influencing surface morphology of anodized TiO2 nanotubes", Electrochimica Acta, 74:244–253.

[70] Yin, L., Ji, S., Liu, G., Xu, G., and Ye, C., (2011). "Understanding the growth behavior of titania nanotubes", Electrochemistry Communications, 13(5):454–457.

[71] Su, Z., and Zhou, W., (2011). "Pore diameter control in anodic titanium and aluminium oxides", Journal of Materials Chemistry, 21(2):357

[72] Su, Z., and Zhou, W., (2011). "Formation, morphology control and applications of anodic TiO2 nanotube arrays", Journal of Materials Chemistry, 21(25):8955

[73] Paulose, M., Prakasam, H. E., Varghese, O. K., Peng, L., Popat, K. C., Mor, G. K., Grimes, C. A., (2007). "TiO 2 nanotube arrays of 1000 m length by anodization of titanium foil: Phenol red diffusion", Journal of Physical Chemistry C, 111(41):14992–14997.

[74] Chen, X., Schriver, M., Suen, T., and Mao, S. S., (2007). "Fabrication of 10 nm diameter TiO2 nanotube arrays by titanium anodization", Thin Solid Films, 515(24):8511–8514.

[75] Yoriya, S., Kittimeteeworakul, W., and Punprasert, N., (2012). "Effect of Anodization Parameters on Morphologies of TiO 2 Nanotube Arrays and Their Surface Properties", 6:686–691.

[76] Wang, J., and Lin, Z., (2009). "Anodic Formation of Ordered TiO2 Nanotube Arrays: Effects of Electrolyte Temperature and Anodization Potential", The Journal of Physical Chemistry C, 113(10):4026–4030.

[77] Byrappa, K., and Yoshimura, M., (2001). Handbook Of Hydrothermal Technology A Technology for Crystal Growth and Materials Processing. Yokohama, Japan: Noyes Publıcations.

[78] Tsai, C., & Teng, H., (2004), "Regulation of the Physical Characteristics of Titania Nanotube Aggregates Synthesized from Hydrothermal Treatment", (24):4352–4358.

[79] Tacchini, I., Ansón-Casaos, a., Yu, Y., Martínez, M. T., and Lira-Cantu, M., (2012). "Hydrothermal synthesis of 1D TiO2 nanostructures for dye sensitized solar cells", Materials Science and Engineering: B, 177(1):19–26.

[80] Yuan, J. J., Li, H. D., Wang, Q. L., Yu, Q., Zhang, X. K., Yu, H. J., and Xie, Y. M., (2012). "Fabrication, characterization, and photocatalytic activity of double-layer TiO2 nanosheet films", Materials Letters, 81:123–126.

[81] Pavasupree, S., Ngamsinlapasathian, S., Suzuki, Y., and Yoshikawa, S., (2007). "Preparation and characterization of high surface area nanosheet titania with mesoporous structure", Materials Letters, 61(14-15):2973–2977.

[82] Wang, B., Xue, D., Shi, Y., and Xie, F., (2008). Nanorods, Nanotubes, and Nanomaterials Research Progress, Nova Publishers

[83] Wong, C. L., Tan, Y. N., and Mohamed, A. R., (2011). "A review on the formation of titania nanotube photocatalysts by hydrothermal treatment.", Journal of environmental management, 92(7):1669–80.

[84] Seo, D., Lee, J., and Kim, H., (2001). "Preparation of nanotube-shaped TiO 2 powder", 229:428–432.

[85] Seo, H.-K., Kim, G.-S., Ansari, S. G., Kim, Y.-S., Shin, H.-S., Shim, K.-H., and Suh, E.-K., (2008). "A study on the structure/phase transformation of titanate nanotubes synthesized at various hydrothermal temperatures", Solar Energy Materials and Solar Cells, 92(11):1533–1539.

[86] Seo, H., Kim, G., Ansari, S. G., and Kim, Y., (2008). "A study on the structure/phase transformation of titanate nanotubes synthesized at various hydrothermal temperatures", Solar Energy Materials, 92(11):1533–1539.

[87] Tsai, C., and Teng, H., (2004). "Regulation of the Physical Characteristics of Titania Nanotube Aggregates Synthesized from Hydrothermal Treatment", (24):4352–4358.

[88] Sreekantan, S., and Wei, L. C., (2010). "Study on the formation and photocatalytic activity of titanate nanotubes synthesized via hydrothermal method", Journal of Alloys and Compounds, 490(1-2):436–442.

[89] Zhang, Y. J., Yan, W., Wu, Y. P., and Wang, Z. H., (2008). "Synthesis of TiO2 nanotubes coupled with CdS nanoparticles and production of hydrogen by photocatalytic water decomposition", Materials Letters, 62(23):3846–3848.

[90] Huang, J., Cao, Y., Wang, M., Huang, C., Deng, Z., Tong, H., and Liu, Z., (2010). "Tailoring of Low-Dimensional Titanate Nanostructures", The Journal of Physical Chemistry C, 114(35):14748–14754.

[91] Bavykin, D. V, Friedrich, J. M., Lapkin, A. A., Walsh, F. C., Engineering, C., Uni, V., December, V., (2006). "Stability of Aqueous Suspensions of Titanate Nanotubes", (22):1124–1129.

[92] Kasuga, T., Hiramatsu, M., Hoson, A., Sekino, T., and Niihara, K., (1998). "Formation of Titanium Oxide Nanotube", Langmuir, 14(12):3160–3163.

[93] Preda, S., Teodorescu, V. S., Musuc, A. M., Andronescu, C., and Zaharescu, M., (2012). "Influence of the TiO2 precursors on the thermal and structural stability of titanate-based nanotubes", Journal of Materials Research, 28(03):294–303.

[94] Yoshida, R., Suzuki, Y., and Yoshikawa, S., (2005). "Effects of synthetic conditions and heat-treatment on the structure of partially ion-exchanged titanate nanotubes", Materials Chemistry and Physics, 91(2-3):409–416.

[95] Tsai, C., Teng, H., Cheng, N., Uni, K., August, R. V, Re, V., September, V., (2006). "Structural Features of Nanotubes Synthesized from NaOH Treatment on TiO 2 with Different Post-Treatments", (4):367–373.

[96] Lee, C.-K., Liu, S.-S., Juang, L.-C., Wang, C.-C., Lyu, M.-D., and Hung, S.-H., (2007). "Application of titanate nanotubes for dyes adsorptive removal from aqueous solution.", Journal of hazardous materials, 148(3):756–60.

[97] Yu, K.-P., Yu, W.-Y., Kuo, M.-C., Liou, Y.-C., and Chien, S.-H., (2008). "Pt/titania-nanotube: A potential catalyst for CO2 adsorption and hydrogenation", Applied Catalysis B: Environmental, 84(1-2):112–118.

[98] Nakahira, A., Kubo, T., and Numako, C., (2010). "TiO2-derived titanate nanotubes by hydrothermal process with acid treatments and their microstructural evaluation.", ACS applied materials & interfaces, 2(9):2611–6.

[99] Zhu, H., Gao, X., Lan, Y., Song, D., Xi, Y., and Zhao, J., (2004). "Hydrogen titanate nanofibers covered with anatase nanocrystals: a delicate structure achieved by the wet chemistry reaction of the titanate nanofibers.", Journal of the American Chemical Society, 126(27):8380–1.

[100] Zhu, H. Y., Lan, Y., Gao, X. P., Ringer, S. P., Zheng, Z. F., Song, D. Y., and Zhao, J. C., (2005). "Phase transition between nanostructures of titanate and titanium dioxides via simple wet-chemical reactions.", Journal of the American Chemical Society, 127(18):6730–6.

[101] Blaauw, C., Naguib, H. M., Ahmad, A., and Ahmed, S. M., (1982). "The preparation of TiO2 thick film anodes for photoelectrochemical solar cells", Solar Energy Materials, 7(3):331–342.

[102] Maruska, H. P., and Ghosh, A. K., (1978). "Photocatalytic decomposition of water at semiconductor electrodes", Solar Energy, 20(6):443–458.

[103] Ou, H., and Lo, S., (2007). "Review of titania nanotubes synthesized via the hydrothermal treatment: Fabrication, modification, and application", Separation and Purification Technology, 58(1):179–191.

[104] Macak, J. M., Tsuchiya, H., Ghicov, a., Yasuda, K., Hahn, R., Bauer, S., and Schmuki, P., (2007). "TiO2 nanotubes: Self-organized electrochemical formation, properties and applications", Current Opinion in Solid State and Materials Science, 11(1-2):3–18.

[105] O'Regan, B., and Grätzel, M., (1991). "A low-cost, high-efficiency solar cell based on dye-sensitized colloidal TiO2 films", Nature, 353:737-740.

[106] Burschka, J., Pellet, N., Moon, S.-J., Humphry-Baker, R., Gao, P., Nazeeruddin, M. K., and Gratzel, M., (2013). "Sequential deposition as a route to high-performance perovskite-sensitized solar cells", Nature, 499(7458):316–319.

[107] Liu, N., Lee, K., & Schmuki, P., (2012), "Small diameter TiO2 nanotubes vs. nanopores in dye sensitized solar cells", Electrochem. Commun., 15(1):1–4.

[108] National Renewable Energy Laboratory, Best Research-Cell Effciences, http://www.nrel.gov/ncpv/images/efficiency_chart.jpg, Access date: 20.05.2015.

[109] Ooyama, Y., Shimada, Y., Inoue, S., Nagano, T., Fujikawa, Y., Komaguchi, K., Harima, Y., (2011). "New molecular design of donor-π-acceptor dyes for dye-sensitized solar cells: control of molecular orientation and arrangement on TiO2 surface", New Journal of Chemistry, 35(1):111.

[110] Yu, J., Fan, J., and Zhao, L., (2010). "Dye-sensitized solar cells based on hollow anatase TiO2 spheres prepared by self-transformation method", Electrochimica Acta, 55(3):597–602.

[111] Park, N. G., Schlichthörl, G., Van De Lagemaat, J., Cheong, H. M., Mascarenhas, A., and Frank, A. J., (1999). "Dye-sensitized TiO2 solar cells: Structural and photoelectrochemical characterization of nanocrystalline electrodes formed from the hydrolysis of TiCl4", Journal of Physical Chemistry B, 103:3308–3314.

[112] Ishihara Sangyo Kaisha LTD, Functional Materials, Photocatalytic Titanium Dioxide, ST/STS Series http://www.iskweb.co.jp/eng/products/functional05.html, 2012 Access Date : 10.05.2015.

[113] Mahmoodi, N. M., and Arami, M., (2006). "Bulk phase degradation of Acid Red 14 by nanophotocatalysis using immobilized titanium(IV) oxide nanoparticles", Journal of Photochemistry and Photobiology A: Chemistry, 182(1):60–66.

[114] Sayilkan, F., Erdemoğlu, S., Asiltürk, M., Akarsu, M., Şener, Ş., Sayilkan, H., Arpaç, E., (2006). "Photocatalytic performance of pure anatase nanocrystallite TiO2 synthesized under low temperature hydrothermal conditions", Materials Research Bulletin, 41(12):2276–2285.

[115] Fujıshıma, A., and Honda, K., (1972). "Electrochemical Photolysis of Water at a Semiconductor Electrode", Nature, 238(5358):37–38.

[116] Thiruvenkatachari, R., Vigneswaran, S., and Naidu, R., (2008). "Permeable reactive barrier for groundwater remediation", Journal of Industrial and Engineering Chemistry, 14(2):145-156.

[117] Vuong, D. D., Tram, D. T. N., Pho, P. Q., and Chien, N. D., (2009). "Hydrothermal Synthesis and Photocatalytic Properties of TiO2 Nanotubes", Physics and Engineering of New Materials, 127: 95–101.

[118] Altomare, M., Pozzi, M., Allieta, M., Bettini, L. G., and Selli, E., (2013). "H2 and O2 photocatalytic production on TiO2 nanotube arrays: Effect of the anodization time on structural features and photoactivity", Applied Catalysis B: Environmental, 136-137:81–88.

[119] Bauer, S., Pittrof, A., Tsuchiya, H., and Schmuki, P., (2011). "Size-effects in TiO2 nanotubes: Diameter dependent anatase/rutile stabilization", Electrochemistry Communications, 13(6):538–541.

[120] Roy, R. K., (2001). Design of Experiments Using The Taguchi Approach: 16 Steps to Product and Process Improvement. John Wiley& Sons.

[121] Saygi, B., (2010), TiO2 Fotokatalizörünün Fotokatalitik Aktivitesi, MSc Thesis, Atatürk University, Graduate School of Natural and Applied Sciences, Erzurum.

CURRICULUM VITAE

PERSONAL INFORMATION

Name Surname : Selen Ezgi (AÇIKYILDIZ) ÇELİK

Date of birth and place : 26/03/1990, Istanbul

Foreign Languages : English- German- Arabic

E-mail : selen@yildiz.edu.tr

EDUCATION

Degree	Department	University	Date of Graduation
Undergraduate	Chemical Engineering Department	Istanbul University	2012
High School	Adnan Menderes Anatolian High School		2007

WORK EXPERIENCE

Year	Corporation/Institute
2013 - recent	Research and Teaching Assistant (Chemical Engineer) Yildiz Technical University, Chemical Engineering Department

2014 - 2014	Research Intern, Imperial Collage, Chemical Engineering Department
2010-2013	Research Student Istanbul University, Chemical Engineering Department, Rheology Lab

PUBLISHMENTS

Papers

1. Beyribey, B., Saygi B., **Acikyildiz, S.E.**, Culcu, L., Mutlu, B., Vardar, D.S., Sarac, H.Effect of V/Mo Ratio on Structural Properties of VxMo(1-x)Oy Nanoparticles used as Alkaline Fuel Cell Catalyzer, Applied Mechanics and Materials Vol. 492 (2014) pp 346-349 ISBN: 978-3-03785-991-9

Conference Papers

1. **Çelik, S. E.**, Genc, U and Sarac, H. Conservation Studies Of 18th Century British Cast Iron Cannon, Seaha Conference, London, 2015 UK
2. **Çelik, S. E.**, and Sarac, H. Archaeometric Investigation of Mortar and Stone Samples of Tercan Mamahatun Complex Within Restoration Project, 37th International Symposium of Excavations, Surveys and Archaeometry, 2015. Erzurum, Turkey
3. **Çelik, S. E.**, and Sarac, H. Optimization of Synthesis Parameters of Tio2 Nanotubes by Using Taguchi Method. International Conference on Engineering, Technology And Sciences (ICETS) – UAE 2014
4. Severoglu, A., Yalcin, B. S., Ozturk, A. B., **Açıkyıldız, S. E.**, and Sarac, H. Determining The Effective Parameters On Moisture Content For Solid Biomass Pellets Produced By Astragalus and Verbascum Thapsus. Venice 2014 Fifth International Symposium On Energy From Biomass and Waste. Italy 2014
5. **Açıkyıldız, S. E.**, Yalcin, B. S., and Sarac, H. A New Approach To Engineering Education: Evolution From Pedagogy To Andragogy/Heutagogy. 21st International Congress Of Chemical And Process Engineering Chisa 2014. Czech Society Of Chemical Engineering. 2014
6. **Acikyildiz, S.E.**, Erpolat, Z., Budan C.B., Asik, I., Sarac, H. Synthesize Of Nanoparticles By Using Living Organisms, Nanokon'14, Istanbul, Turkey 2014
7. **Acikyildiz, S.E.**, Erpolat, Z., Budan C.B., Celikbilek, K., Ates, E., Sarac, H. Preparation Of Moisturizer Formulations By Taguchi Method And Analysis Of Stabilization Parameters, 4thcosmetics Chemistry, Production And Standardization Congress, Antalya, Turkey 2014

8. Aydın, I., **Acikyildiz, S.E.**, Ergin, M.F., Engin, C. Effect Of Salt Addition To Paraffin Wax Emulsions Stabilized By Bentonite, Chemical Engineering Students Congress, Ankara, Turkey 2013
9. Aydın, I., **Acikyildiz, S.E.**, Ergin, M.F., Engin, C. Rheological Investigation Of Bentonite Doped Emulsion Systems, 3rd Cosmetics Chemistry, Production And Standardization Congress, Antalya, Turkey 2013